Collapsible Silicone Tubes: An in Vitro Model for Tracheal Traction

Kevin D. Garman
Marquette University

COLLAPSIBLE SILICONE TUBES: AN IN VITRO MODEL FOR TRACHEAL TRACTION

by

Kevin Garman

A Thesis Submitted to the Faculty of the Graduate School,
Marquette University,
in Partial Fulfillment of the Requirements for
the Degree of Master of Science

Milwaukee, Wisconsin

December 2017

ABSTRACT

COLLAPSIBLE SILICONE TUBES:
AN IN VITRO MODEL FOR
TRACHEAL TRACTION

Kevin Garman

Marquette University, 2017

Obstructive sleep apnea (OSA) is characterized by recurrent episodes of airway collapse and airflow limitation during sleep. Fragmented sleep and reductions in blood oxygen saturation lead to several comorbidities, including hypertension, cardiovascular disease, and cerebrovascular disease. Longitudinal forces (tracheal traction) acting on the soft tissues surrounding the upper airway have been proposed to play a significant role in stabilizing the airway and preventing collapse. However, the relative contribution of longitudinal forces as compared to other factors that affect airway stability (airway geometry, tissue properties, muscle activity) remains unclear. This in-vitro study aimed to investigate to what extent longitudinal forces can stabilize the upper airway against flow-induced collapse.

Collapsible silicone tubes of varying lengths (L = 75 to 125mm), diameters (D = 12.70 to 31.75mm), and wall thicknesses (h = 0.98 to 2.22mm) were fabricated in-house. An experimental setup was developed that included a pressure catheter to measure air pressure in the tube lumen, a pump that generated sinusoidal bidirectional flow, and a laser line scanner to monitor deformations of the tube wall. The buckling pressure (pressure at which the tube collapses) was quantified as a function of tube geometry and longitudinal stretching.

The silicone tubes collapsed at a similar range of transmural pressures (0 to 10 cmH_2O) and flowrates (0 to 250ml/s) as observed in the human airway during sleep. Tube length had no clear effect on the buckling pressure, but mechanical stability increased when the wall-thickness-to-radius ratio ($\gamma = 2h/D$) increased. The buckling pressured measured experimentally was in good agreement with the theory for tubes exposed to transmural pressure alone (zero flow), suggesting that tube collapse was determined primarily by the transmural pressure (rather than by fluid-structure interactions). Longitudinal stretching (5% strain) reduced the buckling pressure by 0.5 to 1.0 cmH_2O, which was smaller than the effect of changes in tube diameter and wall thickness.

Longitudinal stretching improved the stability of cylindrical silicone tubes, but its effect was smaller than the effect of changes in tube geometry.

Keywords: obstructive sleep apnea; tracheal traction; longitudinal strain; starling resistor; airway collapse; buckling pressure; bidirectional cyclic flow; airflow limitation; silicone rubber.

ACKNOWLEDGEMENTS

Kevin Garman

First and foremost, a huge thank you goes to my graduate advisor and mentor, Dr. Guilherme Garcia, for accepting me into his research lab and giving me this incredible opportunity. Starting with my first interview, he has been unbelievably encouraging and supportive. He is an extremely capable advisor who genuinely cares for and encourages his students to be independent and to discern what is best for them. His passion and drive for research and learning to improve lives motivate those in his lab and classroom. Dr. Garcia's innate ability to see the bigger picture and grasp a wide variety of research topics is astounding. His mentorship and support both academically and professionally has proved to be invaluable in many ways, and I genuinely hope to continue this relationship in the future.

I would like to thank my other committee members, Dr. Said Audi and Dr. John LaDisa, for their time and effort in advancing my research project. Dr. Audi and Dr. LaDisa have been instrumental in completing this manuscript by providing their expertise and support. I was under instruction of them both in Dr. LaDisa's cardiopulmonary mechanics class, where I was able to advance my knowledge in areas related to my research and my career passions, and I am incredibly thankful to have had the opportunity to be taught by such brilliant minds.

I thank many other people involved in my thesis. Mrs. Bonnie Freudinger, head of the Medical College of Wisconsin's Engineering Lab, for kindly providing engineering advice, experimental support, and use of workshop tools and machinery. Bonnie also spent hours helping me figure out the best possible way to conduct my experiments and facilitating part orders for the proper equipment I needed to complete the tests. Her support and insights have been vital to advancing my thesis project. Brendan Ryan and Justin Prom created and conducted a significant portion of the 3D Printing work. Ben Dickerhoff aided in DATAQ instrumentation setup. Dr. Masoud Moghaddam wrote the MATLAB code used to analyze pressure data collected from the experimental setup. Andy Milbrath was instrumental in technical support for software and programming setup. I thank Dr. Gerald Harris for his guidance and support in letting me use Marquette University's Biomechanics Lab for materials testing. Mary Wesley has been extremely helpful with various graduate school related logistics and support. I thank other members of Marquette University and the Medical College of Wisconsin for administrative guidance, kindness, and support.

A massive thank you to my sisters, Erin Garman and Angela Garman, for encouraging text messages, cards, and calls from afar. I am beyond grateful to have such

passionate, driven sisters to motivate me and continue to remind me of the little things in life that are worth fighting for. I thank my friends, especially Hien Doan and Brice Ost. Hien has provided crucial emotional support and empathy in many areas of my life and has been a phenomenally motivating study partner throughout this graduate school voyage. Brice has provided constant light-heartedness and has proven to be a true confidant that has lifted my spirits at times when things were going wrong in and outside of graduate school. I would also like to thank many other friends, (Allison Thompson, Kayla Wehkamp, Katie Maxwell, and Brice Ost) for traveling great distances to visit me and show me that there is life beyond this thesis project. Your kind words and support have been instrumental in keeping my sanity intact.

My thesis, along with all of my accomplishments, is dedicated to my parents, Daniel and Vycke Garman. My father and mother have unselfishly devoted their lives to give me opportunities and security they never had growing up. I cannot ever repay them for their many sacrifices, but I truly hope to make them proud with my work. Words will not do justice how much you mean to me; however, I do want to say how unbelievably grateful I am for your unconditional love, whole-hearted acceptance, and unwavering support. I love you with all my heart.

To quote the American Historian, Howard Zinn, “Small acts, when multiplied by millions of people, can transform the world.” Although millions of people may not have been involved in this project, the journey and involvement that each and every person had in this project has significantly changed my world and brought me into a new chapter of life. It took a mountain of support from family, friends, colleagues, mentors, and advisors to finish this thesis. My deepest gratitude to you all.

TABLE OF CONTENTS

LIST OF TABLES

LIST OF FIGURES

LIST OF ABBREVIATIONS, ACRONYMS, & SYMBOLS

(In order of appearance)

OSA: obstructive sleep apnea

AHI: apnea-hypopnea index

CPAP: continuous positive airway pressure

MRI: magnetic resonance imaging

P_{ext}: external air pressure

P_{crit}: critical pressure

P_{us}: upstream pressure

P_{ds}: downstream pressure

V_{lmax}: maximal inspiratory airflow

R_{us}: upstream nasal resistance

ETP: extraluminal tissue pressure

ETPlat: extraluminal tissue pressure of lateral airway walls

ETPant: extraluminal tissue pressure of anterior airway walls

P_s: flow limiting site

Π: non-dimensional pressure

P_{TM}: transmural pressure

K_P: flexural rigidity

α: non-dimension area

A: final area

A_o: initial area

P_B: buckling pressure

Π_{cp}: non-dimensional pressure at contact point

α_{cp}: non-dimensional area at contact point

P_{CP}: contact point pressure

P_{close}: full occlusion pressure

kg/m^3: kilogram per meter cubed

m^2/s: squared meters per second

3D: three-dimensional

C: compliance

♂: Male

♀: Female

PPE: personal protective equipment

ppi: pounds per inch of thickness

psi: pounds per square inch

inHg: inches of mercury

E: Young's modulus

σ: tensile stress

ε: strain

υ: Poisson's ratio

ε_{Axial}: axial strain

ε_{Trans}: transverse strain

MPa: megapascal

cm: centimeters

mm: millimeters

mL/s: milliliters per second

d/D: ratio of the minimal diameter during a breathing cycle to the tube diameter

cmH_2O: centimeters of water

FSI: fluid-structure interaction

SLA: Stereolithography

Q_B: buckling flowrate

Q_{CP}: contact point flowrate

Q_{crit}: critical flowrate

FEA: finite element analysis

BMI: body mass index

UPPP: Uvulopalatopharyngoplasty

CHAPTER 1: BACKGROUND AND INTRODUCTION

1.1 The Problem of Obstructive Sleep Apnea

Obstructive sleep apnea (OSA) affects 2-14% of adults in the United States (White & Younes, 2012). OSA is characterized by recurring collapse of the pharyngeal airway during sleep. The gold standard exam to diagnose OSA is a sleep study in which patients are monitored during sleep. The number of apneas and hypopneas per hour, known as the apnea-hypopnea index (AHI), is used to diagnose and classify the severity of OSA: mild OSA: AHI = 5-15, moderate OSA: AHI = 15-30, and severe OSA: AHI = 30+ (White & Younes, 2012). According to a recent study by White and Younes (2012), while an absolute cause of OSA is unknown, obesity is a strong contributor to OSA onset in 41% to 58% of adults suffering from this condition; moreover, due to increasing obesity rates, the prevalence of OSA is increasing in the United States. In regards to gender, men are 2 to 3 times more likely to have OSA than pre-menopausal women (White & Younes, 2012).

OSA is associated with many neurocognitive and cardiovascular consequences. Neurocognitive consequences of OSA include constant lethargy, lack of focus, fatigue, depression, and overall decreased quality of life; whereas, cardiovascular risks of OSA consist of hypertension, diabetes, cardiac arrhythmias, strokes, myocardial infarction, and increased risk of congestive heart failure (White & Younes, 2012).

The main treatments for OSA are continuous positive airway pressure (CPAP), oral appliances, and upper airway surgery. CPAP utilizes a nasal mask to deliver positive airway pressure that forces open the airway for uninterrupted breathing. CPAP is very

effective, but is often unsuccessful due to patient non-compliance. Oral appliance treatment has better patient compliance than CPAP but a lower effectiveness. Oral appliances displace the mandible anteriorly to increase patency in the retroglossal airspace by pulling the jaw forward (White & Younes, 2012). The final treatment option of upper airway surgery is the most invasive. Surgeries consist of removing or reducing the tissue of the soft palate, moving the jaw anteriorly to enlarge the retroglossal airspace, and/or nasal surgery to reduce nasal resistance (White & Younes, 2012). Although surgery reduces snoring and reduces the AHI, it is rarely a cure for OSA.

In conjunction to the aforementioned treatments, OSA symptoms can be improved by life style changes, such as weight loss, reduction of alcohol consumption, reduction of sedative use before bed, and sleeping on the side (rather than sleeping supine).

1.2 Pathophysiology of Obstructive Sleep Apnea

The upper airway ranges from the external nares to the epiglottis (Figure 1). The main sites of upper airway collapse in OSA patients are the space behind the soft palate (nasopharynx), the space behind the tongue (oropharynx), and the epiglottis (Figure 1). The soft palate is the most common site of collapse (~80% of cases). As the obstruction is caused by surrounding tissue of the pharynx, it is important to understand what the walls are composed of. The anterior wall consists of the soft palate and tongue, the lateral walls consist mainly of muscle and adipose tissues, and the posterior wall consists of the 3 pharyngeal constrictor muscles. The pharyngeal muscles surrounding the oropharynx have a high impact on the degree of patency seen in both healthy individuals

and OSA patients. Therefore, muscle tone plays a key role in OSA pathophysiology. OSA patients have no obstruction while awake due to muscle activity. However, muscle tone is reduced during sleep, decreasing the airway lumen and leading to airflow limitation.

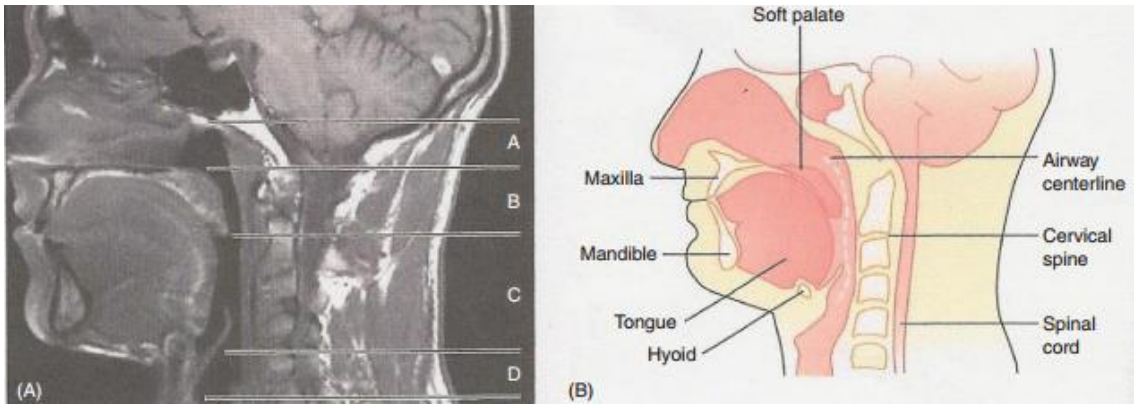

Figure 1: *Upper airway anatomy.*
(A) *Midsagittal MRI in a normal subject, highlighting the four upper airway regions: A = nasopharynx, B = retropalatal nasopharynx (most common site of collapse), C = retroglossal region (oropharynx), and D = the hypopharynx.* ***(B)*** *The diagram illustrates important upper airway, soft tissue, and bone structures. Reproduced from White & Younes (2012).*

The Starling resistor model is often used to explain the mechanism of airway collapse in OSA. In this model (Figure 2), the pharynx is considered a collapsible tube mounted between a rigid upstream segment (the nasal cavity) and a rigid downstream segment (the trachea). The collapsible tube is enclosed by a sealed box where the external air pressure (P_{ext}) can be controlled. When air pressure inside the tube becomes less than the external pressure, the tube collapses. Thus, the external pressure is also known as the critical pressure (P_{crit}) at which the tube collapses (Figure 2).

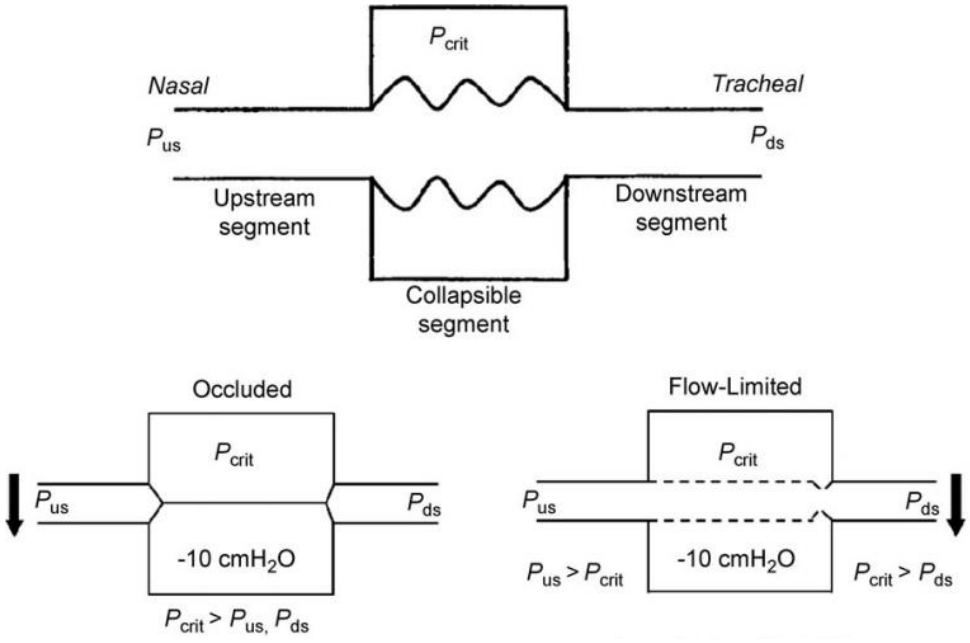

Figure 2: *Starling resistor model.*
P_{crit} = surrounding tissue pressure determining Pharyngeal collapsibility. P_{us} = upstream pressure; P_{ds} = downstream pressure; V_{Imax} = maximal inspiratory airflow. Reproduced from Schwartz & Smith (2013).

Figure 2 shows how the collapsible conduit changes as the external pressure changes. In the bottom left, complete collapse occurs when both the upstream pressure and downstream pressure are less than P_{crit}. In the bottom right, flow-limitation occurs when the downstream pressure becomes less than P_{crit}, while the upstream pressure remains above P_{crit}. During flow limitation, airflow becomes independent of the downstream pressure and the external pressure (P_{crit}) becomes the effective downstream pressure. Thus, during airflow limitation the maximal inspiratory airflow (V_{Imax}) is:

Equation 1: *Max Inspiratory Airflow* $$V_{Imax} = \frac{(P_{us} - P_{crit})}{R_{us}}$$

where P_{us} is the upstream pressure and R_{us} is the upstream nasal resistance.

The Starling resistor model displays several behaviors that are similar to airway collapse in OSA patients, including (1) the pharynx occludes when intraluminal pressure falls below P_{crit}, (2) higher tissue pressure (external pressure) increases collapsibility, (3) longitudinal stretching (tracheal traction) reduces collapsibility, (4) longer airways (longer tubes) are more collapsible, (5) the pressure-flow curve displays hysteresis, and (6) snoring (oscillations).

In a study conducted by Wellman et al. (2014), the concept of flow limitation seen in the starling resistor model was discussed. They explain that in a starling resistor model the upstream segment will incur a fixed amount of airflow under fixed pressure gradient and resistance conditions. Additionally, the upstream and downstream segments see the same amount of flow, thus, the flow through a starling resistor will plateau at a maximum value that remains constant (Figure 3).

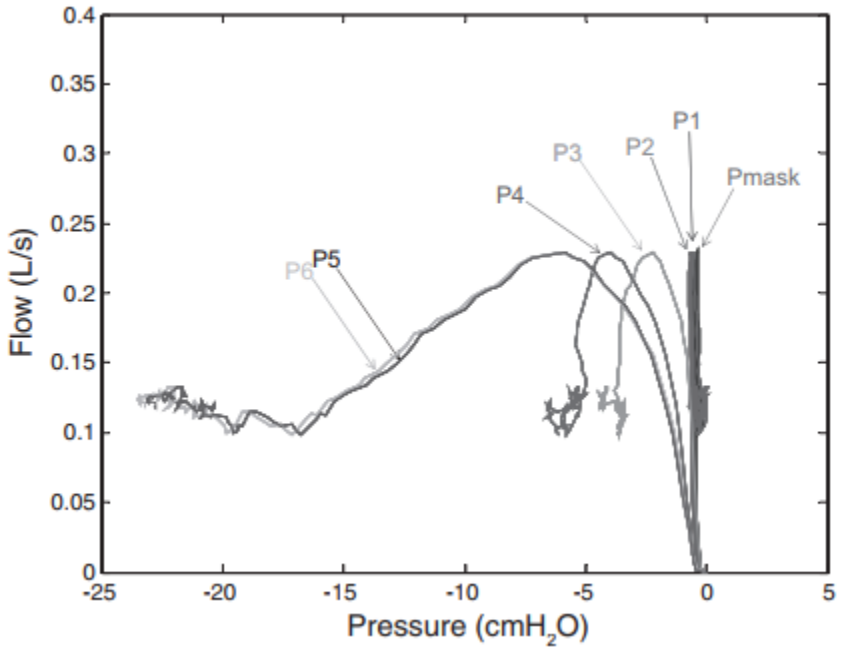

Figure 3: *Pressure-flow relationship for six separate pressure transducers. Sensors P1 and P2 are located in the nares region. Sensors P3 and P4 are located just upstream or at the choke point. Sensors P5 and P6 are located downstream from the choke point. Reproduced from Wellman et al. (2014).*

In Figure 3, there is a maximum flow reached at each location along the upper airway the transducers are placed, which implies that pressures above a certain level will not augment flow. Thus, the flow is effort independent because it has reached its maximal value. Excessive airflow limitation is abnormal and can be indicative of pathological cases in patients with increasingly severe changes in sleep and wakefulness, which may lead to OSA pathogenesis (Arora, Meskill, & Guilleminault, 2015).

The pathogenesis of OSA involves many complicated physiological phenomena, as illustrated in Figure 4.

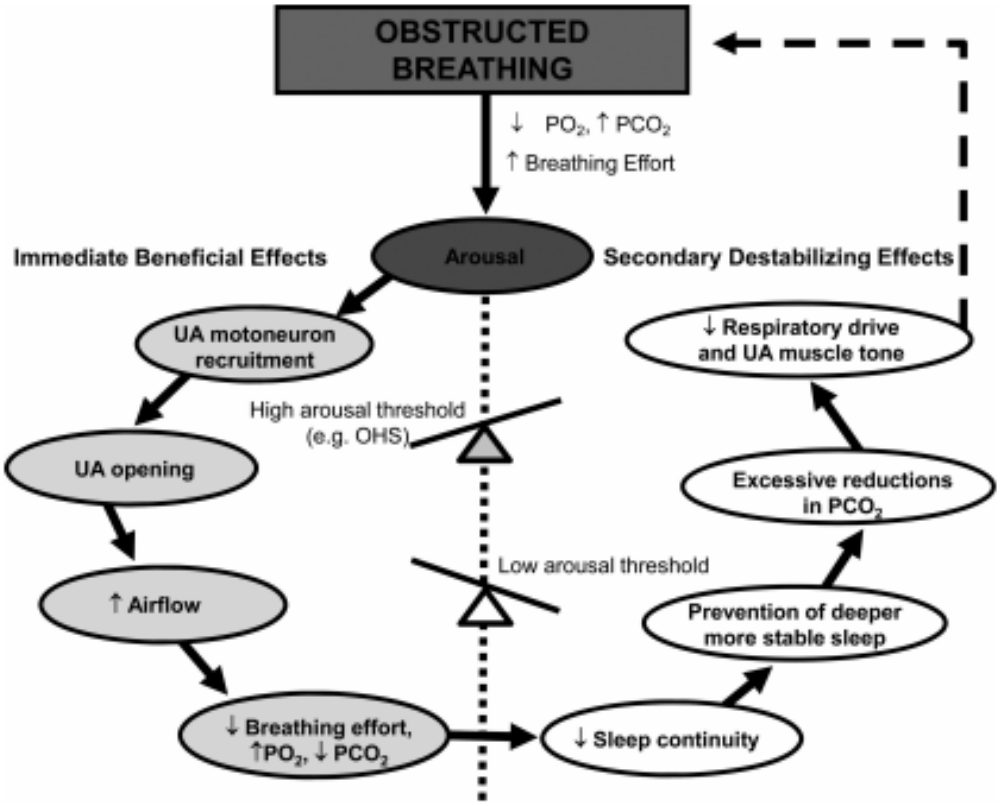

Figure 4: *Diagram modeling the potentially beneficial vs. destabilizing physiological changes linked to respiratory-induced arousals in OSA.*
During obstructed breathing, O_2 levels decrease while CO_2 increase in the blood. This creates a deviation in blood pH balance stimulating increased breathing effort. As the arousal threshold is crossed, a cortical arousal from sleep occurs (dark oval). After approximately 1-2 breaths, immediate beneficial effects are sustained (left-hand side)

including: upper airway motoneuron recruitment, upper airway opening, increased airflow, and homeostasis upon dissipation of hypercapnia and reoxygenation. However, secondary destabilizing effects also arise with arousal (right-hand side) including: disrupted sleep continuity, prevention of deeper, more stable sleep, excessive reduction in CO_2, and decreased respiratory drive and upper airway muscle tone. These effects are likely to propagate this cycle in OSA patients. Reproduced from Eckert & Younes (2013).

Figure 4 shows how arousal from sleep may have both a positive and negative role in OSA pathogenesis. Rapid recruitment of inspiratory upper airway motoneurons is associated with the increased breathing effort as the patient is reintroduced into a wakeful state (Wilkinson, et al., 2008). Upon opening of the airway, a significant increase in airflow is achieved coupled with restoration of blood oxygen levels and reduction in the carbon dioxide buildup that occurs during an obstruction. As noted by Eckert & Younes (2013), OSA patients also experience a number of destabilizing effects upon arousal. Between two possible scenarios, it is unclear in OSA patients which of the following produces a greater risk of cardiovascular disease development: 1) having less arousal events with a lower AHI, which indicates longer obstruction times leading to more significant reductions in blood oxygen levels or 2) having more arousal events with a greater AHI, which indicates shorter obstruction times with less blood oxygen desaturation (Eckert & Younes, 2013). Nonetheless, more complications are known to arise with sleep fragmentation as a higher number of arousal events occur. As homeostasis is regained and the patient becomes less awake, the motoneuron recruitment subsides and the muscle tone dissipates until the cycle is repeated and an obstruction recurs (Figure 4).

1.3 Relevant Findings From Previous Studies

1.3.1 Tracheal Traction

Tracheal traction plays an important role in the pathophysiology of OSA. Increases in lung volume have been shown to reduce pharyngeal collapsibility (White & Younes, 2012). The leading hypothesis is that the effects of lung volume on upper airway collapsibility are mediated by longitudinal forces, i.e., when the lung inflates, longitudinal forces pull the trachea downwards (caudal traction) (Heinzer, et al., 2005). Many animal-based studies have been conducted by applying longitudinal tension to the specimen's airway and observing its effect on collapsibility, which will be explored in the following text.

In two separate studies by Kairaitis et al. (2006) and Amatoury et al. (2014), white male rabbits were anesthetized, tracheotomized, and laid on their backs for tracheal traction studies. In Kairaitis et al. (2006), as tracheal traction force was increased, the extraluminal tissue pressure (ETP) and both the pressures required to close and reopen the upper airway decreased. This suggests that by implementing caudal tracheal traction, the upper airway is stabilized due to reduced wall compliance and surrounding tissue pressure (Kairaitis, et al., 2006) (Figure 5).

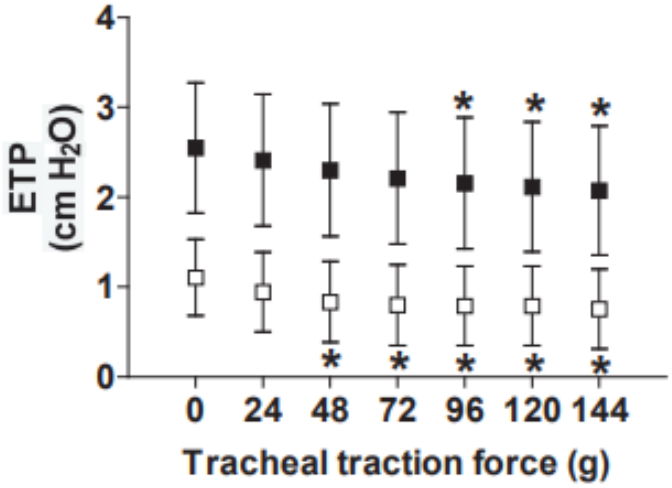

Figure 5: *Data from 17 rabbits showing effect of caudal tracheal traction on Extraluminal Tissue Pressure (ETP).*
*ETP is divided into two sections: (1) mean extraluminal tissue pressure of lateral airway walls (ETPlat) (closed symbols) and (2) mean extraluminal tissue pressure of anterior airway walls (ETPant) (open symbols). *p<0.05 for the corresponding ETP compared with no force. Reproduced from Kairaitis et al. (2006).*

The data presented in Figure 5 suggests that application of longitudinal strain (tracheal traction) propagates transmission of forces to the upper airway extraluminal tissue space and that decompression of those tissues is likely (Kairaitis, et al., 2006). In Amatoury et al. (2014), additional parameters of upper airway geometry and displacement of the thyroid cartilage and hyoid bone were measured and recorded. It was found that upper airway lumen geometry increased non-uniformly with tracheal traction leading to increases in upper airway midsagittal cross-sectional area, length and volume, axial cross-sectional area, anteroposterior diameter, and lateral diameter. These measurements were taken at three regions: R1 = tongue, R2 = hyoid, R3 = epiglottis (Amatoury J. , Kairaitis, Wheatley, Bilston, & Amis, 2014). Among these regions, the most variation due to caudal displacement of the trachea was found along R2. Thus, in

addition to upper airway geometry, both the thyroid cartilage and the hyoid bone underwent caudal displacement when tracheal traction was applied to each animal model. These findings suggest that not only are the effects of tracheal traction on the upper airway complex, but also that the hyoid bone may play a key role due to its mobility in humans and mechanical attachments to the thyroid cartilage and other airway structures.

In a study by Rowley et al. (1996), male cats were premedicated, anesthetized and laid supine for a tracheal and tongue displacement study. In this study, the theory was developed that alterations in upper airway P_{crit} may be due to changes in 1) airway wall intrinsic properties or 2) tissue pressure surrounding the flow limiting site, P_s. Rowley et al. (1996) concluded that the response in P_s to displacement of the trachea is dependent on upper airway dilation caused by tongue displacement (i.e. larger dilation saw less effect in P_s reduction than minimal change in dilation). The maximal inspiratory airflow increased through the upper airway when caudal tracheal displacement was applied. Furthermore, changes in airway wall longitudinal tension were directly associated with caudal tracheal displacement. Based on the data presented in this study, it was concluded that tracheal displacement and tongue displacement had different effects. Tracheal displacement caused airway lengthening and, thus, was influential on the transmural pressure and the luminal area within the collapsible site. On the other hand, natural radially oriented forces were influenced by tongue displacement.

In a study by Schwartz et al. (1996), cats were anesthetized, decerebrated, and ventilated in the supine position for an upper airway collapsibility study. This study was divided into two separate testing mechanisms: airway elongation and airway dilation. For airway elongation, the tracheal stump (created via transection for ventilation) was

moved caudally along with combinations of neck flexion and extension. It was found that P_{crit} decreases as airway length increases, suggesting that longitudinal forces in the wall act as a regulator (Schwartz, Rowley, Thut, Permutt, & Smith, 1996). For airway dilation, the tongue was displaced anteriorly. However, this maneuver only reduced P_{crit} after the airway underwent elongation and not by itself (Schwartz, Rowley, Thut, Permutt, & Smith, 1996). This suggests that elongation and dilation have a complex interacting mechanism.

In a study by Thut et al. (1993), male cats were premedicated, anesthetized and laid supine for a tracheal displacement and neck position study. This study concluded that collapsibility was reduced under the conditions of neck extension and airway elongation.

In two separate studies conducted by Van de Graaf (1988, 1991), mongrel dogs were anesthetized, tracheotomized, and laid supine for tracheal traction studies. These studies showed that thoracic traction has a positive impact on opposing the collapsing action of upper airway negative pressure by producing increased longitudinal tracheal tension. It is theorized that mechanical pull of mediastinal and diaphragmatic structures along with the pressure gradient between intrathroacic and extrathroacic structures produces this tracheal tension effect.

Altogether, these in vivo studies with laboratory animals suggest that longitudinal tracheal traction plays an important role in OSA pathophysiology by reducing the upper airway collapsibility.

1.3.2 Experimental Studies in Collapsible Tubes

Tracheal traction has been studied in many forms. Due to the stigma and cost of animal testing, previous studies have developed in vitro models to observe the effects of tracheal traction. Many collapsible tube-based studies have been conducted with and without longitudinal tension for a better understanding of the fluid mechanics of collapsible tubes in the human body.

In a study by Sakurai et al. (1996), longitudinal tension was applied to five different silicone-rubber tubes of varying cross-sectional areas and then the collapsibility of each tube was observed by applying flow of a sucrose solution with a concentration of 40.6%, density of 1160 kg/m^3, and kinematic viscosity of 3.66×10^{-6} m^2/s. This experiment resulted in decreased collapse and restricted tube wall movement under applied longitudinal tension in every tube tested. Additionally, the effect of lower tube compliance significantly diminished the interaction between tube deformation and flow.

In a study by Oruç et al. (2006), tubes made of silicone rubber and latex were used with varying wall thicknesses to observe the effects of flow on collapsibility. In this study, longitudinal tension was not applied. This experiment was significant as one of the first to use air as the flowing medium instead of aqueous flow. This study showed that aqueous flow in collapsible tubes has negligible fluctuations in behavior upstream when compared to downstream, whereas airflow has significant oscillating behavior upstream of the tube as well as downstream.

In a study by Marzo et al. (2005), computational modeling of viscous fluid through thin-walled and thick-walled deformable tubes was conducted, and the results were used to compare quantitative and qualitative measurements of buckling structure,

location, and flow dynamics to previous literature studies. The authors showed that although the maximal collapse displacement is the same between thick-walled and thin-walled tubes, often the point of collapse is closer to the tube center in the naturally stiffer, thick-walled tubes than in the thinner-walled tubes. In addition to the location of collapse occurring closer to the downstream end, the thinner-walled tubes also produced a secondary buckling pattern downstream. Overall, it was observed that the "location of greatest collapse and the deformed wall shape have a direct effect on the flow patterns" (Marzo, Luo, & Bertram, 2005). Regardless of wall thickness, the most collapsed section of the tube produces a significantly smaller cross-sectional area, which is indicative of higher-speed fluid flow, and, in the case of severe collapse, the flow splits into two separate jets to bypass the obstruction.

Gold and Schwartz (1996) proposed that the starling resistor model is a good model to describe airway collapse in OSA patients. This study recognizes that the simple Starling Resistor model does not resemble the exact geometry of the human upper airway, but does advocate that the pressure-flow relationships in humans are very similar to the starling resistor model. This study found that by using the simple model, prediction of pressure-flow profiles of healthy sleeping subjects' pharyngeal airway is possible. Overall, the use of collapsible tubes to model flow through the pharyngeal airway in humans introduces the parameter P_{crit} that aids in quantifying collapsibility and forecasting treatment outcomes for patients.

In a study by Chouly et al. (2008), an experimental setup involving attachment of a water-filled, deformable latex cylinder (acting as the tongue obstruction in the airway) to a rigid pipe (acting as the airway) is employed to study flow-induced collapse (Figure

6). This setup accounts for variations in patient tissue and bone structure causing different airway patency values among cases by being able to adjust the height at the location of collapse by adding or removing rounded, metallic plates to the "airway" pipe (Figure 6).

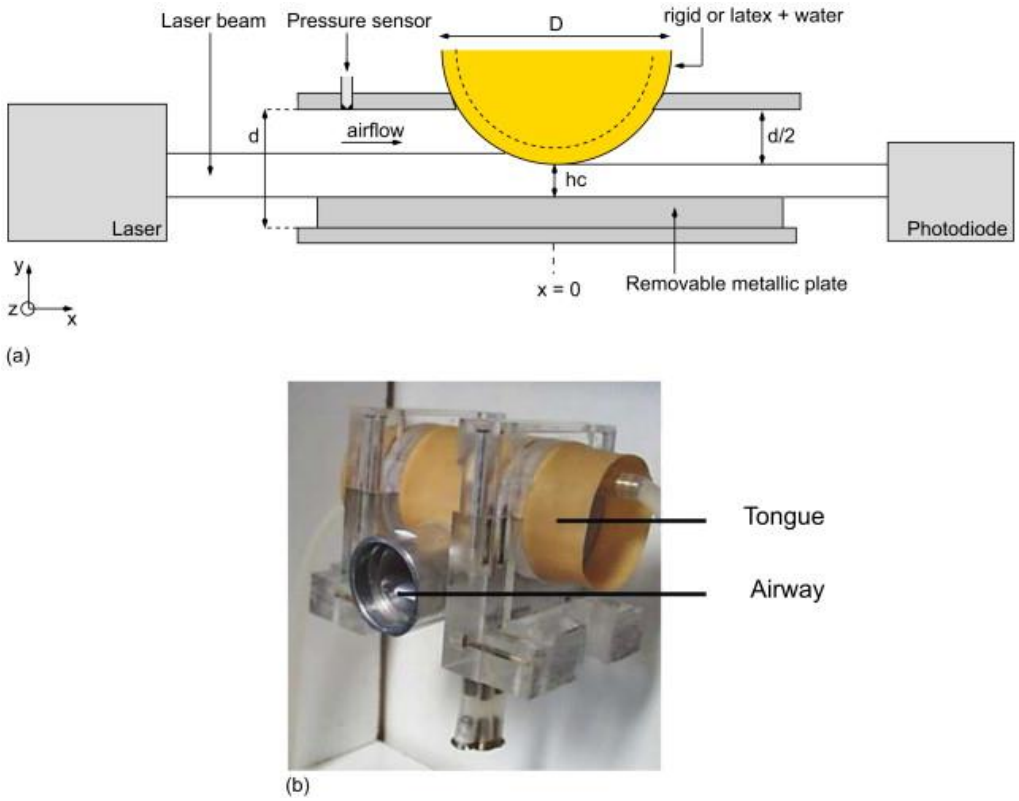

Figure 6: *Experimental setup studied by Chouly et al. (2008). (a) schematic and (b) photograph.*

Results from the study by Chouly et al. (2008) show that movement of the soft palate and the tongue posteriorly play a major role in collapse. However, it is also noted that the pharyngeal walls on either side of the airway are also involved in the collapsing mechanism. Thus, this study advocates further 3D modeling and validation. Furthermore, since this study modeled only uni-directional flow, the authors state that experiments utilizing complete breathing cycles in collapsible tube models could be

pivotal in developing the complete spectrum of anatomical and biomechanical properties that correspond to healthy patients and pathological cases.

Kozlovsky et al. (2014) conducted computer simulations to quantify the area-pressure curve of collapsible tubes and its dependence on wall thickness. An in vitro model using silicone rubber tubes was used to validate computational results by measuring the shape of 2D sections after the tube collapsed. The tubes were filled with water and mounted inside a water-filled tank. This study investigated tube collapsibility due to a transmural pressure gradient alone in the absence of fluid flow (i.e. flowrate was zero). The geometry and behavior demonstrated by Figure 7 shows the pattern of collapse that all tubes underwent in this study.

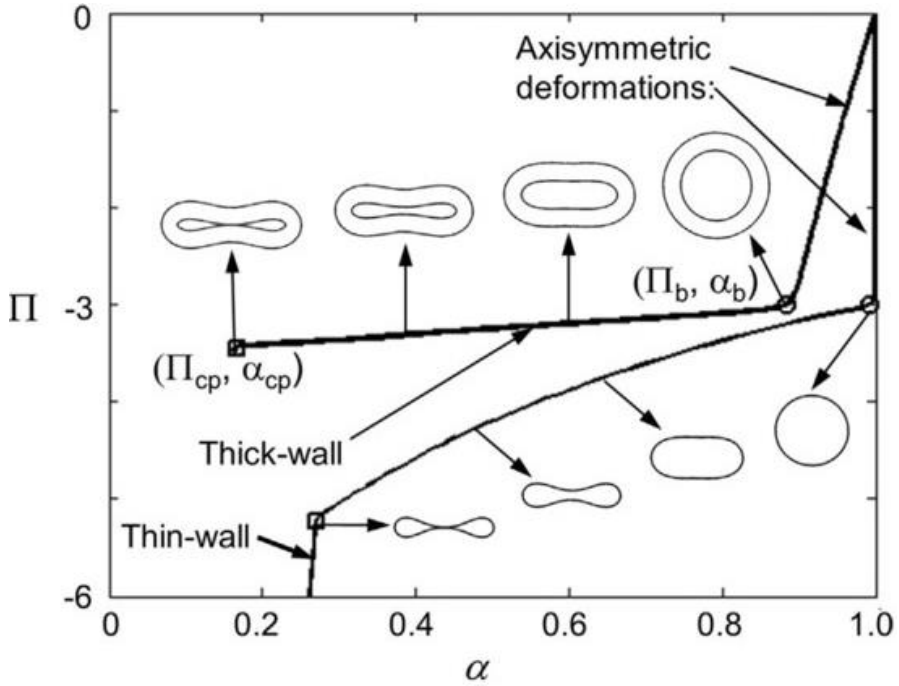

Figure 7: *Pressure-area curves of thin-walled and thick-walled collapsible tubes. Typical non-dimensional pressure-area curves for collapsible tubes with thin (thin line) and thick (thick line) walls. The Buckling point (circle), contact point (square), and tube geometry are marked on the curves. The non-dimensional pressure ($\Pi = P_{TM}/K_P$) is a function of non-dimensional area ($\alpha = A/A_o$), where P_{TM} = transmural pressure, K_p = flexural rigidity of the tube, A = tube cross-sectional area, and A_o = original cross-sectional area. Reproduced from Kozlovsky et al. (2014).*

As seen in Figure 7, when the transmural pressure becomes increasingly more negative the tube cross-section begins to experience small, axisymmetric deformations. As the transmural pressure overcomes the buckling pressure (P_B), the cross-section of the tube rapidly flattens out into an elliptical shape and eventually becomes compressed enough that the opposing walls contact each other (contact point = Π_{cp}, α_{cp}). Unlike in human airways, the collapsible tube segment does not become fully occluded (Shapiro, 1977). After the contact point, the tube stiffens so that an infinitely negative pressure would be required to completely occlude the tube. Therefore, the contact point seen in collapsible tubes has often been considered an equivalent point to full occlusion in the human airway. However, this analogy is imperfect, and therefore, we must distinguish pressures associated with the contact point (P_{CP}) and with full occlusion (P_{close}).

Another factor of importance in studying collapsible tubes with relation to the human upper airway is compliance. Compliance (C) is defined as the slope of a given pressure-area curve, or the change in pharyngeal area (ΔA) for a given change in pressure (ΔP) (Brown, Bradley, Phillipson, Zamel, & Hoffstein, 1985) (**Equation 2**).

Equation 2: *Tube Compliance* $$\boldsymbol{C = \frac{\Delta A}{\Delta P}}$$

Table 1 shows the values of tube compliance in previous in vitro studies compared to human soft tissue compliance. In Table 1, Amatoury et al. (2010) has a compliance similar to OSA patients noted by Isono et al. (1993), but most other studies utilize tubes that are considerably stiffer and less compliant.

For the studies that did not list tube compliance explicitly, a value was calculated based on the area-pressure relationships reported. For those studies, compliance was calculated within the post-buckling region that was bounded by the buckling point and the contact point of each tube (i.e. area and pressure values were used after tube buckling but before opposite wall contact.).

Table 1: *Comparison of in vitro starling resistor model compliance with airway compliance in healthy humans and patients with OSA.*
γ = tube wall thickness-to-internal radius ratio.

STARLING RESISTOR MODEL STUDIES			
MATERIAL	TUBE COMPLIANCE	MEDIUM	REFERENCE
Penrose tube	At γ = 0.029 0.40 cm^2/cmH_2O	Air	Amatoury et al. (2010)
Silicone rubber tubes	At γ = 0.348 0.017 cm^2/cmH_2O	Aqueous Solution	Bertram (1987)
Silicone rubber tubes	At γ = 0.167 0.026 cm^2/cmH_2O	Aqueous Solution (70% Glycerin, 30% H_2O)	Bertram & Tscherry (2006)
Latex tubes	At γ = 0.019 0.141 cm^2/cmH_2O At γ = 0.036 0.043 cm^2/cmH_2O At γ = 0.211 0.011 cm^2/cmH_2O	No Flow	Dion et al. (1995)
Silicone rubber tubes	At γ = 0.01 293.950 cm^2/cmH_2O At γ = 0.24 0.101 cm^2/cmH_2O At γ = 0.333 0.023 cm^2/cmH_2O	No Flow	Kozlovsky et al. (2014)
Silicone rubber tubes	At γ = 0.07 0.196 cm^2/cmH_2O	Sucrose Solution	Sakurai et al. (1996)
Latex tubes	At γ = 0.15 to 0.22 0.00035 to 0.00067 cm^2/cmH_2O	Blood Analogue (33% glycerol, 67% H_2O)	Walker et al. (1999)
HUMAN PHARYNX STUDIES			
MATERIAL	PHARYNGEAL COMPLIANCE	SLEEP / AWAKE	REFERENCE
OSA patients	0.64 ± 0.49 cm^2/cmH_2O	Sleeping	Isono et al. (1993)
Healthy Subjects and OSA patients	Control Group ♂: 0.166 ± 0.002 cm^2/cmH_2O OSA Group ♂: 0.395 ± 0.060 cm^2/cmH_2O	Sleeping	Brown et al. (2015)
Healthy Subjects	Young ♂: 0.083 ± 0.005 cm^2/cmH_2O Young ♀: 0.057 ± 0.005 cm^2/cmH_2O Middle-aged ♂: 0.096 ± 0.007 cm^2/cmH_2O Middle-aged ♀: 0.078 ± 0.006 cm^2/cmH_2O Elderly ♂: 0.104 ± 0.007 cm^2/cmH_2O Elderly ♀: 0.060 ± 0.009 cm^2/cmH_2O	Awake	Huang et al. (1998)

CHAPTER 2: MATERIALS AND METHODS

2.1 INTRODUCTION

The purpose of this study was to quantify the differences in the collapsibility of silicone tubes with and without longitudinal stretching subjected to cyclic bidirectional airflow. The silicone tubes were fabricated to match the airway compliance of patients with obstructive sleep apnea. Adequate airway patency is critical to preventing OSA, and increased airway compliance is the primary determinant of airway collapse during sleep in these patients. Our goal was to quantify the tube collapsibility as a function of tube geometry (tube diameter, length, and wall thickness) and longitudinal stretching. Improved understanding of how longitudinal stretching reduces collapsibility will improve our understanding of OSA pathophysiology and may potentially suggest surgical procedures to reduce airway collapsibility in OSA patients.

2.2 FABRICATION OF COLLAPSIBLE TUBES

Twenty-seven silicone rubber tubes were fabricated and tested in this experiment. Tubes were placed into three experimental groups: varied length (n = 9), varied wall thickness (n = 9), and varied diameter (n = 9). Tube fabrication processes were slightly different between all groups, but maintained the same general procedure. The silicone components were measured and mixed, poured into the mold, allowed to cure for at least 24 hours before removal, and then allowed at least two weeks to completely cure before testing. Pressure, displacement, and flow were measured on each tube tested.

The XP-696 silicone rubber (Silicones, Inc., High Point, NC) is a two-component system (activator + base) that cures at room temperature due to a platinum-catalyzed addition reaction (Figure 8). This material has a high durometer (i.e. high resistance to indentation), high elongation (i.e. high amount of extension under stress), good chemical resistance, exceptional release from molding structure, and is less prone to inhibition when interfaced with 3D printed parts.

The use of 3D printing technology to make molds for uncured silicone rubber is our strategy to create patient-specific collapsible models in future studies. However, certain silicone rubber material can be inhibited during the curing process due to support material residue left on the 3D printed molds. Therefore, the XP-696 material was chosen after comparing its performance with other silicone materials. This platinum-cured silicone was specifically developed to decrease inhibition issues, especially when working with 3D printed parts.

Known silicone properties are listed in Table 2 and Table 3.

Table 2: *Material properties of the uncatalyzed XP-696 Silicone Rubber.*

Uncatalyzed Compound Properties	
Color	Activator (A) = Red Base (B) = Translucent
Mixing Ratio (B/A)	By Weight: 10/1
Viscosity (cps)	Mixed: 25,000
Working Time	35 minutes ± 5 minutes
Cure Time	4-6 hours
Shelf Life	6 months

Table 3: *Material properties of the vulcanized (cured) XP-696 Silicone Rubber.*

Vulcanized Silicone Properties	
Shore A Hardness (±4)	23
Tear Resistance	110 ± 20 ppi
Tensile Strength	450 ± 50 psi
Elongation	425 ± 50%
Shrinkage	Nil
Specific Gravity	1.08

Before official experiments began, two separate tubes were used in a series of identical trials to check that results were reproducible and consistent weeks and months after fabrication. These preliminary experiments demonstrated that material properties were not changing over time.

2.2.1 Fabrication Procedure – Step-by-Step Instructions

All experimental procedures took place in the Biomedical Engineering Lab (BSL-2) at the Medical College of Wisconsin (Milwaukee, WI). Fabrication procedures were conducted in a conventional laboratory setting using aseptic techniques that met local safety guidelines.

Wearing the appropriate personal protective equipment (PPE) (e.g. gloves and eyewear), start the fabrication procedure by mixing 10 parts by weight 696 Base with 1 part by weight 696 Activator in a container that can hold approximately 3 to 4 times the volume being used.

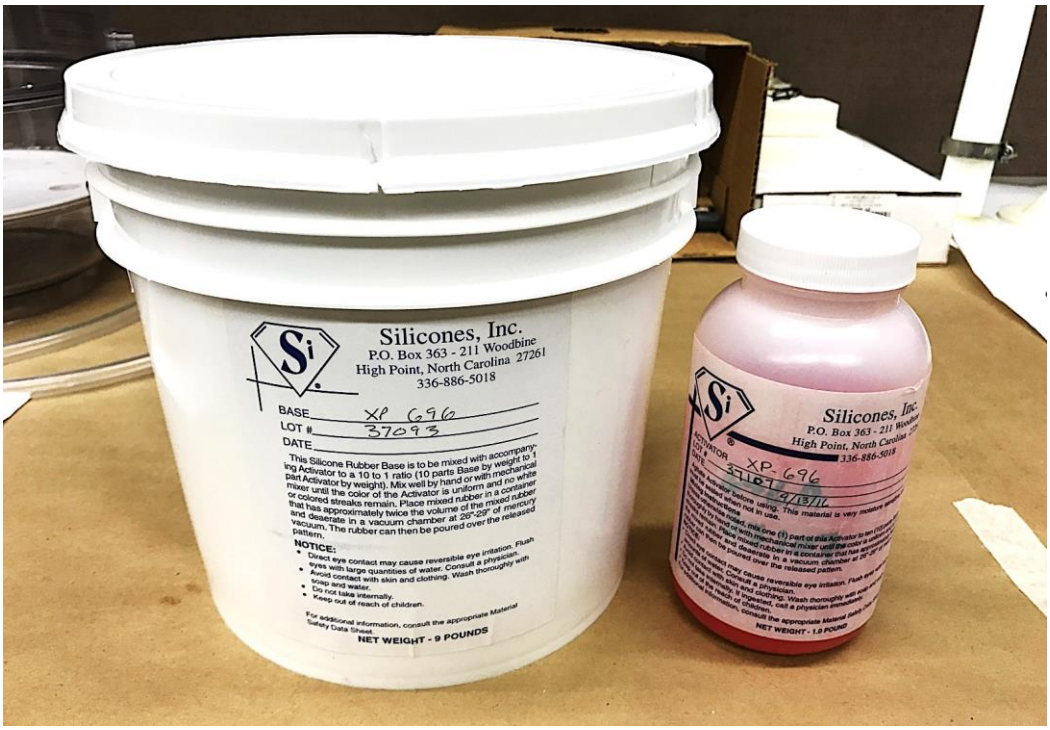

Figure 8: *XP-696 Silicone Rubber base (left) and activator (right).*

Stir the measured mixture thoroughly; making sure uniform color is apparent. To remove all air bubbles, immediately after mixing place the material in a vacuum chamber capable of at least 28 inHg vacuum pressure (Figure 9). The material will expand to double or triple its original volume and then collapse. Maintain vacuum for at least an additional 2 to 3 minutes for complete removal of air bubbles, and then remove the silicone from the vacuum chamber.

Figure 9: *Vacuum chamber (Bel-Art Scienceware Desiccator) used to remove air bubbles after mixing the silicone base and activator.*

Using caution, pour the mixed silicone into the desired mold (Figure 10). Keep in mind that inhibition can occur in the presence of some 3D printed support materials or if the 3D printed part is not cleaned appropriately, which may affect curing time and quality of final model. Additionally, if silicone specimen release is a problem post-cure, then use of a release silicone (e.g. Silicones, Inc. MR-15 Release Silicone) may be beneficial. In this study, the release silicone was applied to the 3D printed mold with a cotton swab and allowed 30 minutes to dry before pouring the XP-696 silicone rubber into the mold. It should be noted that the mold must be cleaned thoroughly with soap and water and dried prior to applying the MR-15 release silicone.

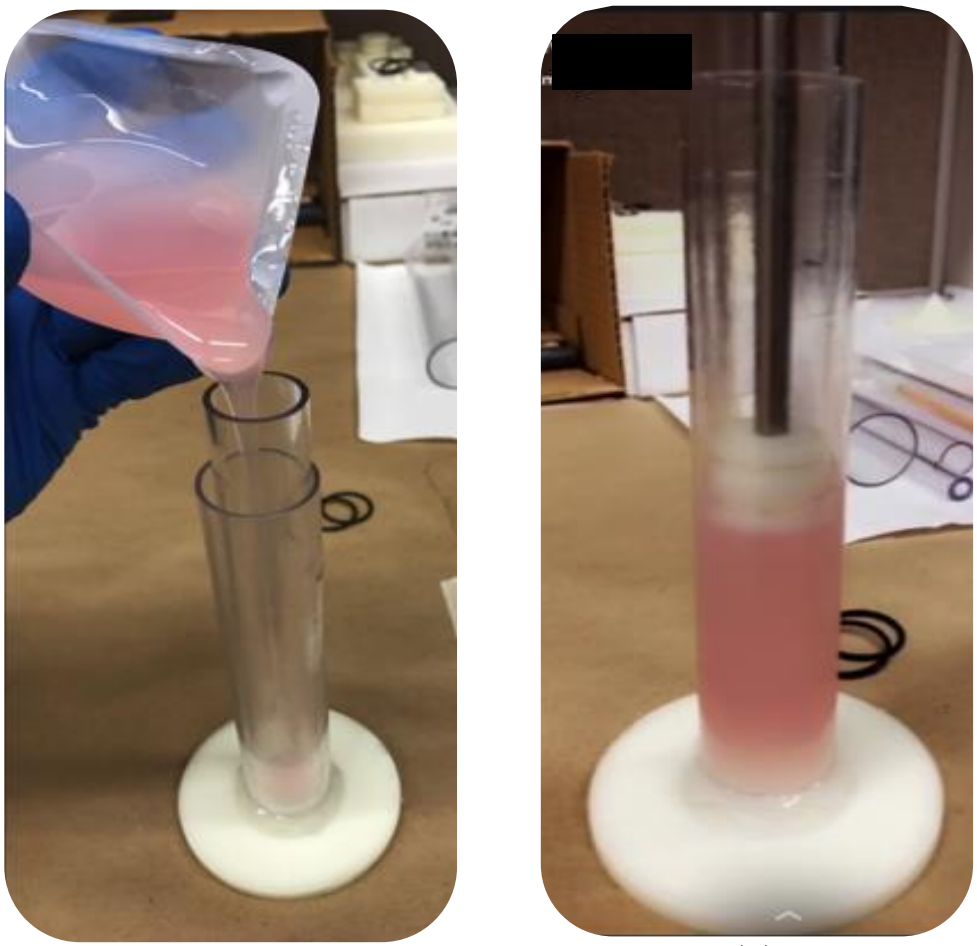

(A) (B)

Figure 10: *Molding process of silicone rubber tubes.*
(A) Pouring silicone into center of mold. (B) Pushing silicone with a piston to force it into the narrow space between inner and outer tubes.

A piston was 3D printed to act as a plunging system to move the poured silicone into the gap between the inner and outer tubes by driving it down the center of the inner tube and up the gap between the inner and outer tubes (Figure 10B). With great care, the piston was placed into the opening of the center tube at which the silicone was poured (Figure 10A). Using a rod, the piston was gently pushed down the center to force the silicone into the gap between the inner and outer tubes (Figure 10B).

Once the desired amount of silicone was pushed into the gap, the system was secured and O-rings were placed at the top edge of the gap. This O-ring keeps the inner and outer tubes concentric and will ensure a uniform wall thickness.

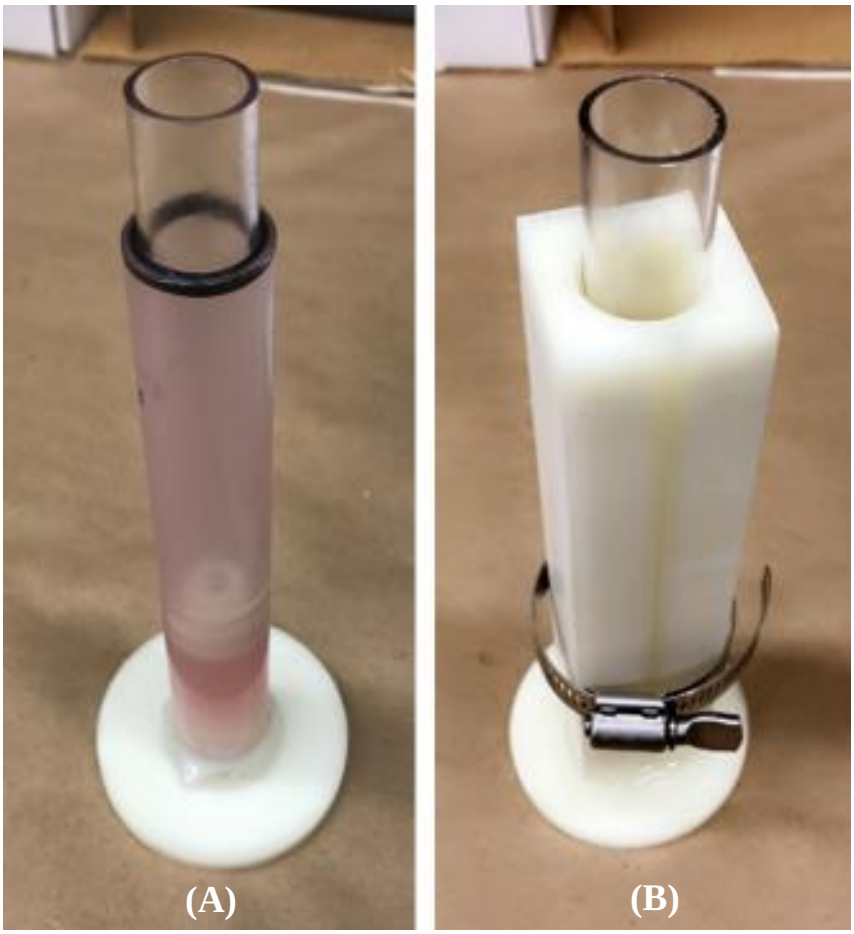

Figure 11: *Variations of silicone mold setup.*
(A) Mold created with off-the-shelf plastic tubes. (B) Mold created with 3D printed parts and an off-the-shelf plastic tube.

Curing takes approximately 24 hours. After curing, to remove the silicone tube, disconnect the mold from its base and use a needle bottle to flush soapy water in between the silicone and the molding walls. The soapy water reduces friction and prevents tearing of the cured silicone.

2.3 Mechanical Properties of the Silicone Material XP-696

Experiments were performed to determine the Young's Modulus and the Poisson's Ratio of the two silicone rubber materials (XP-696 & P-90) that were initially tested. These experiments were conducted in Marquette University's Biomechanics Lab (Engineering Hall, Room 318) using their equipment and safety guidelines. The mechanical properties were tested using a MTS Criterion™ Universal Testing System (MTS Systems Corporation; Eden Prairie, MN) set up for tensile loading at 5 mm/second.

The mechanical tests were performed on test specimens fabricated using the methods described above, except that the test specimens had a flat dumbbell shape (a total length of 6", thickness of ¼", and 2" width ends with a 1" length from the end of the sample to the beginning of the curve inward; the middle region curves down to a 1" width; at least 3" of the middle section is 1" in width). Some of the test specimens used in the mechanical tests are shown in Figure 12.

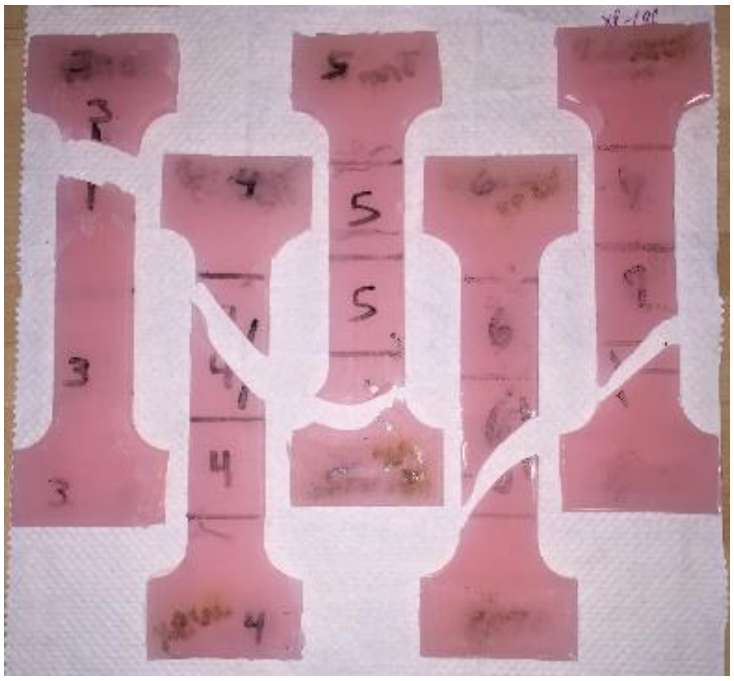

Figure 12: *Silicone rubber specimens used in tensile testing.*

Figure 13 and Figure 14 illustrate how the Young's Modulus and the Poisson's Ratio were calculated from the data collected in the tensile load testing. The Young's Modulus (E) was calculated by plotting the tensile stress (σ) as a function of the strain (ε) and fitting the data (for strain ε < 0.6) with Equation 3.

Equation 3: *Stress — Strain Relationship* $\boldsymbol{\sigma = \mathbf{E} * \boldsymbol{\varepsilon}}$

The Young's Modulus values obtained by applying the discussed approach, for all specimens tested, are listed in Table 4 and Table 5.

Both the P-90 and XP-696 silicone rubber withstand large deformations under tensile loading, hence, the calculations of the Poisson's ratio, υ, in terms of true strain definition is utilized here as,

Equation 4: *Poisson's Ratio* $$\boldsymbol{\upsilon = -\frac{d\epsilon_{Trans}}{d\epsilon_{Axial}}}$$

where ϵ_{Axial} and ϵ_{Trans} are the axial and transverse strains respectively and d represents the small variations in the related quantities. For the axial tensile loading applied to the test specimens in this study with length, L, in the axial direction and width, D, in the transverse direction, the above equation can be extended to,

Equation 5: $$\boldsymbol{-\upsilon \int_{L_o}^{L_o+\Delta L} d\epsilon_L = \int_{D_o}^{D_o+\Delta D} d\epsilon_D}$$

In the above equation, ΔL and ΔD are the changes in the length and width of the test specimen and ϵ_L and ϵ_D are the strains in the axial (length) and transverse (width) directions, respectively. Other forms of the above equation can also be obtained through applying simple mathematical operations,

Equation 6:

$$-\boldsymbol{v}\int_{L_o}^{L_o+\Delta L}\frac{dx}{x}=\int_{D_o}^{D_o+\Delta D}\frac{dy}{y}$$

$$-\boldsymbol{v}[\boldsymbol{ln}\,\boldsymbol{x}]_{L_o}^{L_o+\Delta L}=[\boldsymbol{ln}\,\boldsymbol{y}]_{D_o}^{D_o+\Delta D}$$

$$-\boldsymbol{v}\left[\boldsymbol{ln}\frac{(L_o+\Delta L)}{L_o}\right]=\left[\boldsymbol{ln}\frac{(D_o+\Delta D)}{D_o}\right]$$

$$-\boldsymbol{v}\,\boldsymbol{ln}\left(\mathbf{1}+\frac{\Delta L}{L_o}\right)=\boldsymbol{ln}\left(\mathbf{1}+\frac{\Delta D}{D_o}\right)$$

$$\frac{\Delta D}{D_o}+\mathbf{1}=\left(\frac{\Delta L}{L_o}+\mathbf{1}\right)^{-\boldsymbol{v}}$$

and

Equation 7:

$$\boldsymbol{v}=-\frac{\boldsymbol{ln}\left(\frac{\Delta D}{D_o}+\mathbf{1}\right)}{\boldsymbol{ln}\left(\frac{\Delta L}{L_o}+\mathbf{1}\right)}$$

Equation 7 implies that the Poisson's ratio for the silicone used in this study can be simply determined by finding the slope of the curve obtained by plotting $ln(\frac{\Delta L}{L_o}+1)$ vs. $ln(\frac{\Delta D}{D_o}+1)$ (Figure 14). The Poisson's ratio values obtained by applying the discussed approach, for all specimens tested in the Biomechanics Lab at Marquette University, are listed in Table 4 and Table 5.

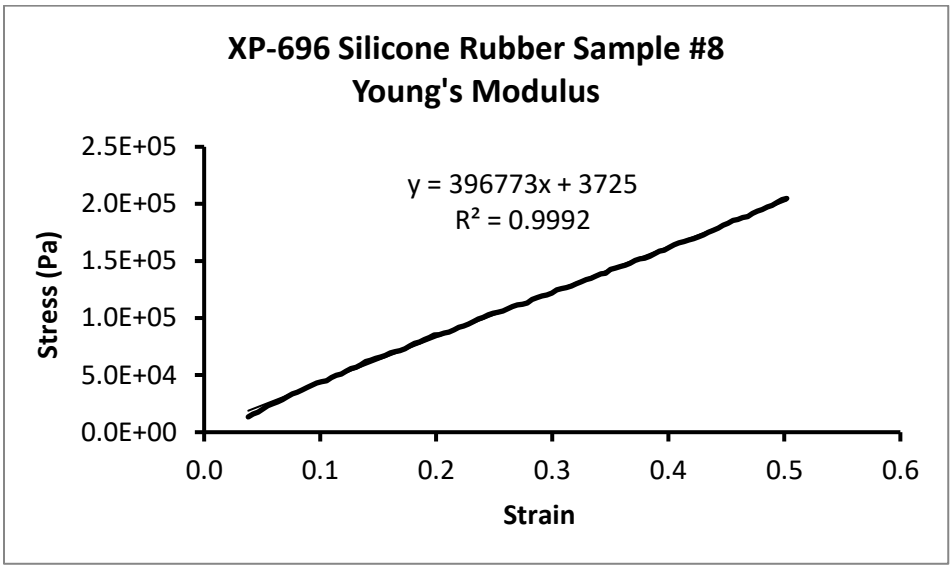

Figure 13: *Young's modulus calculation of sample #8 using XP-696 Silicone Rubber.*

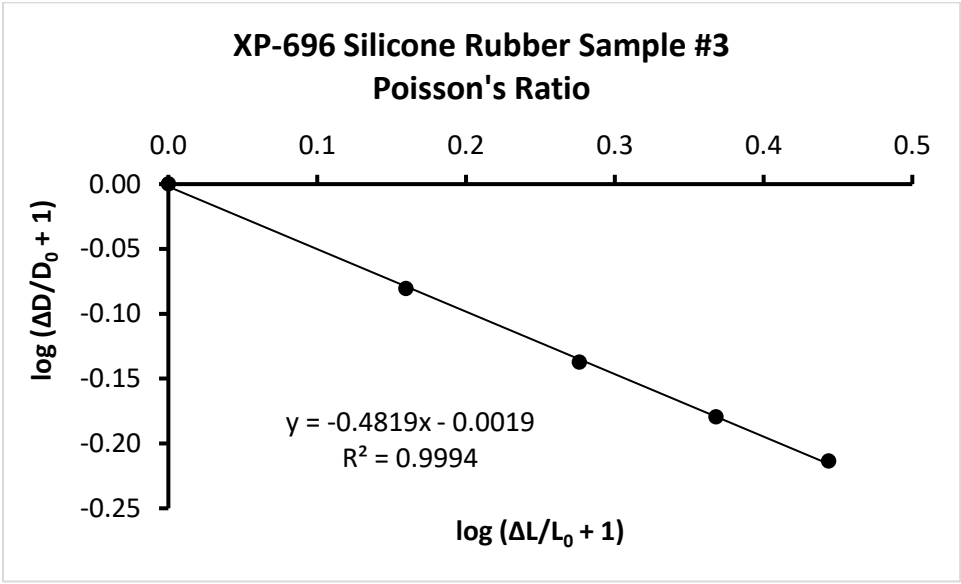

Figure 14: *Poisson's ratio calculation of sample #3 using XP-696 Silicone Rubber.*

Table 4: *Young's modulus and Poisson's ratio values of XP-696 (Fast Cure) Silicone Rubber (Silicones, Inc., High Point, NC).*

XP-696 Silicone Rubber			
SAMPLE	**Young's Modulus (MPa)**	SAMPLE	**Poisson's Ratio**
#8	0.397	#3	0.482
#9	0.344	#4	0.471
#10	0.382	#5	0.496
#11	0.327	#6	0.514
#12	0.355	#7	0.494
AVERAGE	**0.361**	**AVERAGE**	**0.491**
STD	**0.028**	**STD**	**0.016**

Table 5: *Young's modulus and Poisson's ratio of the P-90 (slow cure) Silicone Rubber (Silicones, Inc., High Point, NC).*

P-90 Silicone Rubber			
SAMPLE	**Young's Modulus (MPa)**	SAMPLE	**Poisson's Ratio**
#3	0.290	#3	0.504
#5	0.304	#4	0.520
#7	0.307	#5	0.504
#8	0.285	#6	0.506
#9	0.311	#7	0.504
#10	0.311	-	-
#11	0.332	-	-
#12	0.326	-	-
AVERAGE	**0.308**	**AVERAGE**	**0.507**
STD	**0.016**	**STD**	**0.007**

The P-90 silicone was dropped from the study shortly after mechanical testing because it took much longer to cure than the XP-696 silicone, and it reacted with 3D printed parts, resulting in an unstable curing process in the mold.

Importantly, the young's modulus of the XP-696 silicone selected for this study is approximately 1 order of magnitude lower than in previous studies on collapsible tubes (Table 6), which allowed us to observe tube collapse at pressure gradients similar to those experienced by the human airway (0-10 cmH_2O).

Table 6: *Comparison of XP-696 silicone rubber in this study with other materials used in the literature on collapsible tubes.*

MATERIAL	GEOMETRY	YOUNG'S MODULUS	STRAIN	MEDIUM	MAX FLOWRATE (@ FLOW LIMITATION)	REFERENCE
XP-696 silicone rubber	L: 75-125mm D: 12.7-31.75mm H: 0.98-2.22mm	0.361 ± 0.028 MPa	0.5cm (4 to 6.66 %)	Air	Could not Characterize Flow Limitation	This study
Penrose tube	L: 80mm D: 16mm H: 0.23mm	1.5 to 3.5 MPa	0 to 62.5%	Air	150 to 300 mL/s	Amatoury et al. (2010)
Silicone rubber	L: 230mm D: 12.7mm	3.8 to 4.0 MPa	0.7 to 12%	Water	-	Bertram (1987)
Silicone rubber	L: 728mm D: 12.0mm H: 1.0mm	Not given	N/A	70% Glycerin 30% H_2O	42 to 65 mL/s	Bertram & Tscherry (2006)
Thin Latex tube filled with water	D: 49mm H: 0.3mm	1.68 MPa	N/A	Air	-	Chouly et al. (2008)
Latex rubber tube	L: 1100mm D: 25.4mm H: 0.86mm	Not given	Conducted but values not given	Glycerin/ Water Mix	- (steady, supercritical flow)	Kececioglu et al. (1981)
Silicone rubber filled with water	L: At least 10x's longer than D_{OUT} D_{IN}: 18-25mm H: 3mm	2.4 to 4.0 MPa	N/A	N/A	No-Flow Experiments	Kozlovsky et al. (2014)
Penrose tube OR Silicone Rubber	Penrose D: 25.4mm H: 0.55mm Silicone Rubber D: 25.4mm H: 1-3mm	Not given	N/A	Air	- (constant flow)	Oruc et al. (2007)
Thin-walled silicone rubber	L: 160mm D: 5.70-8.00mm H: 0.20-0.30mm	Not given	0 to 100%	Sucrose Solution	N/A (cyclic flow)	Sakurai et al. (1996)

For additional comparison, the young's modulus of the XP-696 silicone selected for this study was compared to the young's modulus estimated or assumed in previous studies of upper airway collapse (Table 7), which allowed us to understand the difference in material properties and guide our decision making process in choosing tube geometry for our in vitro experiments.

Table 7: *Comparison of Young's Modulus of the XP-696 silicone rubber used in this study with the Young's Modulus of the human airway estimated or assumed in previous studies of upper airway collapse.*

MATERIAL	EXPERIMENT TYPE	YOUNG'S MODULUS	REFERENCE
XP-696 silicone rubber	In vitro (benchtop)	0.361 ± 0.028 MPa	This study
Human soft palate	FEA model	At hard palate: 100.64 kPa At uvula: 0.51 kPa	Berry et al. (1999)
Human soft palate	FSI model	1.0×10^6 Pa	Sun et al. (2007)
Human soft palate	FSI model	7539 Pa	Zhu et al. (2012)
Muscle	FSI model	Soft Palate: 0.025 MPa Bilateral palatal muscles: 0.98 MPa	Wang et al. (2012)
Human Tissue	FEM model	Soft tissue: 1.00×10^4 Pa Nasopharynx: 1.37×10^{10} Pa Epiglottis cartilages: 2.02×10^6 Pa Tracheal cartilage: 2.02×10^6 Pa	Huang et al. (2013)
Human upper airway tissue	FSI model	7.54 kPa	Zhao et al. (2013)
3D Stereolithography (SLA) – Human upper airway	In vitro (benchtop)	325 kPa	
Human soft palate	Ex vivo (cadavers)	Range from Uvula to Hard Palate: 585 Pa – 1410 Pa	Birch & Srodon (2009)

2.4 GEOMETRY OF THE COLLAPSIBLE TUBES

Three (n=3) tubes were tested for each tube geometry (Table 8 and Figure 15) to account for variations in the fabrication process. The standard tube dimensions chosen were 10cm in length, 22.22mm in diameter, and 1.60mm in wall thickness (Table 8). Tube dimension variances tested were then above and below this standard tube dimension for each given study (Figure 15).

Table 8: *Dimensions (length, diameter, and wall thickness) of the silicone rubber tubes fabricated for this study.*

	# tubes	Length (cm)	Diameter (mm)	Wall thickness (mm)
Tube length study	n = 3	7.5	22.22	1.60
	n = 3	10.0	22.22	1.60
	n = 3	12.5	22.22	1.60
Tube diameter study	n = 3	10.0	12.70	1.60
	n = 3	10.0	22.22	1.60
	n = 3	10.0	31.75	1.60
Wall thickness study	n = 3	10.0	22.22	0.80
	n = 3	10.0	22.22	1.60
	n = 3	10.0	22.22	2.40

Figure 15: *Comparisons of each tube geometry (length, diameter, and wall thickness). (★) Indicates the standard dimension tube (L = 10cm, D = 22.22mm, W = 1.60mm) for easier comparison with the varied dimensions in each study.*

The considerations for selecting these specific geometries to study were 2-fold: known physiological values (Table 9) and current model material properties (Table 7). More specifically, the range of lengths and diameters of our silicone tubes (Table 8) overlap with the length and diameter of the human pharynx (Table 9). However, our silicone tubes had a much smaller wall thickness (0.8 to 2.4mm) than the wall thickness of the human pharynx (20 to 40mm, Table 9). To match the compliance of the human upper airway (Table 1), we had to study tubes with relatively thin walls because the young's modulus of the current study's silicone rubber (0.361 MPa) was much higher

than the young's modulus of the soft tissues surrounding the human pharynx (~0.001 MPa) (Table 7).

Table 9: *Comparison of the geometrical dimensions used in this study with the dimensions of the human airway.*

	Standard Dimension (current study)	Measured Physiological Value (human measurements)	Reference
Airway Length	L = 100mm	♂ Airway Length[1]: 62 – 84mm ♀ Airway Length[1]: 42 – 78mm	Malhotra et al. (2002)
Airway Diameter	D = 22.22mm	Minimum Diameter[2]: 8.54mm Maximum Diameter[2]: 22.07mm	Van Holsbeke et al. (2014)
		Control Patients[3]: 26.22mm OSA Patients[3]: 22.85mm	Bradley et al. (1986)
Airway Wall Thickness	W = 1.60mm	Normal Patients[4]: 27.6 ± 7.1mm Mild Apnea[4]: 35.2 ± 6.8mm Apneic Patients[4]: 33.0 ± 8.7mm	Schwab et al. (1995)

[1] *Length measured from hard palate to base of epiglottis.*
[2] *Minimum Diameter: Minimal CSA measured between top boundary of hard palate and the end of the uvula to bottom boundary of epiglottis and the larynx.*
Maximum Diameter: Region between epiglottis and larynx.
[3] *Control Patients: Average CSA of 9 subjects at functional residual capacity.*
OSA Patients: Average CSA of 10 subjects at functional residual capacity.
[4] *All cases were measured as lateral pharyngeal wall thickness.*

The amount of longitudinal stretch of 0.5cm was chosen because of the past strain percentages seen by previous airway studies in collapsible tubes and airway muscle models. Amatoury et al. (2010) conducted experiments in Penrose tubing with strain ranges from 0-60% of the original length, but it is speculated that beyond 25% strain the model underwent plastic deformation. Fredberg et al. (1997) conducted experiments in bovine trachea muscle with strain ranges from 0-8% of the original length. Kairaitis et al. (2012) studied pharyngeal stretch by applying average stretch of 7mm (ΔL) in rabbits, where the original pharyngeal length of rabbits is approximated to be 42mm (L_o)

(Amatoury J. , Kairaitis, Wheatley, Bilston, & Amis, 2015). Therefore, the strain seen in the rabbit model is calculated by taking ΔL and dividing by the original length, L_o:

$$\frac{7}{42} \approx 17\%$$

Because every tube tested in the current study was subjected to a longitudinal stretch of 0.5cm, the strain values were as follows: 6.66% at L = 7.5cm, 5.00% at L = 10cm, and 4.00% at L = 12.5cm. Therefore, although there is potential for future studies to be conducted at higher strain values, the longitudinal strain conducted in the current study was within the ranges seen in previous literature.

A large quantity of tubes was fabricated for each variable being tested. However, many tubes were deemed unacceptable post-fabrication because their wall thickness was not uniform or small air pockets had formed in the catalyzed product (Figure 16). Those tubes were not used and thrown out of the study due to inhomogeneous character.

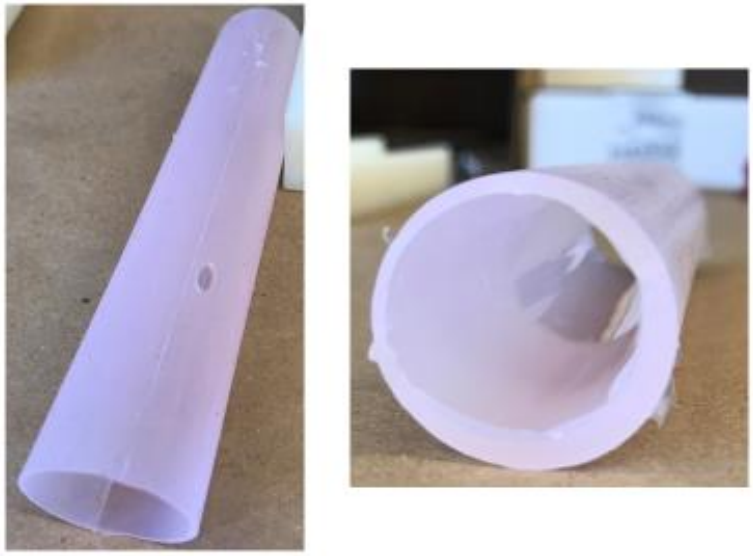

Figure 16: *Examples of tubes that were thrown out of this study. (Left) Air pocket formation. (Right) Severe wall thickness inhomogeneity.*

2.5 EXPERIMENTAL SETUP

The experimental setup is illustrated in Figure 17 and Figure 18. A cyclic air pump (Harvard Apparatus, Model #607) was used to reproduce cyclic breathing (inspiration and expiration) with airflow rates (Q = [0, 250] mL/s) and frequency (20 cycles/min) in the same range of breathing in adult humans (Benchetrit, 2000). This pump was attached to a flexible hose with two pressure relief valves for safety measures in case the flow of air becomes blocked by unforeseen deterrents. The flexible hose is then attached to a rigid tube that is mounted on a custom-fabricated, rigid scaffold for stability. At the center of this scaffold is a gap where the XP-696 silicone rubber collapsible tube specimen is placed. Approximately 1 inch away from the gap on either end is a pressure transducer (Omega, Model #PX409-015GUSBH), which monitors the pressure upstream and downstream of the collapsible tube. On the downstream rigid tube segment, a small hole was drilled so that a pressure catheter (Millar, Mikro-Cath™ Diagnostic Pressure Catheter) could be introduced into the tubing system housing the flow. Before each test and after each collapsible tubing specimen was secured, the pressure catheter was guided to the center of the collapsible tube specimen in order to record pressure at the flow-limiting site. Directly above the collapsible tube specimen is a laser line scanner used for displacement measurements (Micro-Epsilon, Model #2600-100). At the far upstream end of the scaffold, the rigid tubing converts into a short, flexible rubber tubing segment that connects to a flowmeter (TSI Inc., Model #4045 G), which is open to the atmosphere. All aforementioned sensors are connected to a laptop via USB hub or a data acquisition system.

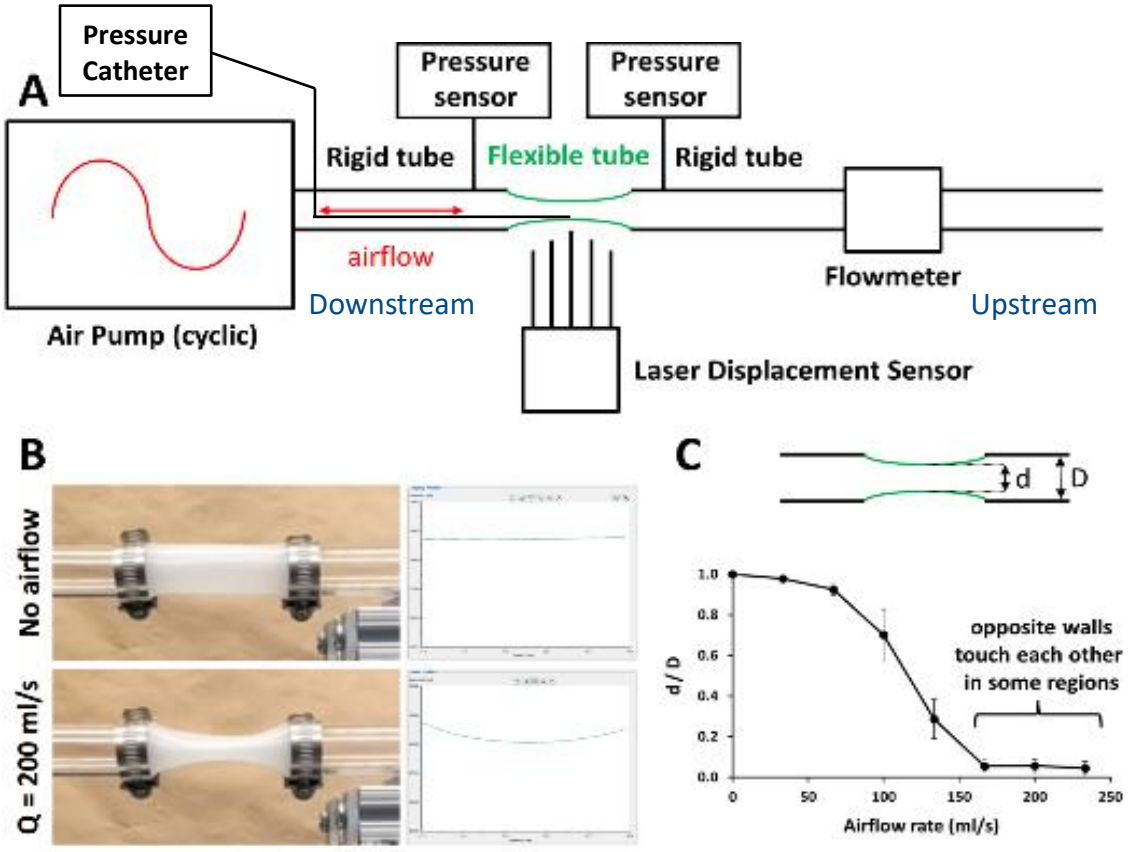

Figure 17: *Experimental setup design and examples.*
A) Diagram of experimental setup. B) Example of tube collapse and displacement measured with the laser line scanner. C) Example of collapsibility curve.

The ratio (d/D) of the minimal internal diameter (d) during a breathing cycle to the tube internal diameter with zero flow (D) is plotted against the mean airflow rate during the inspiratory phase of the breathing cycle (Figure 17C).

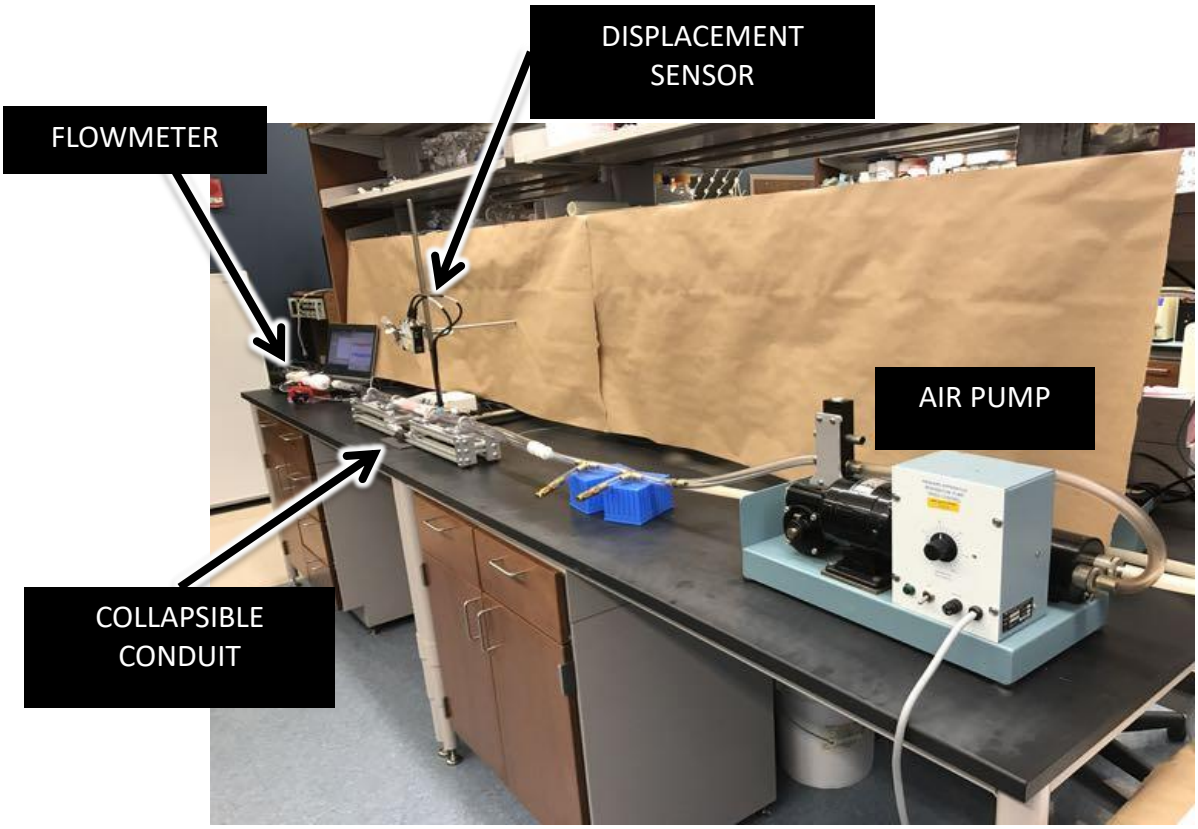

Figure 18: *Experimental setup.*
The air pump produces bidirectional, cyclic airflow through piston action. The air is forced out the back to a flexible tubing that folds over the top of the air pump and connects to the tubing in line with the collapsible tube. Pressure relief valves are directly upstream of pump to ensure pressure relief safety and mitigation of pump damage in case the flow of air is completely blocked during the experiment. The laser line displacement sensor is situated directly above the collapsible tube with a vertical distance of approximately 1 foot away from the tube. The flowmeter is at the opposite end of the air pump (upstream) and marks the end of the tubing system.

The equipment used in the experimental setup is listed in Table 10.

Table 10: *Equipment used in the experimental setup.*

Item	Company	Model #	Resolution
Air Pump	Harvard Apparatus	607	N/A
Pressure Relief Valves	McMaster Carr	N/A	N/A
High Speed USB Output Pressure Transducer	Omega	PX409-015GUSBH	Up to 1000 Hz
Mikro-Cath™ Diagnostic Pressure Catheter	Millar	825-0101	Flat to ~10kHz (Limited by PCU to 1 kHz)
Pressure Control Unit (PCU) with Patient Isolation	Millar	PCU-2000	1000 Hz
Laser Line Scanner – Compact Class	Micro-Epsilon	scanCONTROL 2600-100	Up to 300 Hz
Mass Flowmeter (High Flow Series)	TSI Inc.	4045 G	250 Hz (Standard for steady flow)
			4 ms to 63% of full scale flow (Large volume fluctuations)

2.6 MEASUREMENT PROTOCOL

All sensors were calibrated prior to beginning the experiments. Additionally, the pressure catheter and the laser line scanner were placed as close to the centerline of the collapsible tube as possible without disrupting the sensor readings. Therefore, both may need to be moved when the longitudinal tension is applied to the tube.

At the beginning of each experiment, the pump was off. Recording was started in the pressure transducers and the flowmeter (total recording time = 1 minute) and then the pump was turned on shortly after the recording was initiated. The increase in flow and pressure after turning on the pump was the event used to synchronize the measurements before beginning the data recording.

To quantify the stretching, a ruler was secured against the mechanical system as shown in Figure 19. From the initial position, the rail car slides along the guiderails, which is attached to the silicone tube under examination. The tube is then stretched 0.5cm, which is measured via the stationary ruler.

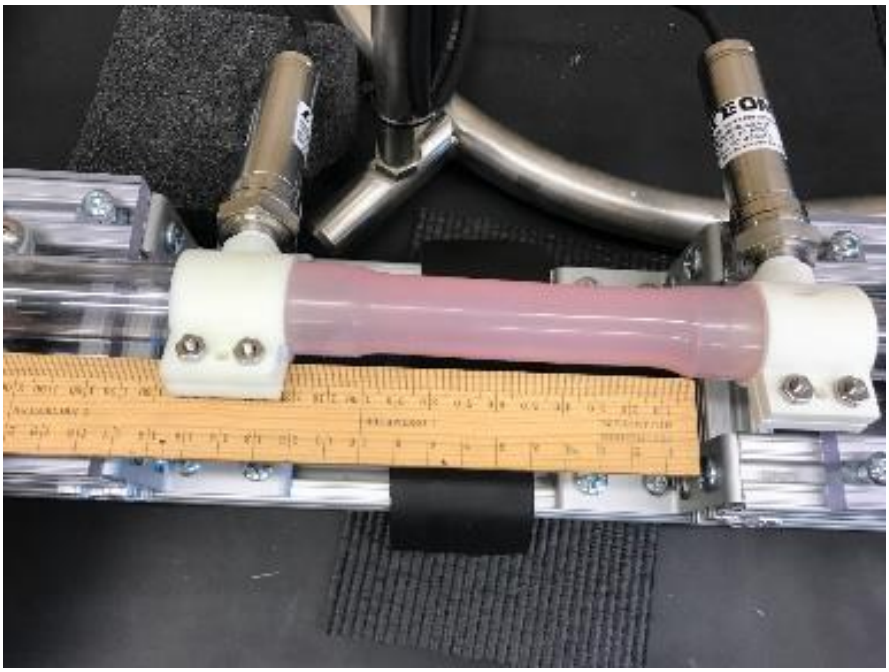

Figure 19: *A ruler was used to measure longitudinal stretching.*

2.7 Reproducibility Analysis

The reproducibility of the experiment was a concern due to the in-house fabrication of collapsible tubes and the possibility that the tube mechanical properties could be changing over time. Therefore, the reproducibility was tested by taking five separately constructed silicone tubes and testing them all and comparing the results (Figure 20). Additionally, the reproducibility over time was tested by taking two separate tubes and testing them five separate times over a period of 2 months (Figure 21).

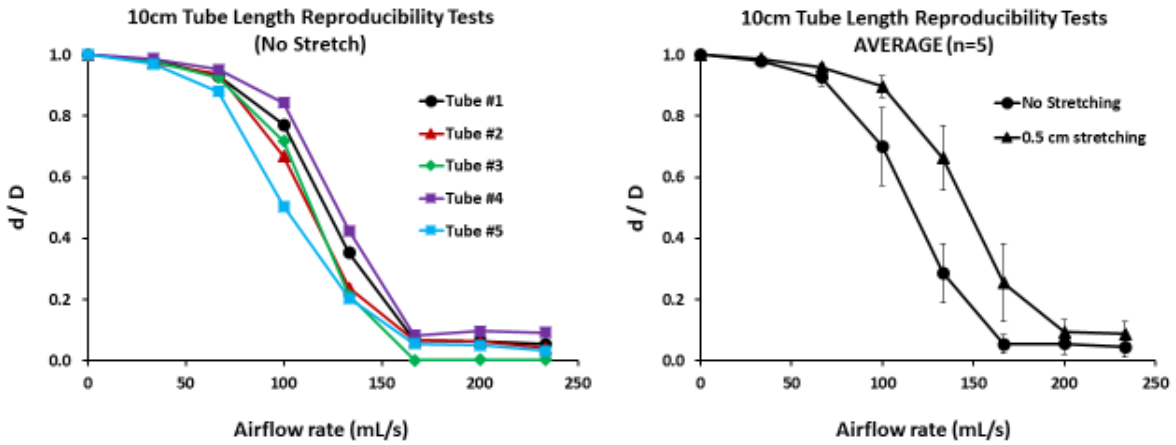

Figure 20: *Reproducibility results of 5 separate silicone tubes.*
On the left, all tubes tested in the reproducibility experiments are plotted for comparison between each other (no stretch condition only). On the right, the error bars indicate variability of independent measurements performed between tubes for the no stretch condition and a 0.5cm stretch condition.

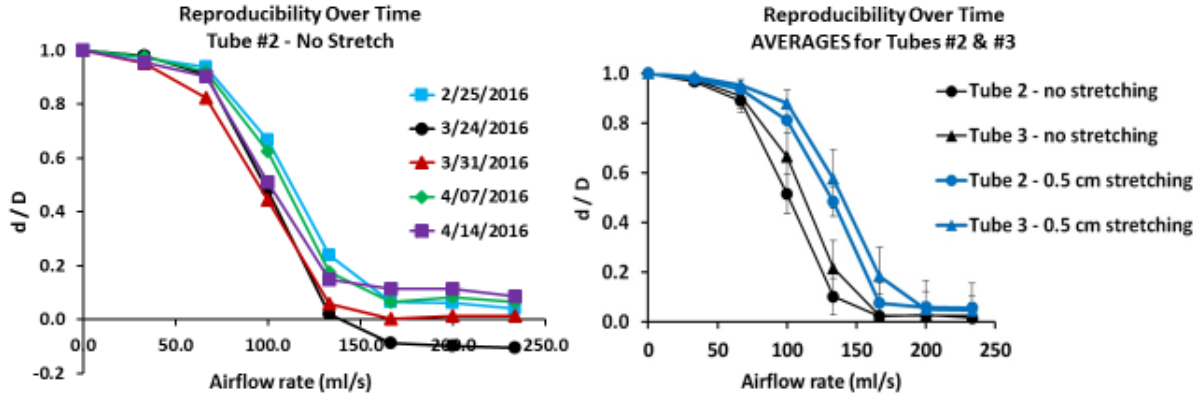

Figure 21: *Reproducibility over time experiments.*
Indicated on the left, the variability of independent measurements performed in the no stretch condition on the same tube (Tube #2) over a period of approximately 2 months. Indicated on the right, the average recordings and standard deviations for tubes #2 and #3 in the no stretch and stretch condition. The averages for both tubes are based on 5 separate testing cycles over a period of approximately 2 months. There was no systematic pattern of change over time.

The analysis showed that there is no clear pattern of change over time. Therefore, it was concluded that the silicone tubes were not fatigued and the mechanical properties were not significantly affected by conducting tests within our experimental scope. The

standard deviations of the variability among tubes and within the same tube provide a measure of the experimental error.

2.8 DATA ANALYSIS

2.8.1 Data Collection

Digital recordings of the displacement taken perpendicular to flow were obtained for qualitative and quantitative observations. In this experiment, collapse is seen during inspiration. Therefore, "airflow" is the average airflow during the inspiratory phase of the pump cycle. The displacement recordings for each tube were taken individually at each increment of air volume along the appropriate pump volume range tested (Table 11).

Table 11: *Pump settings and displacement measurement parameters for each tube study.*

	Dimension Tested	Pump Volume Range Tested (ml)	Increments per Test	Increment Value (ml)	Pump Frequency (cycles/min)
Tube length study	7.50cm	0-700	8	100	20
	10.0cm	0-700	8	100	20
	12.5cm	0-700	8	100	20
Tube diameter study	12.70mm	0-700	8	100	20
	22.22mm	0-700	8	100	20
	31.75mm	0-700	8	100	20
Wall thickness study	0.98mm	0-350	8	50	20
	1.60mm	0-700	8	100	20
	2.22mm	0-700	8	100	20

From each increment of air volume tested, a recording of d/D is measured (Figure 17), and this measurement corresponds to the maximum value of d/D, which corresponds to the maximum deformation during the inspiratory phase of the pump cycle. In addition to displacement, pressures were recorded upstream, downstream, and at the flow-limiting site.

2.8.2 Pressure Analysis

MATLAB codes were written to evaluate the data collected from the upstream and downstream pressure transducers and the Millar pressure catheter (Figure 22). The MATLAB code identified and averaged the minimum pressure of approximately 10 consecutive breathing cycles. This analysis revealed that there was minimal variation from cycle to cycle.

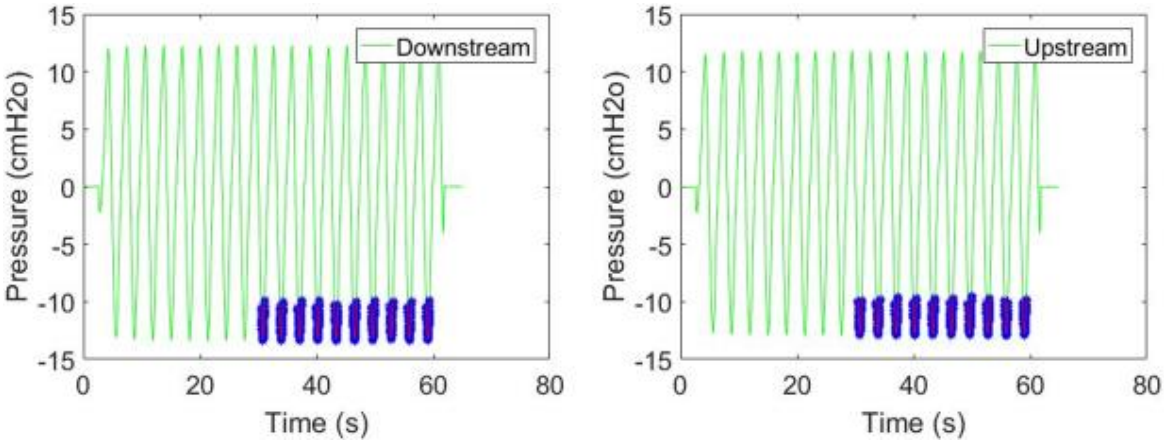

Figure 22: *MATLAB calculation of downstream and upstream minimum pressure. Starting at 30 seconds, the code finds the minimum pressure values for every cycle. Once the minimum value is found the code analyzes 50 points before and 50 points after to make sure no other minimum values exist and calculates an average of the minimum values found between those cycles.*

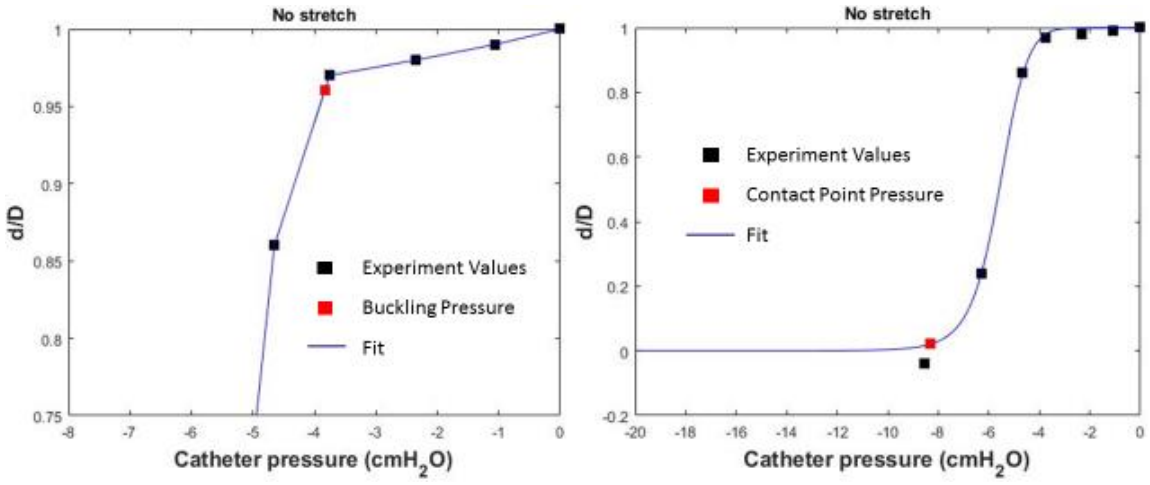

Figure 23: *Method to calculate buckling pressure (P_B) and contact point pressure (P_{CP}).*

Additionally, another code was written to evaluate the buckling pressure and contact point pressure (P_B and P_{CP}, respectively) associated with each study (Figure 23). Both the graphs presented here are for the no stretch condition. The red square on each graph displays the calculated P_B (left) and P_{CP} (right). The P_B is calculated on a curve formed from a linear piece function. The P_{CP} is calculated on a curve formed from the Michaelis-Menten function. The buckling pressure was defined as the catheter pressure corresponding to d/D = 0.96. The contact point pressure was defined as the catheter pressure corresponding to d/D = 0.02.

2.9 Statistical Analysis

For each tube geometry (diameter, length, and wall thickness), the results were averaged for the n=3 tubes studied and the associated standard deviations were calculated. Additional statistical analysis was conducted in the form of a paired two sample t-test on all three tube geometries. These tests were an analysis of the difference between the 0.5cm stretch versus no stretch on buckling pressure for each geometry. For these tests, a sample population of n=9 was utilized for both the length and wall thickness studies, and a sample population of n=7 was utilized for the diameter study. Further analysis employed calculation of the average difference and standard deviation within each geometrical case to analyze the effect of applying 0.5cm stretch on buckling pressures for each tube dimension.

CHAPTER 3: RESULTS

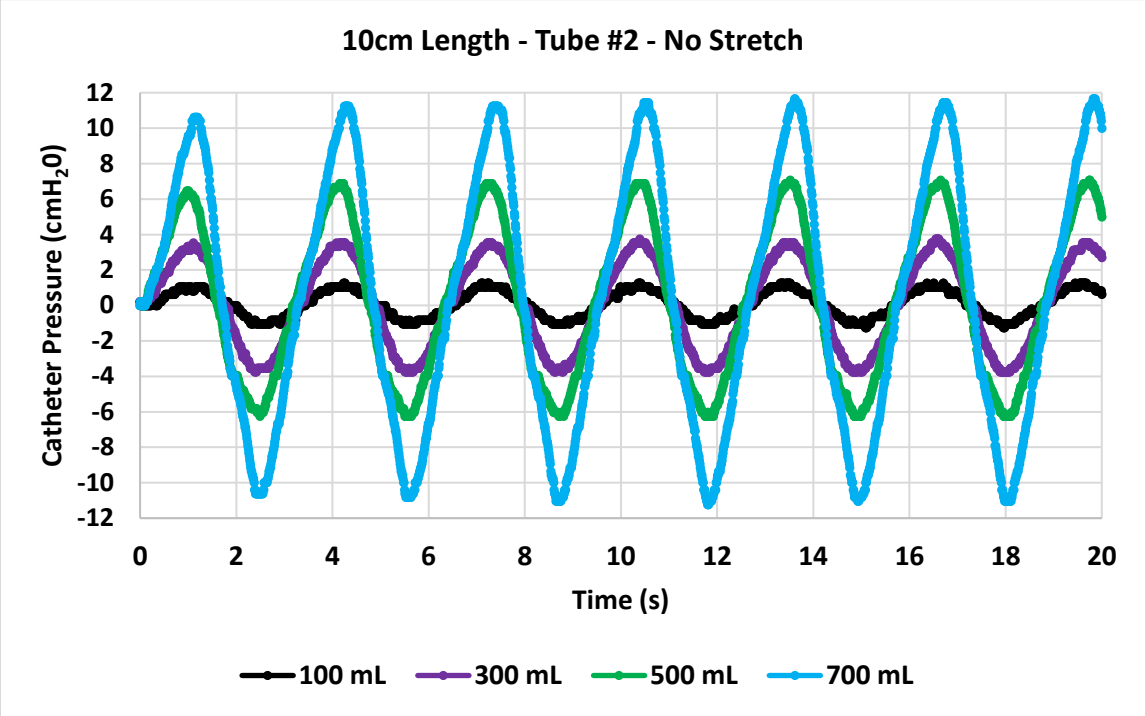

Figure 24: *Synchronized catheter profiles for non-stretch length study, (10cm) tube #2. Pressure at the center of a 10cm silicone tube as a function of time with pump at 20 cycles/min and tidal volumes of 100mL, 300mL, 500mL, and 700mL.*

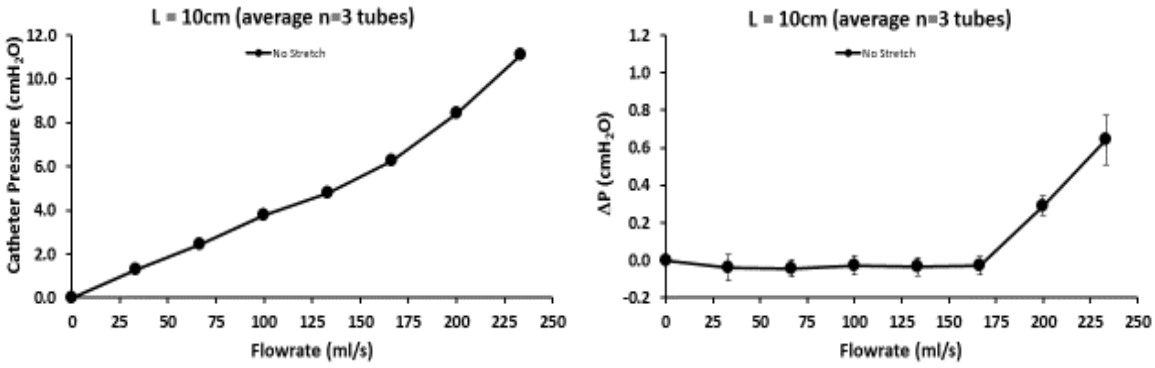

Figure 25: *Averages of all 3 tubes at 10cm length.*
(Left) Pressure at center of silicone tube as a function of flowrate. (Right) Pressure Drop across silicone tube. Opposite walls touched each other for flowrates above 200 mL/s.

The pressure recordings were consistent with an increase in airflow as the pump tidal volume was increased (Figure 24). Typical curves for the relationship between flowrate and pressure are displayed in Figure 25. The pressure at the center of the tube increased almost linearly with the flowrate (Figure 25, left panel). The pressure drop across the tube was nearly zero (within experimental error) until opposite walls touched each other (Figure 25, right panel).

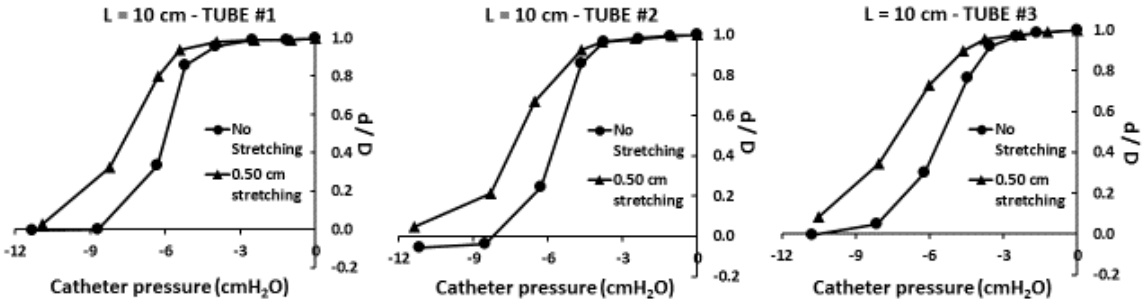

Figure 26: *Comparison between tubes – length study with 10cm tubes.*
The ratio (d/D) of the minimal diameter (d) during a breathing cycle to the tube diameter with zero flow (D) is plotted against the minimum pressure at the center of the tube (catheter pressure) during the inspiratory phase of the breathing cycle.

For each tube geometry, we fabricated and measured n=3 tubes to account for imperfections in the fabrication process that could affect tube collapsibility. Figure 26 illustrates typical variability among tubes with the same geometry.

3.1 TUBE LENGTH STUDY

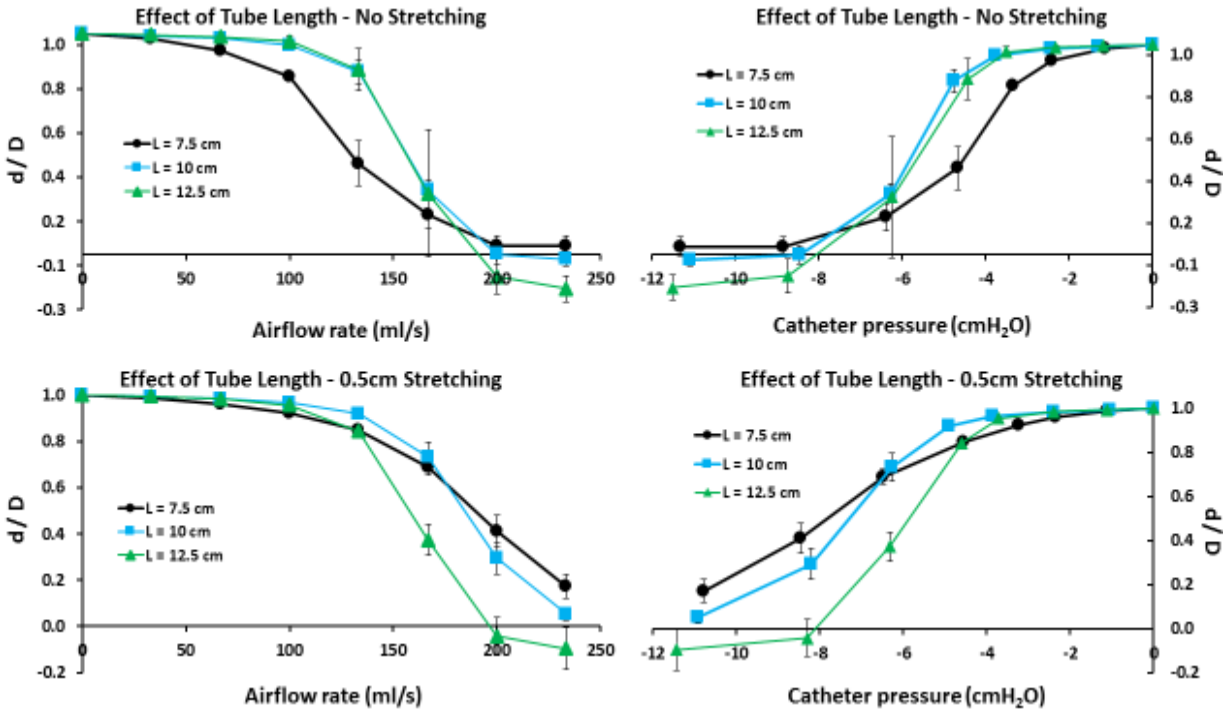

Figure 27: *Effects of tube length (L) on tube collapsibility. (Top) No longitudinal stretch. (Bottom) With 0.5cm longitudinal stretch. Each curve is an average for n=3 tubes. Error bars indicate standard deviations.*

Figure 27 displays the effects of length and the effects of 0.5cm longitudinal strain on an average of three 22.22mm diameter silicone tubes with 1.59mm wall thickness at lengths of 7.5cm, 10cm, and 12.5cm. The left column displays diameter ratio (see Figure 17C) as a function of airflow rate. The right column displays the diameter ratio (d/D) as a function of the pressure at the center of the silicone tube. Tube length had no clear pattern on the collapsibility curves. Longitudinal strain had a greater effect on the shorter tube (L = 7.5cm), while it had almost no effect on the longer tube (L = 12.5cm).

The average buckling pressure (P_B) for a tube length of 7.5cm was -1.5 ± 0.2 cmH_2O without stretch and -2.38 ± 0.09 cmH_20 with stretch (Table 12). For the 10cm tubes, the average P_B increased its magnitude to -3.36 ± 0.61 cmH_20 without stretch and -4.04 ± 0.53 cmH_2O with stretch. Almost a two-fold increase from 7.5cm tube length to 10.0cm tube length for each scenario. For the 12.5cm tubes, the average P_B was similar to the 10cm tubes with values of -3.39 ± 0.51 cmH_2O without stretch and -3.52 ± 0.27 cmH_2O with stretch. Figure 28 shows the tube length effect on average buckling pressure, P_B.

The overall paired t-Test results show significant difference for the buckling pressure with longitudinal stretch and without longitudinal stretch ($p \leq 0.0108$ at $\alpha = 0.05$ at n=9). We defined the change in buckling pressure caused by 0.5cm stretch as $\Delta P_B = (P_B)_{\text{No Stretch}} - (P_B)_{\text{Stretch}}$. The average change in P_B was $\Delta P_B = 0.87 \pm 0.17$ cmH_2O for 7.5cm length tubes, $\Delta P_B = 0.65 \pm 0.50$ cmH_2O for 10cm length tubes, and $\Delta P_B = 0.13 \pm 0.41$ cmH_2O for 12.5cm length tubes.

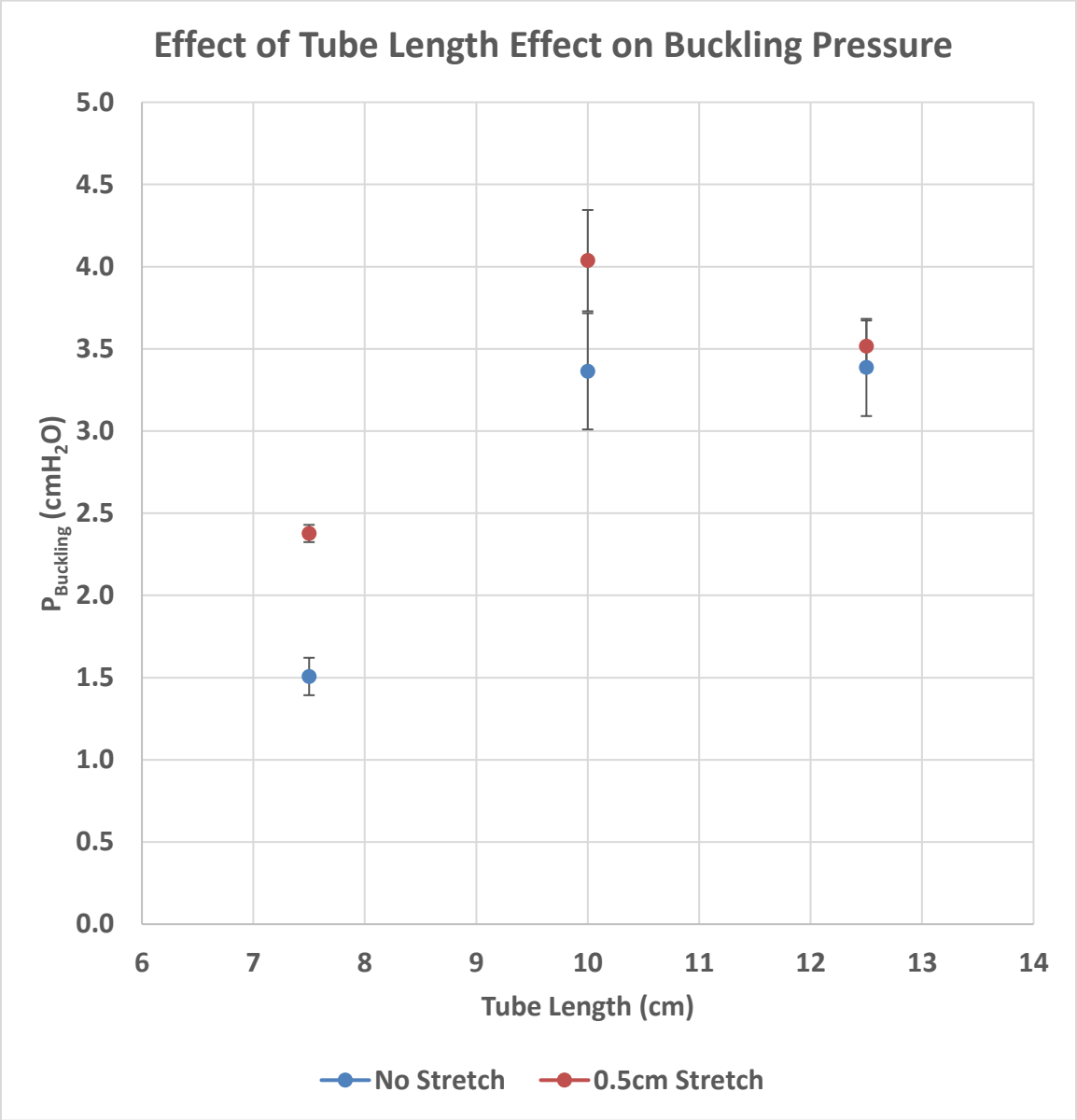

Figure 28: *Effect of tube length on average buckling pressure at tube lengths of 7.5cm, 10cm, and 12.5cm with 0.5cm stretch (red) and without stretch (blue).*

Error bars indicate standard errors, where $standard\ error = \frac{standard\ deviation}{\sqrt{n}}$.

Table 12: *Tube length study results.*

Abbreviations: L = Length; D = diameter; H = wall thickness; P_B = Buckling pressure; Q_B = Flowrate at buckling; P_{CP} = Contact point pressure; Q_{CP} = Flowrate at contact point.

Tube Length = 7.5 cm							
No Stretch							
Tube	L (cm)	D (mm)	H (mm)	P_B (cmH_2O)	Q_B (mL/s)	P_{CP} (cmH_2O)	Q_{CP} (mL/s)
1cut	7.5	22.22	1.59	-1.64	43.9	-10.96	272.0
2cut				-1. 60	46.0	-8.15	210.5
3cut				-1.28	38.4	-12.72	271.3
Average				-1.5 ± 0.2	42.8 ± 3.9	-10.96 ± 2.31	251.3 ± 35.3
0.5 cm Stretch							
Tube	L (cm)	D (mm)	H (mm)	P_B (cmH_2O)	Q_B (mL/s)	P_{CP} (cmH_2O)	Q_{CP} (mL/s)
1cut	7.5	22.22	1.59	-2.34	65.6	-20.00	363.7
2cut				-2.48	74.2	-17.33	322.6
3cut				-2.31	65.1	-20.00	408.1
Average				-2.38 ± 0.09	68.3 ± 5.1	-19.11 ± 1.54	364.8 ± 42.8
Tube Length = 10 cm							
No stretch							
Tube	L (cm)	D (mm)	H (mm)	P_B (cmH_2O)	Q_B (mL/s)	P_{CP} (cmH_2O)	Q_{CP} (mL/s)
1	10	22.22	1.59	-3.59	90.9	-8.81	229.3
2				-3.83	102.8	-8.30	225.1
3				-2.67	72.7	-10.01	232.6
Average				-3.36 ± 0.61	88.8 ± 15.2	-9.04 ± 0.88	229.0 ± 3.8
0.5 cm Stretch							
Tube	L (cm)	D (mm)	H (mm)	P_B (cmH_2O)	Q_B (mL/s)	P_{CP} (cmH_2O)	Q_{CP} (mL/s)
1	10	22.22	1.59	-4.65	115.9	-11.91	275.0
2				-3.78	98.4	-11.88	261.4
3				-3.68	98.4	-14.11	285.9
Average				-4.04 ± 0.53	104.2 ± 10.1	-12.63 ± 1.28	274.1 ± 12.3
Tube Length = 12.5 cm							
No stretch							
No stretch	L (cm)	D (mm)	H (mm)	P_B (cmH_2O)	Q_B (mL/s)	P_{CP} (cmH_2O)	Q_{CP} (mL/s)
1	12.5	22.22	1.59	-2.85	82.6	-8.88	215.3
2				-3.87	108.1	-7.46	216.9
3				-3.44	105.0	-15.51	281.4
Average				-3.39 ± 0.51	98.6 ± 13.9	-10.62 ± 4.30	237.9 ± 37.7
0.5 cm Stretch							
Tube	L (cm)	D (mm)	H (mm)	P_B (cmH_2O)	Q_B (mL/s)	P_{CP} (cmH_2O)	Q_{CP} (mL/s)
1	12.5	22.22	1.59	-3.24	87.8	-10.93	239.4
2				-3.53	98.9	-9.50	227.9
3				-3.78	98.4	-9.54	234.6
Average				-3.52 ± 0.27	95.0 ± 6.3	-9.99 ± 0.81	234.0 ± 5.8

3.2 TUBE DIAMETER STUDY

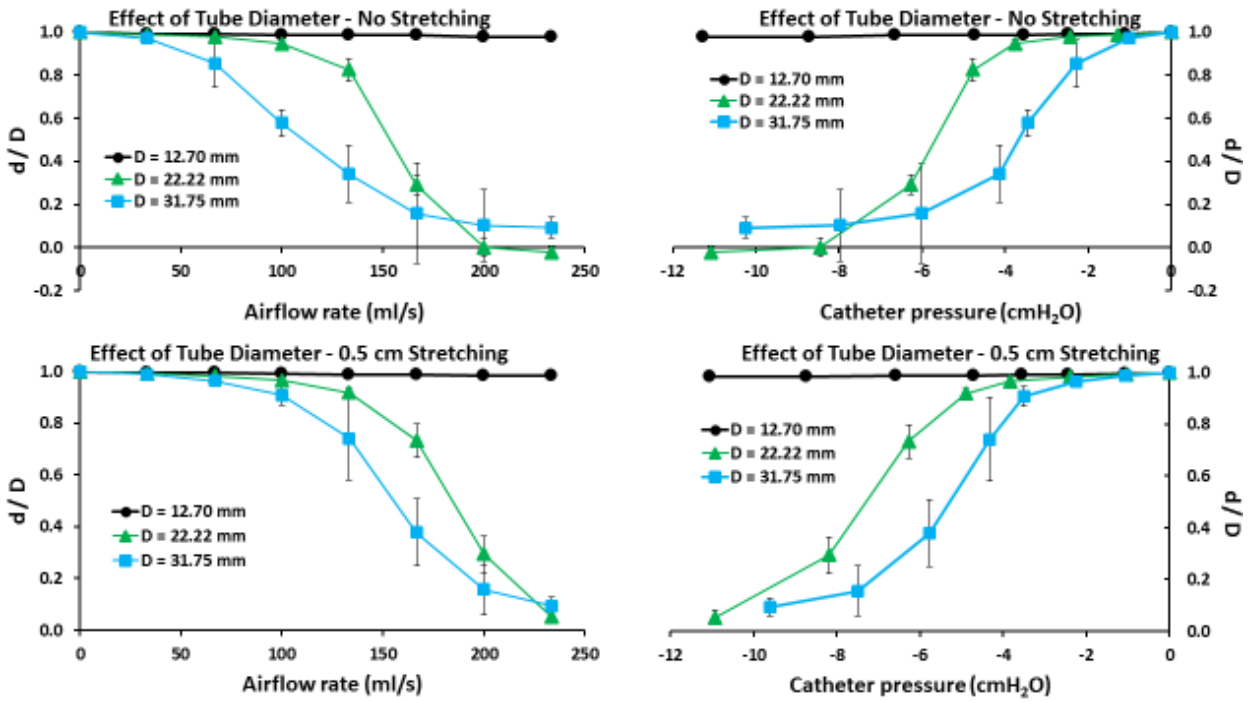

Figure 29: *Effects of tube diameter (D) on tube collapsibility. (Top) No longitudinal stretch. (Bottom) With 0.5cm longitudinal stretch. Each curve is an average for n=3 tubes. Error bars indicate standard deviations.*

Figure 29 displays the effects of diameter and the effects of 0.5cm longitudinal strain on 10cm long silicone tubes with 1.59mm wall thickness and diameters of 12.70mm, 22.22mm, and 31.75mm. The left column displays the diameter ratio (d/D) as a function of airflow rate (see Figure 17C). The right column displays the diameter ratio as a function of the pressure at the center of the silicone tube. Tube diameter had a clear effect on the collapsibility curves. Tubes with larger diameters had greater collapse.

The buckling pressure (P_B) for a tube diameter of 12.70mm was less than -12.00 cmH_20 and less than -15.00 ± 0.09 cmH_20 without stretch and with stretch, respectively (Table 13). For the 22.22mm tubes, the P_B was -3.36 ± 0.61 cmH_20 without stretch and -4.04 ± 0.53 cmH_20 with stretch, respectively. Thus, at least a three-fold reduction in the

P_B magnitude was observed when tube diameter increased from 12.70mm to 22.22mm (Figure 30). For the 31.75mm tubes, the magnitude of buckling pressure decreased slightly as compared to the 22.22mm tubes with buckling pressures at -1.29 ± 0.40 cmH_20 and -2.34 ± 0.44 cmH_20 without stretch and with stretch, respectively.

The overall paired t-Test results show significant difference between all points ($p \leq 0.0064$ at $\alpha = 0.05$ at n=7). We defined the change in buckling pressure caused by 0.5cm stretch as $\Delta P_B = (P_B)_{No\ Stretch} - (P_B)_{Stretch}$. The average change in P_B was $\Delta P_B = 2.21$ cmH_2O for 12.70mm diameter tubes, $\Delta P_B = 0.65 \pm 0.50$ cmH_2O for 22.22mm diameter tubes, and $\Delta P_B = 1.05 \pm 0.35$ cmH_2O for 31.75mm diameter tubes.

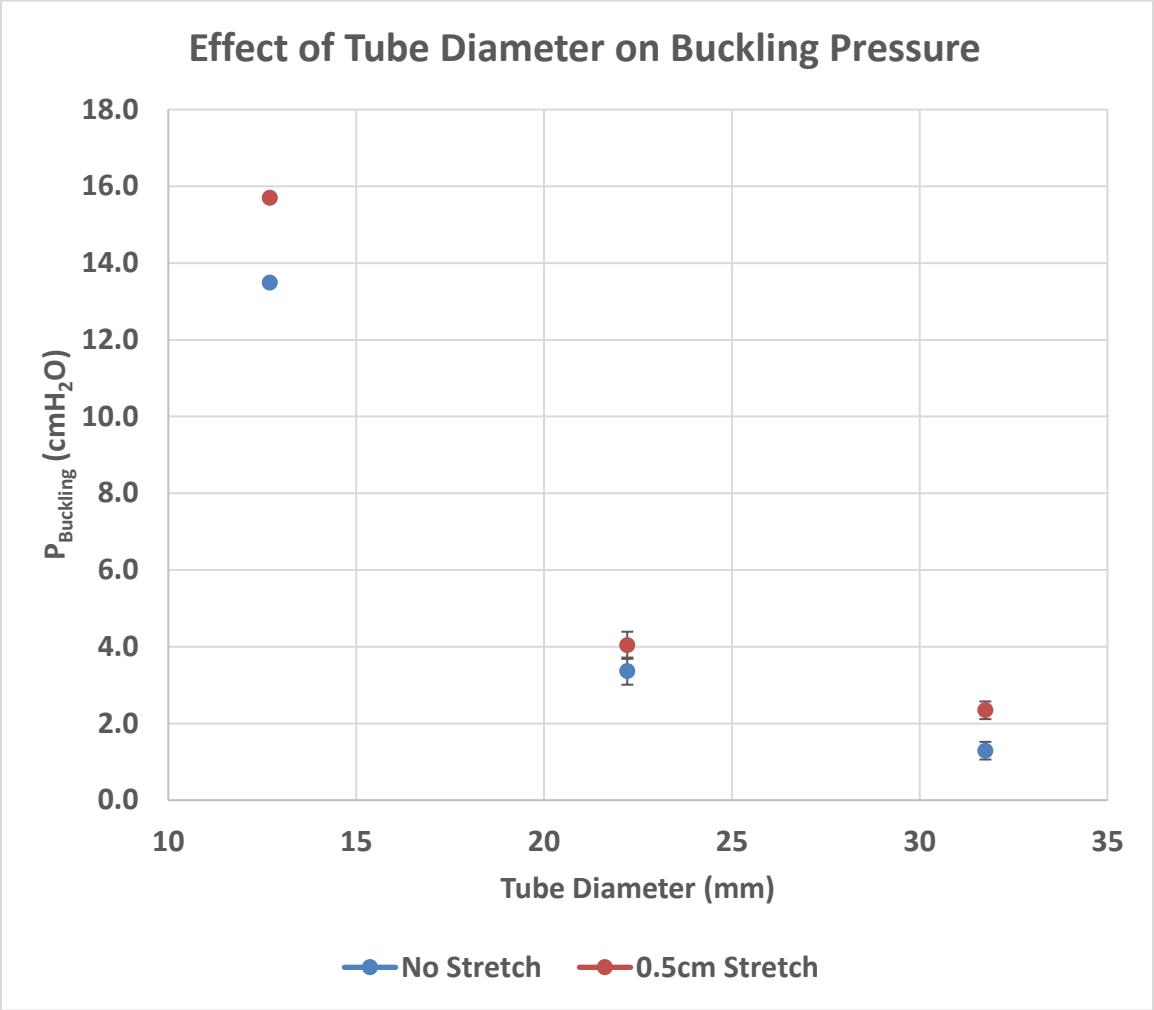

Figure 30: *Effect of tube diameter on average buckling pressure at diameters of 12.70mm, 22.22mm, and 31.75mm with 0.5cm stretch (red) and without stretch (blue). Error bars indicate standard errors, where* $standard\ error = \frac{standard\ deviation}{\sqrt{n}}$.

Table 13: *Tube diameter study results.*

Abbreviations: L = Length; D = diameter; H = wall thickness; P_B = Buckling pressure; Q_B = Flowrate at buckling; P_{CP} = Contact point pressure; Q_{CP} = Flowrate at contact point.

Tube Diameter = 12.70 mm							
No Stretch							
Tube	L (cm)	D (mm)	H (mm)	P_B (cmH_2O)	Q_B (mL/s)	P_{CP} (cmH_2O)	Q_{CP} (mL/s)
d1	10	12.70	1.59	< -11.00	>250	<-20.00	>500
d2				-13.49	263.3	<-20.00	566.8
d3				< -12.00	>250	<-20.00	>500
Average				-	-	-	-
0.5 cm Stretch							
Tube	L (cm)	D (mm)	H (mm)	P_B (cmH_2O)	Q_B (mL/s)	P_{CP} (cmH_2O)	Q_{CP} (mL/s)
d1	10	12.70	1.59	< -13.00	>250	<-20.00	>500
d2				-15.70	296.6	<-20.00	530.6
d3				< -13.00	>250	<-20.00	>500
Average				-	-	-	-
Tube Diameter = 22.22 mm							
No Stretch							
Tube	L (cm)	D (mm)	H (mm)	P_B (cmH_2O)	Q_B (mL/s)	P_{CP} (cmH_2O)	Q_{CP} (mL/s)
1	10	22.22	1.59	-3.59	90.9	-8.81	229.3
2				-3.83	102.8	-8.30	225.1
3				-2.67	72.7	-10.01	232.6
Average				-3.36 ± 0.61	88.8 ± 15.2	-9.04 ± 0.88	229.0 ± 3.8
0.5 cm Stretch							
Tube	L (cm)	D (mm)	H (mm)	P_B (cmH_2O)	Q_B (mL/s)	P_{CP} (cmH_2O)	Q_{CP} (mL/s)
1	10	22.22	1.59	-4.65	115.9	-11.91	275.0
2				-3.78	98.4	-11.88	261.4
3				-3.68	98.4	-14.11	285.9
Average				-4.04 ± 0.53	104.2 ± 10.1	-12.63 ± 1.28	274.1 ± 12.3
Tube Diameter = 31.75 mm							
No Stretch							
Tube	L (cm)	D (mm)	H (mm)	P_B (cmH_2O)	Q_B (mL/s)	P_{CP} (cmH_2O)	Q_{CP} (mL/s)
D1	10	31.75	1.59	-1.08	36.1	-11.33	325.2
D2				-1.04	32.5	-7.51	253.7
D3				-1.75	52.7	-11.38	294.2
Average				-1.29 ± 0.40	40.4 ± 10.8	-10.07 ± 2.22	291.0 ± 35.9
0.5 cm Stretch							
Tube	L (cm)	D (mm)	H (mm)	P_B (cmH_2O)	Q_B (mL/s)	P_{CP} (cmH_2O)	Q_{CP} (mL/s)
D1	10	31.75	1.59	-2.53	71.7	-14.02	317.5
D2				-1.84	57.6	-9.49	265.4
D3				-2.66	76.7	-9.59	260.2
Average				-2.34 ± 0.44	68.7 ± 9.9	-11.03 ± 2.59	281.0 ± 31.7

3.3 TUBE WALL THICKNESS STUDY

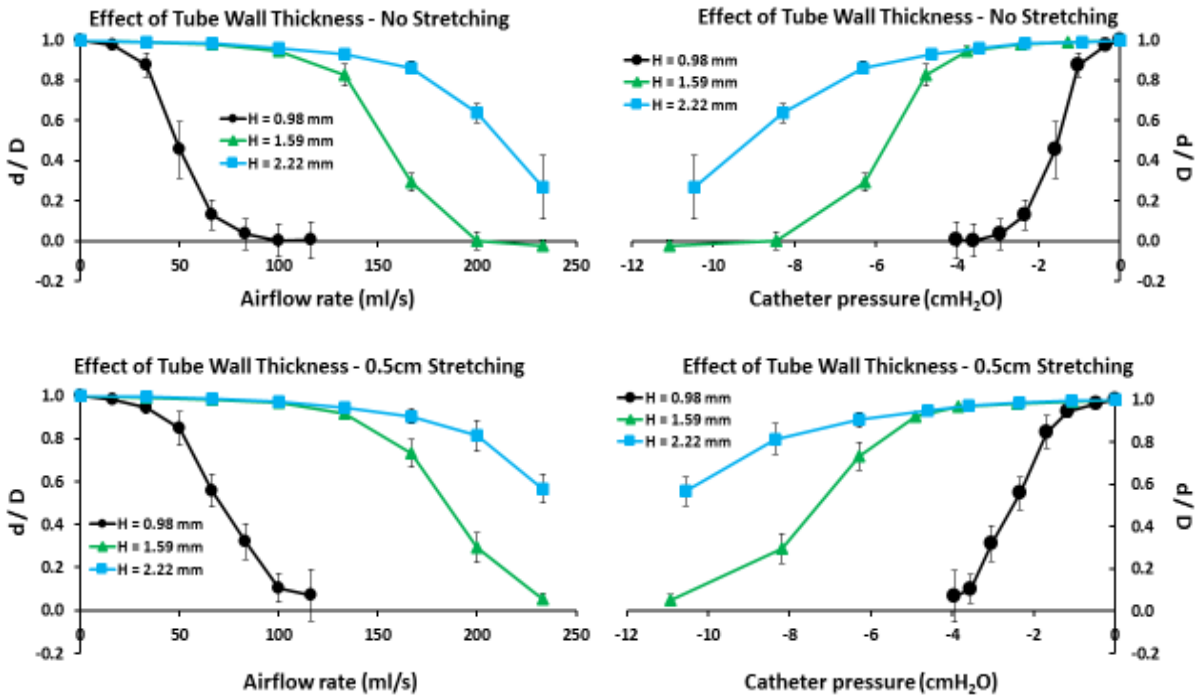

Figure 31: *Effects of tube wall thickness (H) on airflow rate and catheter pressure. (Top) No longitudinal stretch. (Bottom) With 0.5cm longitudinal stretch. Each curve is an average for n=3 tubes. Error bars indicate standard deviations.*

Figure 31 displays the effects of wall thickness and the effects of 0.5cm longitudinal strain on 10cm long silicone tubes of 22.22mm diameter with wall thicknesses of 0.98mm, 1.59mm, and 2.22mm. The left column displays the diameter ratio (d/D) as a function of airflow rate (see Figure 17C). The right column displays the diameter ratio as a function of the pressure at the center of the silicone tube. Wall thickness also had a clear effect on tube collapsibility. Tubes with thinner walls had greater collapse.

The buckling pressure (P_B) for a tube wall thickness of 0.98mm averages -0.47 ± 0.20 cmH_20 without stretch and -0.91 ± 0.27 cmH_20 with stretch, respectively (Table 14). For tubes with 1.59mm wall thickness, the P_B was more negative with values of -3.36 ±

0.61 cmH_20 and -4.04 ± 0.53 cmH_20 without stretch and with stretch, respectively. Thus, the buckling pressure magnitude increased nearly 3-fold when the wall thickness increased from 0.98mm to 1.59mm (Figure 32). For the 2.22mm wall thickness, the buckling pressure was slightly more negative with values of -3.70 ± 0.84 cmH_20 without stretch and -4.27 ± 1.05 cmH_20 with stretch (Table 14 and Figure 32).

The overall paired t-Test results show significant difference between all points ($p \leq 0.0015$ at $\alpha = 0.05$) at n=9. We defined the change in buckling pressure caused by 0.5cm stretch as $\Delta P_B = (P_B)_{No\ Stretch} - (P_B)_{Stretch}$. The average change in P_B was $\Delta P_B = 0.44 \pm 0.13$ cmH_2O for 0.98mm wall thickness tubes, $\Delta P_B = 0.65 \pm 0.50$ cmH_2O for 1.59mm wall thickness tubes, and $\Delta P_B = 0.57 \pm 0.24$ cmH_2O for 2.22mm wall thickness tubes.

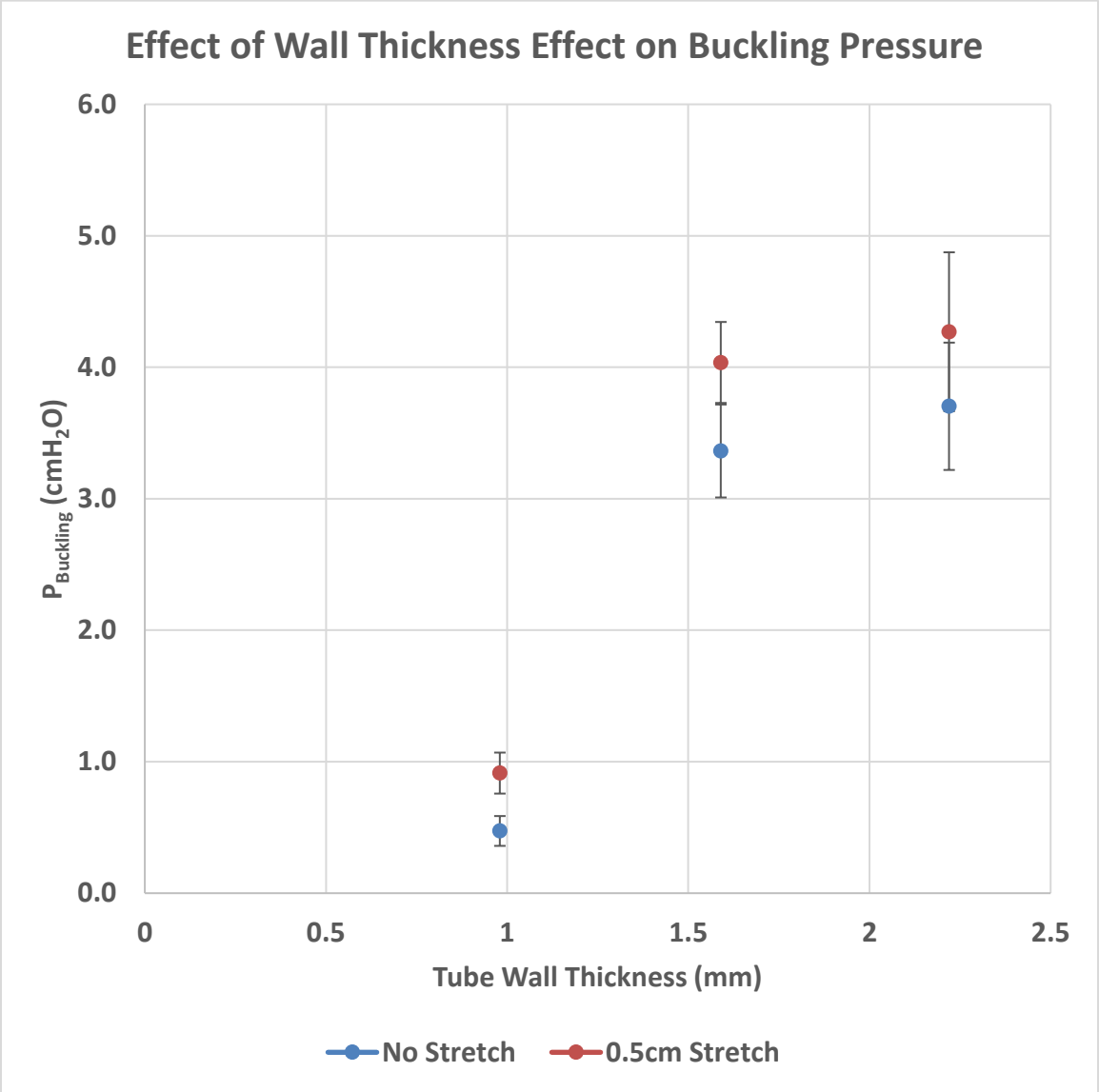

Figure 32: *Effect of tube wall thickness on average buckling pressure at wall thicknesses of 0.98mm, 1.59mm, and 2.22mm with 0.5cm stretch (red) and without stretch (blue). Error bars indicate standard errors, where* $standard\ error = \frac{standard\ deviation}{\sqrt{n}}$.

Table 14: *Tube wall thickness study results.*

Abbreviations: L = Length; D = diameter; H = wall thickness; P_B = Buckling pressure; Q_B = Flowrate at buckling; P_{CP} = Contact point pressure; Q_{CP} = Flowrate at contact point.

Tube Wall Thickness = 0.98 mm							
No Stretch							
Tube	L (cm)	D (mm)	H (mm)	P_B (cmH_2O)	Q_B (mL/s)	P_{CP} (cmH_2O)	Q_{CP} (mL/s)
D	10	22.22	0.98	-0.70	26.4	-4.23	108.2
E				-0.35	18.0	-3.52	99.7
F				-0.37	16.3	-2.73	86.6
Average				-0.47 ± 0.20	20.2 ± 5.4	-3.49 ± 0.75	98.2 ± 10.9
0.5 cm Stretch							
Tube	L (cm)	D (mm)	H (mm)	P_B (cmH_2O)	Q_B (mL/s)	P_{CP} (cmH_2O)	Q_{CP} (mL/s)
D	10	22.22	0.98	-1.18	35.9	-5.03	139.2
E				-0.64	21.3	-5.50	143.6
F				-0.92	27.3	-6.63	187.6
Average				-0.91 ± 0.27	28.2 ± 7.3	-5.72 ± 0.82	156.8 ± 26.8
Tube Wall Thickness = 1.59 mm							
No Stretch							
Tube	L (cm)	D (mm)	H (mm)	P_B (cmH_2O)	Q_B (mL/s)	P_{CP} (cmH_2O)	Q_{CP} (mL/s)
1	10	22.22	1.59	-3.59	90.9	-8.81	229.3
2				-3.83	102.8	-8.30	225.1
3				-2.67	72.7	-10.01	232.6
Average				-3.36 ± 0.61	88.8 ± 15.2	-9.04 ± 0.88	229.0 ± 3.8
0.5 cm Stretch							
Tube	L (cm)	D (mm)	H (mm)	P_B (cmH_2O)	Q_B (mL/s)	P_{CP} (cmH_2O)	Q_{CP} (mL/s)
1	10	22.22	1.59	-4.65	115.9	-11.91	275.0
2				-3.78	98.4	-11.88	261.4
3				-3.68	98.4	-14.11	285.9
Average				-4.04 ± 0.53	104.2 ± 10.1	-12.63 ± 1.28	274.1 ± 12.3
Tube Wall Thickness = 2.22 mm							
No Stretch							
Tube	L (cm)	D (mm)	H (mm)	P_B (cmH_2O)	Q_B (mL/s)	P_{CP} (cmH_2O)	Q_{CP} (mL/s)
A	10	22.22	2.22	-3.27	98.4	-17.43	324.3
B				-4.67	130.0	-13.49	303.3
C				-3.17	87.8	-20.00	480.2
Average				-3.70 ± 0.84	105.4 ±22.0	-16.97 ± 3.28	369.3 ± 96.6
0.5 cm Stretch							
Tube	L (cm)	D (mm)	H (mm)	P_B (cmH_2O)	Q_B (mL/s)	P_{CP} (cmH_2O)	Q_{CP} (mL/s)
A	10	22.22	2.22	-3.86	110.0	-20.00	485.7
B				-5.46	148.4	-17.66	351.0
C				-3.49	98.4	-20.00	700.0
Average				-4.27 ± 1.05	118.9 ± 26.2	-19.22 ± 1.35	512.2 ± 176.0

3.4 Buckling Pressures vs. Gamma

The experimental buckling pressures measured from every tube in this study were compiled and displayed in Figure 33 (blue dots). Theoretical buckling pressures were calculated from Kozlovsky et al. (2014) and displayed in Figure 33 (black bars) for comparison to the experimental results. The buckling pressure was calculated using the following equation:

Equation 8: *Buckling Pressure* $P_B = (-3)(K_P)$

where the flexural rigidity (K_P) increases as the wall thickness-to-radius ratio increases (Kozlovsky, Zaretsky, Jaffa, & Elad, 2014). K_P in the above equation can be defined as,

Equation 9: *Flexural Rigidity* $K_P = \frac{\mathrm{E}}{12(1-\nu^2)}(\ln(1+\gamma))^3$

Which includes the Young's Modulus (E), the Poisson's Ratio (ν), and the wall thickness-to-radius ratio (γ). By substituting Equation 9 into Equation 8 for K_P, the following equation can be utilized to calculate theoretical values of buckling pressure:

Equation 10: *Buckling Pressure* $P_B = (-3)(\frac{\mathrm{E}}{12(1-\nu^2)}(\ln(1+\gamma))^3)$

Table 15: *Theoretical buckling pressures for each tube study (black bars on Figure 33).*
$\gamma = H/R_i$ = the ratio of the wall thickness to the radius.

Study Type	Length (cm)	Radius (mm)	Wall Thickness (mm)	γ	P_B (MPa)	P_B (cmH_2O)
Length Study	7.5	11.11	1.6	0.144	-0.000289627	-2.95
	10			0.144	-0.000289627	-2.95
	12.5			0.144	-0.000289627	-2.95
Diameter Study	10	6.35	1.6	0.252	-0.001349461	-13.76
		11.11		0.144	-0.000289627	-2.95
		15.875		0.101	-0.000105297	-1.07
Wall Thickness Study	10	11.11	0.8	0.072	-0.000039978	-0.41
			1.6	0.144	-0.000289627	-2.95
			2.4	0.216	-0.000889724	-9.07

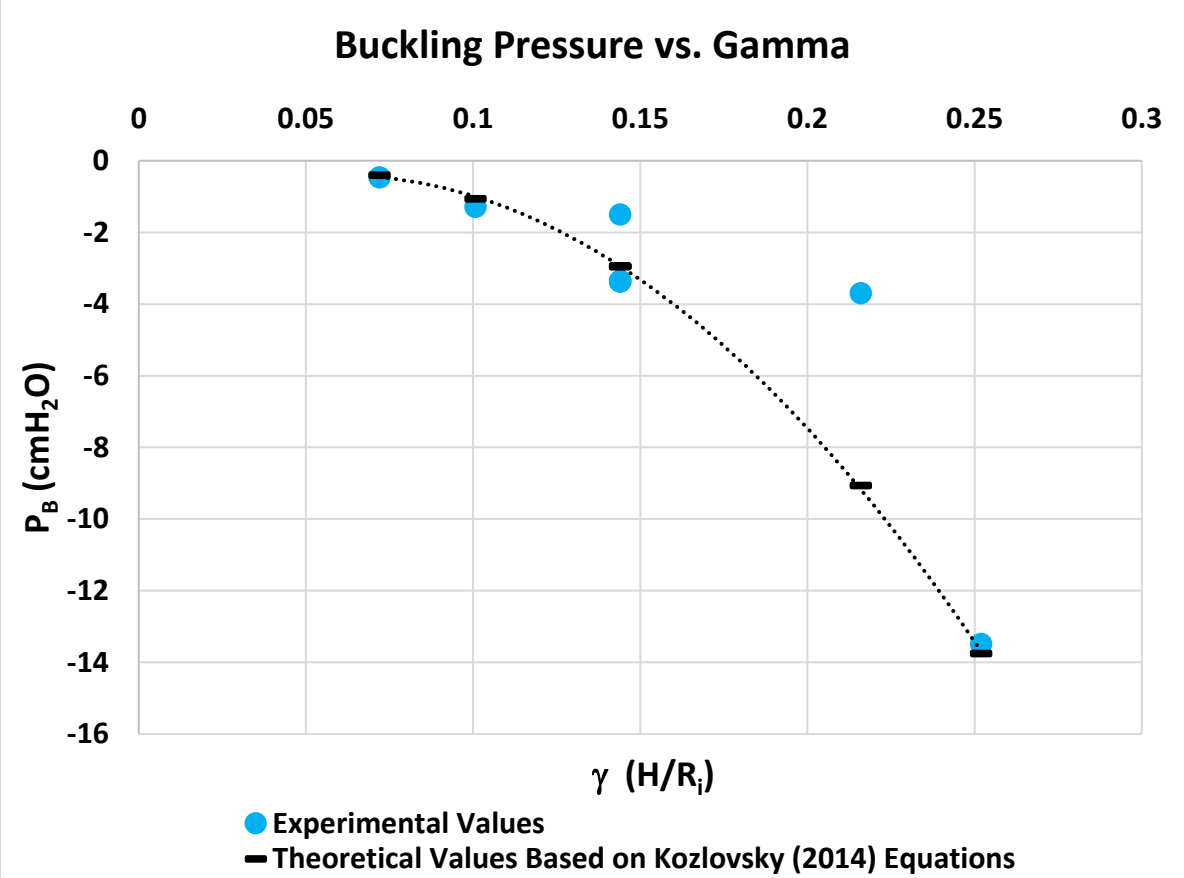

Figure 33: Comparison of experimental values (blue) to theoretical values (black) and the e*ffects of γ on the buckling pressure.*
$\gamma = H/R_i$ = tube wall thickness-to-internal radius ratio.

CHAPTER 4: MAJOR FINDINGS AND FUTURE DIRECTIONS

4.1 DISCUSSION

This study was conducted on an experimental setup that was designed, fabricated, and validated in-house. The experimental setup was developed to quantify the collapsibility of cylindrical silicone tubes that behave similarly to the human pharynx in OSA patients. A significant part of this project was devoted to designing and fabricating this new experimental setup.

Additionally, a large part of this project was also devoted to identifying the proper material for fabricating the collapsible tubes and, once a material was chosen, developing methods for a fabrication process and performing mechanical testing to quantify the material properties. It is important to note that the compliance of the silicone tubes investigated was in the same range of airway compliance found in the human upper airway (Oliven, et al., 2010). The tubes tested collapsed with transmural pressures in the range of 0 to 15 cmH_20 and flowrates in the range of 0 to 250 mL/s, like in OSA patients.

4.1.1 Summary of Major Findings

As the tube length increased from 7.5 cm to 10 cm, the buckling pressure (P_B) decreased from -1.5 ± 0.2 cmH_20 to -3.36 ± 0.61 cmH_20. However, as the length increased from 10 cm to 12.5 cm, P_B did not change. In theory, longer tubes are expected to be more collapsible. In contrast with this expectation, the shorter tube (L=7.5cm) was the most collapsible in this study. Meanwhile, there was no substantial difference

between tubes with lengths of 10cm and 12.5cm. These results contradict our preliminary results (Figure 34).

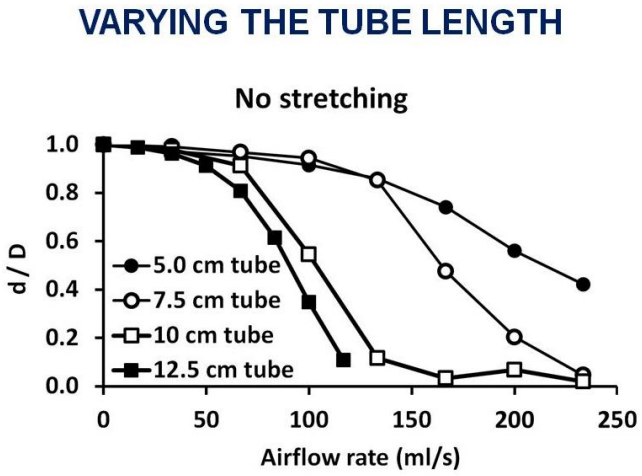

Figure 34: *Preliminary results showing expected effect of length on tube collapsibility.*

Longitudinal strain had greater effects on the shorter tube (P_B reduced from -1.5 ± 0.2 cmH_20 without stretching to -2.38 ± 0.09 cmH_20 with 0.5cm stretching in the 7.5cm tube) than in longer tubes (P_B reduced from -3.4 ± 0.5 cmH_20 without stretching to -3.5 ± 0.3 cmH_20 with 0.5cm stretching in the 12.5cm tube). The greater effect of longitudinal stretching in the shorter tube was expected given that 0.5cm stretch caused a higher strain in the shorter tube.

As the tube diameter increased from 12.70 mm to 31.75 mm, the magnitude of P_B was markedly decreased (Figure 30). The greatest effect was seen as the diameter increased from 12.70 mm to 22.22 mm, where the buckling pressure decreased nearly three-fold. As the diameter increased from 22.22 mm to 31.75 mm, the magnitude of P_B decreased in half approximately. The trend arises that naturally narrower airways tend to have more structural support from surrounding tissues. However, this conclusion needs further testing to corroborate the claim that tissues in the airway do provide this structural

support, and behave similarly to silicone tubes. It is important to note that the wall thickness of the tissue surrounding the human pharynx is much greater than in our silicone tubes and that the soft tissue is not expected to behave as a homogenous material (Brown, Bradley, Phillipson, Zamel, & Hoffstein, 1985). Longitudinal strain increased airway stability at all diameters by requiring higher buckling pressures to achieve collapse, and the magnitude of buckling pressure change was nearly the same for all diameters (Figure 30).

As the tube wall thickness increased from 0.98 mm to 2.22 mm, the magnitude of buckling pressure increased. The greatest effect was seen as the wall thickness increased from 0.98 mm to 1.59 mm, where the buckling pressure decreased from -0.47 ± 0.20 cmH_20 to -3.4 ± 0.6 cmH_20. When wall thickness increased from 1.59 mm to 2.22 mm, the magnitude of P_B increased only slightly. The trend arises that tubes with thicker walls are more stable. Longitudinal strain reduced collapsibility at all wall thicknesses.

4.1.2 Relationship to Previous Work & Unique Contribution

To the best of our knowledge, this study is the first to investigate cyclic, bi-directional airflow (modeling the complete breathing cycle) through collapsible silicone tubes in reference to modeling tracheal traction in OSA patients. This is not the first study to model tracheal traction in collapsible silicone tubes, but may be the first to do so using cyclic airflow. The findings suggest that applying a longitudinal strain or "tracheal traction" reduces airway collapsibility. This supports previous studies showing reductions in airway collapsibility in models with collapsible tubes (Sakurai, Ohba,

Futagami, & Tsujimoto, 1996). The current model suggests that tracheal traction produces a stabilizing effect in the human airways.

Some interesting observations can be made when we compare findings from our in vitro study with in vivo observations in OSA patients. First, OSA severity is correlated with body mass index (BMI). Obese OSA patients have narrower airway lumens and thicker soft tissue walls as compared to non-obese OSA patients. Weight loss has been shown to decrease OSA severity by reducing the pharyngeal critical pressure (Gold & Schwartz, 1996). In our experiments, the silicone tubes became more collapsible when wall thickness decreased. However, the opposite seems to occur in humans, namely obese patients have a more collapsible airway but thicker soft tissue walls. We speculate that the greater stability provided by thicker walls in obese OSA patients is counter-balanced by a greater tissue pressure. In our experiments, air pressure external to the tube was kept constant (atmospheric pressure). We speculate that in obese patients the tissue pressure is greater than in non-obese patients, in such a way that the greater stability of thicker soft tissue walls is offset by a higher tissue pressure that induces airway collapse at lower lumen pressure.

A second interesting observation is regarding the effect of upper airway surgery on pharyngeal collapsibility. Often, surgical intervention for OSA is aimed at removing tissue, such as tonsillectomy, Uvulopalatopharyngoplasty (UPPP). In our experiments, a reduction in wall thickness increased the collapsibility of silicone tubes. This contrasts to the observation that removal of soft tissue surrounding the human pharynx via UPPP surgery either reduces pharyngeal collapsibility (reduces Pcrit) or does not affect it (Gold & Schwartz, 1996). Thus, we speculate that the beneficial effect of UPPP surgery is not

the reduction in wall thickness itself, but rather it is due to a reduction in soft tissue pressure.

The current experiment produced pressure-flowrate curves representative of a flowrate limitation study. Figure 35 displays a previous study's flowrate-limitation curve produced by testing collapsible Penrose tubing under varying external pressures (P_C = Chamber Pressure). Our results (Figure 25) look similar to the low range of pressure drops across the tube in Figure 35.

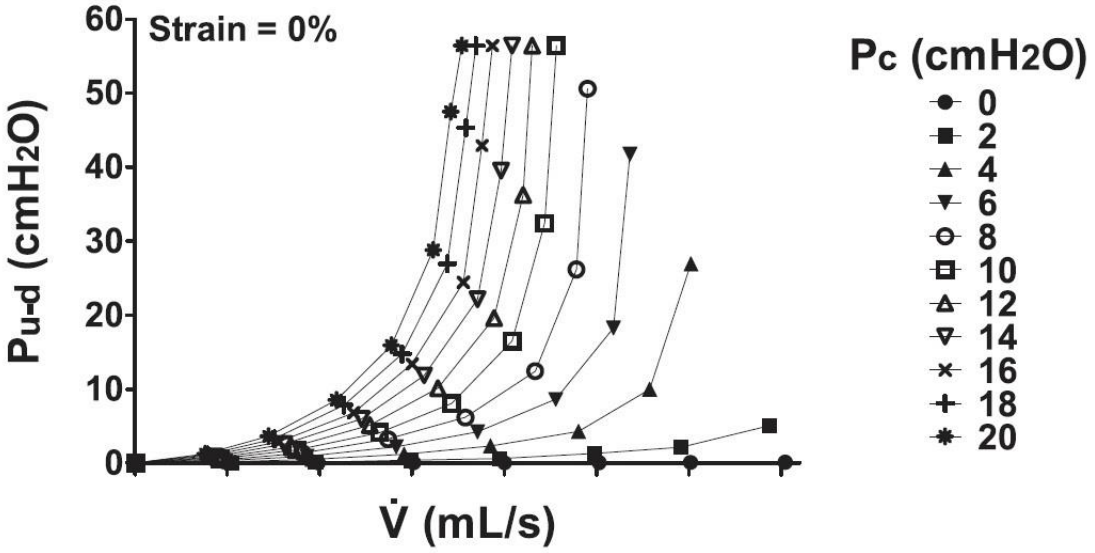

Figure 35: *Flowrate limitation (or pressure drop-independent flowrate) relationship. Reproduced from Amatoury et al. (2010).*

Tube wall thickness is a highly important parameter that determines collapsibility of flexible tubes. As the wall thickness-to-radius ratio (γ) increases, the flexural rigidity increases and the tubes become more and more resistant to bending (Kozlovsky, Zaretsky, Jaffa, & Elad, 2014). This phenomenon has been simulated numerically with finite element analysis (FEA) in ADINA software in a study by Kozlovsky et al. (2014) (Figure 36).

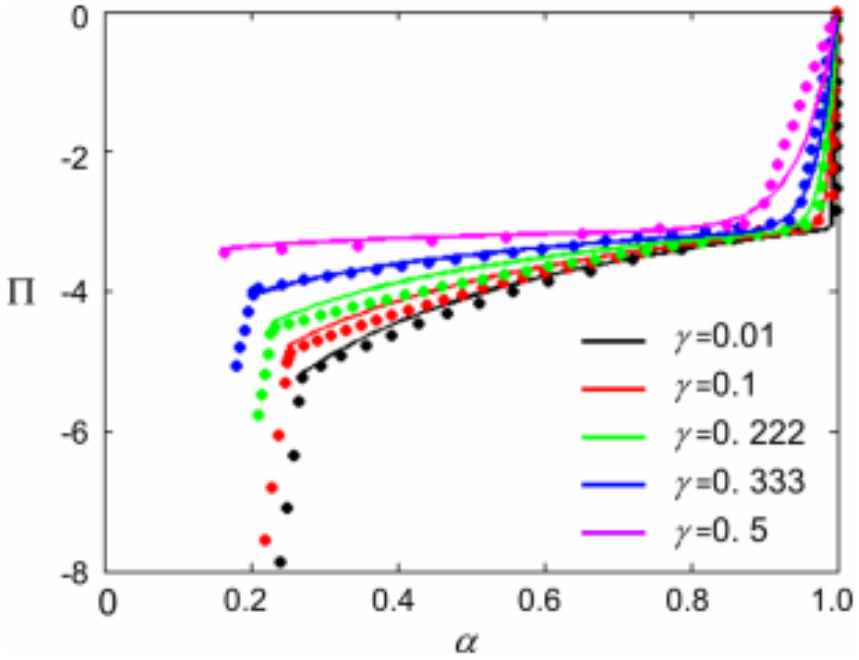

Figure 36: *Non-dimensional pressure-area curves as obtained from computer simulations (circles) for tubes with different wall thickness ratios, γ.*
The wall thickness-to-radius ratio is defined as, $\gamma = \frac{H}{R_i}$*, where H = wall thickness and* R_i *= tube radius. Reproduced from Kozlovsky et al. (2014).*

The results from the current study agree with their conclusions. As wall thickness increases a greater magnitude of negative pressure is required to buckle the collapsible tube (Equation 10). Moreover, in the tube diameter study, it was observed that the small diameter tubes were significantly more rigid than all other conduits tested. This is due to the larger wall-thickness-to-radius ratio of a tube of constant wall thickness but decreasing diameter.

4.1.3 Study Limitations

Results from this study should be interpreted within the constraints of potential limitations, including small inconsistencies in tube placement (rotation, stretching) when being put onto the experimental setup, lack of airflow measurements in the flowmeter to

validate the flowrate set in the pump, measuring catheter pressure at the exact tube center, and relatively low sample sizes.

Tube placement was accomplished in the same manner every time a tube was placed within the experimental setup. However, because this was done by hand, inconsistencies in placement (minor rotation, minor stretching) were inevitable.

The airflow measurement data recorded produced choppy results. This is speculated to have been partially due to the fact that the flowmeter available was a flowmeter for measuring uni-directional flow, and not cyclic flow.

The Mikro-Cath™ Diagnostic Pressure Catheter used in this experiment was fed into the collapsible silicone tube by penetrating the wall of the downstream rigid tubing and then being pushed upstream until resting right next to the measurement site of the displacement line scanner. However, the catheter was simply resting on the bottom of the lumen and not placed concentrically within the tube lumen.

The sample size of the current study was limited (n=3 tubes for each geometry). This study was meant to be exploratory. However, our significant findings and the validation of the experimental setup and its capabilities have allowed for further interest and exploration with a larger more anatomically-correct collapsible silicone airway study to be conducted.

4.2 Conclusion & Future Directions

This study suggests that tube length, diameter, and wall thickness have an effect on the collapsibility of silicone rubber tubes. Additionally, this study also suggests that longitudinal strain increases lumen patency in cylindrical silicone rubber tubes. These

findings coupled with the results found in animal models and other collapsible tube experiments, support previous evidence that tracheal traction in the human upper airway could decrease the severity of OSA by stabilizing peripharyngeal tissues and reducing airway collapse.

Future research in cylindrical tubes could explore the effects of constant airflow experiments and the theory of negative effort dependence (Owens, et al., 2014). Other areas of interest could look into the effects of zero airflow experiments (transmural pressure alone) and quantifying the tube law or pressure-area relationship and measure the buckling pressure in these conditions and how it compares to cyclic flow experiments (Genta, et al., 2016) (Kozlovsky, Zaretsky, Jaffa, & Elad, 2014). In regards to cyclic flow experiments, there is potential to study pump frequency and its effect on buckling pressure, because it has been noted that fluid-solid coupling in shells conveying viscous flow can have a substantial impact on the location and behavior of buckling deformation (Heil & Pedley, 1996).

Future research also includes assessing effects of greater longitudinal strains and the impact on buckling pressure. Moreover, assessing length, diameter, wall thickness, and longitudinal strain in silicone rubber patient-specific models and comparing with the results of this study. Additionally, future studies could look into fabrication of patient-specific models with homogenous wall thickness, wall thickness that varies along the perimeter, greater wall thickness as seen in the human airway, and varying elastic properties (young's modulus, etc.) along the perimeter or longitudinally.

REFERENCES

Amatoury, J., Kairaitis, K., Wheatley, J. R., Bilston, L. E., & Amis, T. C. (2010). Onset of airflow limitation in a collapsible tube model: Impact of surrounding pressure, longitudinal strain, and wall folding geometry. *Journal of Applied Physiology,* (109), 1467-1475. doi:10.1152/japplphysiol.0096.2010

Amatoury, J., Kairaitis, K., Wheatley, J. R., Bilston, L. E., & Amis, T. C. (2014). Peripharyngeal tissue deformation and stress distributions in response to caudal tracheal displacement: Pivotal influence of the hyoid bone? *Journal of Applied Physiology, 116*(7), 746-756. doi:10.1152/japplphysiol.01245.2013

Amatoury, J., Kairaitis, K., Wheatley, J. R., Bilston, L. E., & Amis, T. C. (2015). Peripharyngeal tissue deformation, stress distributions, and hyoid bone movement in response to mandibular advancement. *Journal of Applied Physiology*, *118*(3), 282-291. doi:10.1152/japplphysiol.00668.2014.

Arora, N., Meskill, G., & Guilleminault, C. (2015). The role of flow limitation as an important diagnostic tool and clinical finding in mild sleep-disordered breathing. *Sleep Science, 8*(3), 134-142. doi:10.1016/j.slsci.2015.08.003

Benchetrit, G. (2000). Breathing pattern in humans: Diversity and individuality. *Respiration Physiology, 122*(2-3), 123-129.

Berry, D. A., Moon, J. B., & Kuehn, D. P. (1999). A finite element model of the soft palate. *The Cleft Palate-Craniofacial Journal, 36*(3), 217-23. doi:10.1597/1545-1569(1999)036<0217:AFEMOT>2.3.CO;2.

Bertram, C. D. (1987). The effects of wall thickness, axial strain and end proximity on the pressure-area relation of collapsible tubes. *Journal of Biomechanics, 20*(9), 863-876.

Bertram, C. D. (1995). The dynamics of collapsible tubes. *The Society for Experimental Biology*, (49), 253-264.

Bertram, C. D., & Godbole, S. A. (1995). Area and pressure profiles for collapsible-tube oscillations of three types. *Journal of Fluids and Structures, 9*, 257-277.

Bertram, C. D., & Tscherry, J. (2006). The onset of flow-rate limitation and flow-induced oscillations in collapsible tubes. *Journal of Fluids and Structures,* , 1026-1045. doi:10.1016/j.jfluidstructs.2006.07.005.

Birch, M. J., & Srodon, P. D. (2009). Biomechanical properties of the human soft palate. *The Cleft Palate-Craniofacial Journal, 46*(3), 268-74. doi:10.1597/08-012.1

Bradley, T. D., Brown, I. G., Grossman, R. F., Zamel, N., Martinez, D., Phillipson, E. A., & Hoffstein, V. (1986). Pharyngeal size in snorers, nonsnorers, and patients with obstructive sleep apnea. *The New England Journal of Medicine, 315*(21), 1327-21.

Brown, I. G., Bradley, T. D., Phillipson, E. A., Zamel, N., & Hoffstein, V. (1985). Pharyngeal compliance in snoring subjects with and without obstructive sleep apnea. *The American Review of Respiratory Diseases, 132*(2), 211-5. doi:10.1164/arrd.1985.132.2.211

Chouly, F., Van Hirtum, A., Lagrée, P. -., Pelorson, X., & Payan, Y. (2008). Numerical and experimental study of expiratory flow in the case of major upper airway obstructions with fluid-structure interaction. *Journal of Fluids and Structures, 24*(2), 250-269.

Chouly, F., Van Hirtum, A., Lagrée, P. -., Pelorson, X., & Payan, Y. (2009). Modelling the human pharyngeal airway: Validation of numerical simulations using in vitro experiments. *Medical & Biological Engineering & Computing, 47*(1), 49-58. doi:10.1007/s11517-008-0412-1

Conrad, W. A. (1969). Pressure-flow relationships in collapsible tubes. *IEEE Transactions on Biomedical Engineering, BME-16*(4), 284-295. doi:10.1109/TBME.1969.4502660

Dion, B., Naili, S., Renaudeaux, J. P., & Ribreau, C. (1995). Buckling of elastic tubes: Study of highly compliant device. *Medical and Biological Engineering and Computing, 33*, 196-201.

Eckert, D. J., & Malhotra, A. (2008). Pathophysiology of adult obstructive sleep apnea. *Proceedings of the American Thoracic Society, 5*, 144-153. doi:10.1513/pats.200707-114MG

Eckert, D. J., & Younes, M. K. (2013). Arousal from sleep: Implications for obstructive sleep apnea pathogenesis and treatment. *Journal of Applied Physiology, 116*, 302-313. doi:10.1152/japplphysiol.00649.2013.

Elliott, E. A., & Dawson, S. V. (1977). Test of wave-speed theory of flow limitation in elastic tubes. *Journal of Applied Physiology: Respiratory, Environmental, and Exercise Physiology, 43*(3), 516-22.

Fredberg, J. J., Inouye, D., Miller, B., Nathan, M., Jafari, S., Raboudi, S. H., . . . Shore, S. A. (1997). Airway smooth muscle, tidal stretches, and dynamically determined

contractile states. *American Journal of Respiratory and Critical Care Medicine, 156*(6), 1752-59.

Genta, P. R., Edwards, B. A., Sands, S. A., Owens, R. L., Butler, J. P., Loring, S. H., . . . Wellman, A. (2016). Tube law of the pharyngeal airway in sleeping patients with obstructive sleep apnea. *Sleep, 39*(2), 337-43. doi:10.5665/sleep.5440

Gold, A. R., & Schwartz, A. R. (1996). The pharyngeal critical pressure: The whys and hows of using nasal continuous positive airway pressure diagnostically. *Chest, 110,* 1077-1088.

Grotberg, J. B., & Jensen, O. E. (2004). Biofluid mechanics in flexible tubes. *Annual Review of Fluid Mechanics, 36*, 121-47. doi:10.1146/annurev.fluid.36.050802.121918.

Heil, M., & Pedley, T. J. (1996). Large post-buckling deformations of cylindrical shells conveying viscous flow. *Journal of Fluids and Structures, 10*(6), 565-599.

Heinzer, R. C., Stanchina, M. L., Malhotra, A., Fogel, R. B., Patel, S. R., Jordan, A. S., . . . White, D. P. (2005). Lung volume and continuous positive airway pressure requirements in obstructive sleep apnea. *American Journal of Respiratory and Critical Care Medicine, 172*(1), 114-7. doi:10.1164/rccm.200404-552OC

Huang, J., Shen, H., Takahashi, M., Fukunaga, T., Toga, H., Takahashi, K., & Ohya, N. (1998). Pharyngeal cross-sectional area and pharyngeal compliance in normal males and females. *Respiration, 65*(6), 458-68.

Huang, R., Li, X., & Rong, Q. (2013). Control mechanism for the upper airway collapse in patients with obstructive sleep apnea syndrome: A finite element study. *Science China Life Sciences, 56*(4), 366-372.

Isono, S., Morrison, D. L., Launois, S. H., Feroah, T. R., Whitelaw, W. A., & Remmers, J. E. (1993). Static mechanics of the velopharynx of patients with obstructive sleep apnea. *Journal of Applied Physiology, 75*(1), 148-54.

Kairaitis, K., Byth, K., Parikh, R., Stavrinou, R., Wheatley, J. R., & Amis, T. C. (2006). Tracheal traction effects on upper airway patency in rabbits: The role of tissue pressure. *Sleep, 30*(2), 179-86.

Kairaitis, K., Howitt, L., Wheatley, J. R., & Amis, T. C. (2009). Mass loading of the upper airway extraluminal tissue space in rabbits: effects on tissue pressure and pharyngeal airway lumen geometry. *Journal of Applied Physiology, 106*(3), 887-92. doi:10.1152/japplphysiol.91236.2008

Kairaitis, K., Parikh, R., Stavrinou, R., Garlick, S., Kirkness, J. P., Wheatley, J. R., & Amis, T. C. (2003). Upper airway extraluminal tissue pressure fluctuations during breathing in rabbits. *Journal of Applied Physiology, 95*(4), 1560-1566. doi:10.1152/japplphysiol.00432.2003

Kairaitis, K., Stavrinou, R., Parikh, R., Wheatley, J. R., & Amis, T. C. (2006). Mandibular advancement decreases pressures in the tissues surrounding the upper airway in rabbits. *Journal of Applied Physiology, 100*(1), 349-356. doi:10.1152/japplphysiol.00560.2005

Kamm, R. D. (1999). Airway wall mechanics. *Annual Review of Biomedical Engineering, 1*, 47-72. doi:10.1146/annurev.bioeng.1.1.47

Kececioglu, I., McClurken, M. E., Kamm, R. D., & Shapiro, A. H. (1981). Steady, supercritical flow in collapsible tubes. part 1. experimental observations. *Journal of Fluid Mechanics, 109*, 367-389.

Kozlovsky, P., Zaretsky, U., Jaffa, A. J., & Elad, D. (2014). General tube law for collapsible thin and thick-wall tubes. *Journal of Biomechanics, 47*(10), 2378-2384.

Malhotra, A., Huang, Y., Fogel, R. B., Pillar, G., Edwards, J. K., Kikinia, R., . . . White, D. P. (2002). The male predisposition to pharyngeal collapse: Importance of airway length. *American Journal of Respiratory and Critical Care Medicine, 166*(10), 1388-95. doi:10.1164/rccm.2112072.

Marzo, A., Luo, X. Y., & Bertram, C. D. (2005). Three-dimensional collapse and steady flow in thick-walled flexible tubes. *Journal of Fluids and Structures, 20*(6), 817-835.

Oliven, A., Kaufman, E., Kaynan, R., Oliven, R., Steinfeld, U., Tov, N., . . . Kimmel, E. (2010). Mechanical parameters determining pharyngeal collapsibility in patients with sleep apnea. *Journal of Applied Physiology, 109*(4), 1037-44. doi:10.1152/japplphysiol.00019.2010

Oruc, K., & Carpinhoglu, M. O. (2007). A test rig for the investigation of airflow through collapsible tubes. *Journal of Mechanical Engineering Science, 221*, 275-80.

Owens, R. L., Eckert, D. J., Yeh, S. Y., & Malhotra, A. (2008). Upper airway function in the pathogenesis of obstructive sleep apnea: A review of the current literature. *Current Opinion in Pulmonary Medicine, 14*, 519-524. doi:10.1097/MCP.0b013e3283130f66

Owens, R. L., Edwards, B. A., Sands, S. A., Butler, J. P., Eckert, D. J., White, D. P., . . . Wellman, A. (2014). The classical starling resistor model often does not predict

inspiratory airflow patterns in the human upper airway. *Journal of Applied Physiology, 116*, 1105-1112. doi:10.1152/japplphysiol.00853.2013

Pedersen, O. F., & Butler, J. P. (2011). Expiratory flow limitation. *Comprehensive Physiology, 1*(4), 1861-82. doi:10.1002/cphy.c100025.

Pirnar, J., Dolenc-Grošelj, L., Fajdiga, I., & Žun, I. (2015). Computational fluid-structure interaction simulation of airflow in the human upper airway. *Journal of Biomechanics, 48*(13), 3685-91. doi:10.1016/j.jbiomech.2015.08.017.

Rowley, J. A., Permutt, S., Willey, S., Smith, P. L., & Schwartz, A. R. (1996). Effect of tracheal and tongue displacement on upper airway airflow dynamics. *Journal of Applied Physiology, 80*(6), 2171-8.

Sakurai, A., Ohba, K., Futagami, Y., & Tsujimoto, M. (1996). The effect of longitudinal tension on flow in collapsible tube. *JSME International Journal, 39*(2), 361-367.

Schwab, R. J., Gupta, K. B., Gefter, W. B., Metzger, L. J., Hoffman, E. A., & Pack, A. I. (1995). Upper airway and soft tissue anatomy in normal subjects and patients with sleep-disordered breathing. Significance of the Lateral Pharyngeal Walls. *American Journal of Respiratory and Critical Care Medicine, 152*(5), 1673-89.

Schwartz, A. R., Rowley, J. A., Thut, D. C., Permutt, S., & Smith, P. L. (1996). Structural basis for alterations in upper airway collapsibility. *Sleep, 19*, S184-S188.

Schwartz, A. R., & Smith, P. L. (2013). CrossTalk proposal: The human upper airway does behave like a starling resistor during sleep. *The Journal of Physiology, 591*, 2229-2232. doi:10.1113/jphysiol.2012.250654

Shapiro, A. H. (1977). Physiologic and medical aspects of flow in collapsible tubes., 883-906.

Shapiro, A. H. (1977). Steady flow in collapsible tubes. *Journal of Biomechanical Engineering*, *99*(3), 126-147. doi:10.1115/1.3426281

Smith, P. L., Wise, R. A., Gold, A. R., & Schwartz, A. R. (1985). Upper airway pressure-flow relationships in obstructive sleep apnea. *Journal of Applied Physiology, 64*(2), 789-95.

Stanchina, M. L., Malhotra, A., Fogel, R. B., Trinder, J., Edwards, J. K., Schory, K., & White, D. P. (2003). The influence of lung volume on pharyngeal mechanics, collapsibility, and genioglossus muscle activation during sleep. *Sleep, 26*(7), 851-6.

Sun, X., Yu, C., Wang, Y., & Liu, Y. (2007). Numerical simulation of soft palate movement and airflow in human upper airway by fluid-structure interaction method. *Acta Mechanica Sinica, 23*(4), 359-367.

Thut, D. C., Schwartz, A. R., Roach, D., Wise, R. A., Permutt, S., & Smith, P. L. (1993). Tracheal and neck position influence upper airway airflow dynamics by altering airway length. *Journal of Applied Physiology, 75*(5), 2084-90.

Van de Graaff, W. B. (1988). Thoracic influence on upper airway patency. *Journal of Applied Physiology, 65*(5), 2124-31.

Van de Graaff, W. B. (1991). Thoracic traction on the trachea: Mechanisms and magnitude. *Journal of Applied Physiology, 70*, 1328-36.

Van Holsbeke, C. S., Verhulst, S. L., Vos, W. G., De Backer, J. W., Vinchurkar, S. C., Verdonck, P. R., . . . De Backer, W. A. (2014). Change in upper airway geometry between upright and supine position during tidal nasal breathing. *Journal of Aerosol Medicine and Pulmonary Drug Delivery, 27*(1), 51-57. doi:10.1089/jamp.2012.1010.

Walker, R. D., Smith, R. E., Sherriff, S. B., & Wood, R. F. M. (1999). Latex vessels with customized compliance for use in arterial flow models. *Physiological Measurement, 20*(3), 277-286.

Wang, Y., Wang, J., Liu, Y., Yu, S., Sun, X., Li, S., . . . Zhao, W. (2012). Fluid–structure interaction modeling of upper airways before and after nasal surgery for obstructive sleep apnea. *International Journal for Numerical Methods in Biomedical Engineering, 28*(5), 528-546. doi:10.1002/cnm.1486.

Wellman, A., Genta, P. R., Owens, R. L., Edwards, B. A., Sands, S. A., Loring, S. H., . . . Butler, J. P. (2014). Test of the starling resistor model in the human upper airway during sleep. *Journal of Applied Physiology, 117*, 1478-1485. doi:10.1152/japplphysiol.00259.2014.

White, D. P., & Younes, M. K. (2012). Obstructive sleep apnea. *Comprehensive Physiology, 2*, 2541-94. doi:10.1002/cphy.c110064

Wilkinson, V., Malhotra, A., Nicholas, C. L., Worsnop, C., Jordan, A. S., Butler, J. E., . . . Trinder, J. (2008). Discharge patterns of human genioglossus motor units during sleep onset. *Sleep, 31*(4), 525-533.

Winter, W. C., Gampper, T., Gay, S. B., & Suratt, P. M. (1995). Enlargement of the lateral pharyngeal fat pad space in pigs increases upper airway resistance. *Journal of Applied Physiology, 79*(3), 726-31.

Yang, X. L., Liu, Y., & Yang, J. M. (2009). Expiratory flow in a rigid three-generation airway with one collapsible segment. *International Journal for Numerical Methods in Biomedical Engineering, 25*(5), 553-563. doi:10.1002/cnm.1198

Zhu, J. H., Lee, H. P., Lim, K. M., Lee, S. J., Teo, L. S. L., & Wang, D. Y. (2012). Passive movement of human soft palate during respiration: A simulation of 3D fluid/structure interaction. *Journal of Biomechanics, 45*(11), 1992-2000.

APPENDIX

MATLAB CODE

Downstream & Upstream Pressure Code

Code #1 – Convergence Identification

```
%%%%%%%%%%%%%%%%%%%%%%%%%%%%%%%%%%%%%%%%%%%%%%%%%%%%%%%%%%%%%%%%%%%%%%%%%%%%%%%
%%%%%%%%%%%%%%%%%%%%%%%%%%%%%%%%%%%%%%%%%%%%%%%%%%%%%%%%%%%%%%%%%%%%%%%%%%%%%%%
%AUTHOR: Masoud Moghaddam, Ph.D.
%LAST MODIFIED: 6/16/2017 by Kevin Garman
%DESCRIPTION: This code is a function that conducts analysis of
%downstream and upstream pressures measured by two separate OMEGA High
%Speed USB Output Pressure Transducers on either end of the collapsible
%conduit implemented in the experimental setup.  Outputs are graphical
%representations of average mean pressure and standard deviation
%associated with taking varying numbers of points around the minimum
%pressure value of each cycle after 30 seconds of run time.
%Specifically, this studies the variation between 1 - 100 points to
%allow the user to identify what range would be best to set for each
%case.
%%%%%%%%%%%%%%%%%%%%%%%%%%%%%%%%%%%%%%%%%%%%%%%%%%%%%%%%%%%%%%%%%%%%%%%%%%%%%%%
%%%%%%%%%%%%%%%%%%%%%%%%%%%%%%%%%%%%%%%%%%%%%%%%%%%%%%%%%%%%%%%%%%%%%%%%%%%%%%%

clear all;
clc;
close all;

%%%%%%%%%%%%%%%%%%%%%%%%%%%%%%%%%%%%%%%%%%%%%%%%%%%%%%%%%%%%%%%%%%%%%%%%%%%%%%%
%%%%%%%%%%%%%%%%%%%%%%%%%%%%%    Inputs    %%%%%%%%%%%%%%%%%%%%%%%%%%%%%%%%%
%%%%%%%%%%%%%%%%%%%%%%%%%%%%%%%%%%%%%%%%%%%%%%%%%%%%%%%%%%%%%%%%%%%%%%%%%%%%%%%

file1='D+UPress_Diameter_12,70_Tube#d1_100_NoStretch';

threshold_time=30;

%%%inputs related to the polynomial fit
num_points_before_after_min_for_polyfit=100;
studied_points_num=1:5:num_points_before_after_min_for_polyfit;
%For the given range of points you can check the variations in minimum
%pressure and Standard Deviation for the upstream and Downstream the
%given points are the chosen number of points for the curve fit before
%and after the minimum pressure of the cycles in the original data set!
%so num_point

fit_order=3;
cycle_per_min=20;
```

```
%%%%%%%%%%%%%%%%%%%%%%%%%%%%%%%%%%%%%%%%%%%%%%%%%%%%%%%%%%%%%%%%%%%%%%%%%%%%
%%%%%%%%%%%%%%%%%%%%%%   Reading from the files    %%%%%%%%%%%%%%%%%%%%%%
%%%%%%%%%%%%%%%%%%%%%%%%%%%%%%%%%%%%%%%%%%%%%%%%%%%%%%%%%%%%%%%%%%%%%%%%%%%%

file_size=size(xlsread(file1));
rows_in_text=num2str(file_size(1));
file_range=strcat('A13:H',rows_in_text);
imported_data=xlsread(file1, file_range);

%%%% reading the time, downstream pressure and upstream pressure
time=imported_data(:,3);
pressure_downstream=imported_data(:,5);
pressure_upstream=imported_data(:,8);

%%%%%%%%%%%%%%%%%%%%%%%%%%%%%%%%%%%%%%%%%%%%%%%%%%%%%%%%%%%%%%%%%%%%%%%%%%%%
%%%%%%%%%%%%%%%%%    Finding the minimum pressure     %%%%%%%%%%%%%%%%%
%%%%%%%%%%%%%%%%%%%%%%%%%%%%%%%%%%%%%%%%%%%%%%%%%%%%%%%%%%%%%%%%%%%%%%%%%%%%

%%%% assigning a starting time_Threshold (neglecting the cycles before
%%%% that threshold) and finding the indices corresponding to the
%%%% start of the cycles.

threshold_time_indice=find(time>threshold_time,1);
period_cycle_sec=60/cycle_per_min;
time_cycles=threshold_time:period_cycle_sec:max(time);
num_cycles_after_threshold_time=size(time_cycles,2);
for i=1:num_cycles_after_threshold_time
    time_cycle_start_indice(i)=find(time>time_cycles(i),1);
end

%%%% Finding the minimum pressure in each of the cycles

for j=1: num_cycles_after_threshold_time-1

% This section looks for the minimum values in each cycle starting from
% 10 indices after the initial index of start of the cycle
% 10 is added here because in some cases the start of the cycle
% coincides with the minimum pressure value (resulting in some errors)

cycles_minpressure_downstream(j)=min(pressure_downstream((time_cycle_st
art_indice(j)+10):time_cycle_start_indice(j+1)));

cycles_minpressure_upstream(j)=min(pressure_upstream(time_cycle_start_i
ndice(j)+10:time_cycle_start_indice(j+1)));

% finding the indices corresponding to the min pressure
%%% The min pressure value found in each of the cycles (in previous
%%% step) can be "not unique" and there is a chance that pressure with
%%% such value exit in other cycles as well. However, we are only
%%% interested in the index corresponding to the minimum pressure in
%%% the associated cycle. The find (...,10) finds the possible existing
%%% 10 indices corresponding to each minimum pressure and then the
%%% commands afterward make sure that the chosen index falls in the
```

```
%%% range of the corresponding cycle.

temp_downstream=find(pressure_downstream==cycles_minpressure_downstream
(j),10); %saving the index temporarily
temp_upstream=find(pressure_upstream==cycles_minpressure_upstream(j),10
); %saving the index temporarily

%%%%%%%%%%%%%%%%%%%%%%%%%%%%%%  Downstream  %%%%%%%%%%%%%%%%%%%%%%%%%%%%%%

    if j==1
       for k=1:size(temp_downstream,1)
            if temp_downstream(k)>time_cycle_start_indice(j)
                 min_pressure_indice_downstream(j)=temp_downstream(k);
                 break
            end
       end
    else

        for k=1:size(temp_downstream,1)
            if temp_downstream(k)>=time_cycle_start_indice(j) &&
temp_downstream(k)>min_pressure_indice_downstream(j-1)
                 min_pressure_indice_downstream(j)=temp_downstream(k);
                 break
            end
        end
    end

%%%%%%%%%%%%%%%%%%%%%%%%%%%%%%  Upstream  %%%%%%%%%%%%%%%%%%%%%%%%%%%%%%

    if j==1
       for k=1:size(temp_upstream,1)
            if temp_upstream(k)>time_cycle_start_indice(j)
                 min_pressure_indice_upstream(j)=temp_upstream(k);
                 break
            end
       end
    else

        for k=1:size(temp_upstream,1)
            if temp_upstream(k)>=time_cycle_start_indice(j) &&
temp_upstream(k)>min_pressure_indice_upstream(j-1)
                 min_pressure_indice_upstream(j)=temp_upstream(k);
                 break
            end
        end
    end
end
```

```
%%%%%%%%%%%%%%%%%%%%%%%%%%%%%%%%%%%%%%%%%%%%%%%%%%%%%%%%%%%%%%%%%%%%%%%%%%%%
%%%%%%%%%%%%%%%          PLOTTING Original DATA          %%%%%%%%%%%%%%%
%%%%%%%%%%%%%%%%%%%%%%%%%%%%%%%%%%%%%%%%%%%%%%%%%%%%%%%%%%%%%%%%%%%%%%%%%%%%

set(0,'DefaultAxesFontSize', 18);

%%% Original data
xlabel('Time (s)')
ylabel('Pressure (cmH2o)')
figure(1)
plot(time,pressure_downstream, 'g')
xlabel('Time (s)')
ylabel('Pressure (cmH2o)')
legend('Downstream')

hold on
figure(2)
plot(time,pressure_upstream, 'g')
xlabel('Time (s)')
ylabel('Pressure (cmH2o)')
legend('Upstream')

%%%%%%%%%%%%%%%%%%%%%%%%%%%%%%%%%%%%%%%%%%%%%%%%%%%%%%%%%%%%%%%%%%%%%%%%%%%%
%%%%%%%   Making cuts and fitting a polynomial curve and plot   %%%%%%%
%%%%%%%%%%%%%%%%%%%%%%%%%%%%%%%%%%%%%%%%%%%%%%%%%%%%%%%%%%%%%%%%%%%%%%%%%%%%

% In this section a range of points before and after the priorly found
% indices corresponding to the minimum pressure in each cycle is
% considered ( a cut of the data around minumum pressure in each
% cycle). This would allow fitting a polynomial in that smaller range
% of data (in order to remove the noise and getting a smoother curve
% and finally a more accurate minimum value for the pressure in each of
% the cycle)

counter=0;
for kk=studied_points_num;

    counter=counter+1;


time_polyfit_downstream=zeros(size(min_pressure_indice_downstream,2),
2*kk+1);

pressure_polyfit_downstream=zeros(size(min_pressure_indice_downstream,2
), 2*kk+1);
    p_downstream=zeros(size(min_pressure_indice_downstream,2),
fit_order+1);

polynomial_fit_curve_downstream=zeros(size(min_pressure_indice_downstre
am,2), 2*kk+1);
```

```
    time_polyfit_upstream=zeros(size(min_pressure_indice_upstream,2),
2*kk+1);

pressure_polyfit_upstream=zeros(size(min_pressure_indice_upstream,2),
2*kk+1);
    p_upstream=zeros(size(min_pressure_indice_upstream,2),
fit_order+1);

polynomial_fit_curve_upstream=zeros(size(min_pressure_indice_upstream,2
), 2*kk+1);


%%%%%%%%%%%%%%%%%%%%%%%%%     Downstream      %%%%%%%%%%%%%%%%%%%%%%%%%

    for i=1:size(min_pressure_indice_downstream,2)

        %%% defining the cut range

cut_range_in_each_cyle_downstream=(min_pressure_indice_downstream(i)-
kk):(min_pressure_indice_downstream(i)+kk);

        %%% time and pressure in the cut range

time_polyfit_downstream(i,:)=time(cut_range_in_each_cyle_downstream);

pressure_polyfit_downstream(i,:)=pressure_downstream(cut_range_in_each_
cyle_downstream);

        %%% plotting the time and pressure in the cut range
        figure(1)
        hold on

plot(time_polyfit_downstream(i,:),pressure_polyfit_downstream(i,:),
'b*')
        hold on

        %%% polynomially fitting the time and pressure in the cut range
        p_downstream(i,:)=polyfit(time_polyfit_downstream(i,:),
pressure_polyfit_downstream(i,:), fit_order);

polynomial_fit_curve_downstream(i,:)=polyval(p_downstream(i,:),time_pol
yfit_downstream(i,:));

        %%% plotting the polynomial fit of the time and pressure in the
cut range
        figure(1)
        hold on

plot(time_polyfit_downstream(i,:),polynomial_fit_curve_downstream(i,:),
'r')
        hold on
    end
```

```
%%%%%%%%%%%%%%%%%%%%%%%%%%%%%%%  Upstream  %%%%%%%%%%%%%%%%%%%%%%%%%%%%%%%

    for j=1:size(min_pressure_indice_upstream,2)


cut_range_in_each_cyle_upstream=(min_pressure_indice_upstream(j)-
kk):(min_pressure_indice_upstream(j)+kk);

time_polyfit_upstream(j,:)=time(cut_range_in_each_cyle_upstream);

pressure_polyfit_upstream(j,:)=pressure_upstream(cut_range_in_each_cyle
_upstream);

        figure(2)
        hold on
        plot(time_polyfit_upstream(j,:),pressure_polyfit_upstream(j,:),
'b*')
        hold on

        p_upstream(j,:)=polyfit(time_polyfit_upstream(j,:),
pressure_polyfit_upstream(j,:), fit_order);

polynomial_fit_curve_upstream(j,:)=polyval(p_upstream(j,:),time_polyfit
_upstream(j,:));

        figure(2)
        hold on

plot(time_polyfit_upstream(j,:),polynomial_fit_curve_upstream(j,:),
'r')
        hold on
    end


%%%%%%%%%%%%%%%%%%%%%%%%%%%%%%%%%%%%%%%%%%%%%%%%%%%%%%%%%%%%%%%%%%%%%%%%%%%
%%%%%%%%%%%%%%%%%%%  Final average min pressure   %%%%%%%%%%%%%%%%%%%
%%%%%%%%%%%%%%%%%%%%%%%%%%%%%%%%%%%%%%%%%%%%%%%%%%%%%%%%%%%%%%%%%%%%%%%%%%%

%%%%%%%%%%%%%%%%%%%%%%%%%%    Downstream    %%%%%%%%%%%%%%%%%%%%%%%%%%%

min_fit_pressure_downstream=min(polynomial_fit_curve_downstream,[],2);
average_min_pressure_downstream(counter)=mean(min_fit_pressure_downstre
am);
STD_min_pressure_downstream(counter)=std(min_fit_pressure_downstream);

%%%%%%%%%%%%%%%%%%%%%%%%%       Upstream       %%%%%%%%%%%%%%%%%%%%%%%%%

min_fit_pressure_upstream=min(polynomial_fit_curve_upstream,[],2);
average_min_pressure_upstream(counter)=mean(min_fit_pressure_upstream);
STD_min_pressure_upstream(counter)= std(min_fit_pressure_upstream);
```

```
end

figure (3)
plot(studied_points_num, average_min_pressure_downstream)
hold on
plot(studied_points_num, average_min_pressure_upstream)
xlabel('Number of Points')
ylabel('Average Mean Pressure')
legend('downstream','upstream')

figure (4)
plot(studied_points_num, STD_min_pressure_downstream)
hold on
plot(studied_points_num, STD_min_pressure_upstream)
xlabel('Number of Points')
ylabel('Standard Deviation')
legend('downstream','upstream')
```

Code #2 – Downstream & Upstream Pressure Analysis

```
%%%%%%%%%%%%%%%%%%%%%%%%%%%%%%%%%%%%%%%%%%%%%%%%%%%%%%%%%%%%%%%%%%%%%%%%%%%%%%%
%%%%%%%%%%%%%%%%%%%%%%%%%%%%%%%%%%%%%%%%%%%%%%%%%%%%%%%%%%%%%%%%%%%%%%%%%%%%%%%
%AUTHOR: Masoud Moghaddam, Ph.D.
%LAST MODIFIED: 6/16/2017 by Kevin Garman
%DESCRIPTION: This code is a function that conducts quantification of
%downstream and upstream pressures measured by two separate OMEGA High
%Speed USB Output Pressure Transducers on either end of the collapsible
%conduit implemented in the experimental setup.  Outputs are an average
%of ten cycles' minimum pressure values and the the associated standard
%deviation. Outputs from this code are used to acquire data for all
%post-analysis calculations and discussion.
%%%%%%%%%%%%%%%%%%%%%%%%%%%%%%%%%%%%%%%%%%%%%%%%%%%%%%%%%%%%%%%%%%%%%%%%%%%%%%%
%%%%%%%%%%%%%%%%%%%%%%%%%%%%%%%%%%%%%%%%%%%%%%%%%%%%%%%%%%%%%%%%%%%%%%%%%%%%%%%

clear all;
clc;

%%%%%%%%%%%%%%%%%%%%%%%%%%%%%%%%%%%%%%%%%%%%%%%%%%%%%%%%%%%%%%%%%%%%%%%%%%%%%%%
%%%%%%%%%%%%%%%%%%%%%%%%%%%%%%%%%%%%%%%%%%%%%%%%%%%%%%%%%%%%%%%%%%%%%%%%%%%%%%%
%%%%%%%%%%%%%%%%%%%%%%%%%%%%%%%%%%%%%%%%%%%%%%%%%%%%%%%%%%%%%%%%%%%%%%%%%%%%%%%

file1='D+UPress_Diameter_12,70_Tube#d3_700_Stretch';

threshold_time=30;

%%%inputs related to the polynomial fit
num_points_before_after_min_for_polyfit=50;
fit_order=3;
```

```
cycle_per_min=20;

%%%%%%%%%%%%%%%%%%%%%%%%%%%%%%%%%%%%%%%%%%%%%%%%%%%%%%%%%%%%%%%%%%%%%%%%%%%%
%%%%%%%%%%%%%%%%%%%%   Reading from the files    %%%%%%%%%%%%%%%%%%%%
%%%%%%%%%%%%%%%%%%%%%%%%%%%%%%%%%%%%%%%%%%%%%%%%%%%%%%%%%%%%%%%%%%%%%%%%%%%%

file_size=size(xlsread(file1));
rows_in_text=num2str(file_size(1));
file_range=strcat('A13:H',rows_in_text);
imported_data=xlsread(file1, file_range);

%%%% reading the time, downstream pressure and upstream pressure
time=imported_data(:,3);
pressure_downstream=imported_data(:,5);
pressure_upstream=imported_data(:,8);


%%%%%%%%%%%%%%%%%%%%%%%%%%%%%%%%%%%%%%%%%%%%%%%%%%%%%%%%%%%%%%%%%%%%%%%%%%%%
%%%%%%%%%%%%%%%%%    Finding the minimum pressure     %%%%%%%%%%%%%%%%%
%%%%%%%%%%%%%%%%%%%%%%%%%%%%%%%%%%%%%%%%%%%%%%%%%%%%%%%%%%%%%%%%%%%%%%%%%%%%

%%%% assigning a starting time_Threshold (neglecting the cycles before
%%%% that threshold) and finding the indices corresponding to the
%%%% start of the cycles

threshold_time_indice=find(time>threshold_time,1);
period_cycle_sec=60/cycle_per_min;
time_cycles=threshold_time:period_cycle_sec:max(time);
num_cycles_after_threshold_time=size(time_cycles,2);
for i=1:num_cycles_after_threshold_time
    time_cycle_start_indice(i)=find(time>time_cycles(i),1);
end

%%%% Finding the minimum pressure in each of the cycles

for j=1: num_cycles_after_threshold_time-2

% This section looks for the minimum values in each cycle starting from
% 10 indices after the initial index of start of the cycle 10 is added
% here because in some cases the start of the cycle coincides with the
% minimum pressure value (resulting in some errors)


cycles_minpressure_downstream(j)=min(pressure_downstream((time_cycle_st
art_indice(j)+10):time_cycle_start_indice(j+1)));

cycles_minpressure_upstream(j)=min(pressure_upstream(time_cycle_start_i
ndice(j)+10:time_cycle_start_indice(j+1)));
```

```
% finding the indices corresponding to the min pressure

%%% the min pressure value found in each of the cycles (in previous
%%% step) can be "not unique" and there is a chance that pressure with
%%% such value exit in other cycles as well. However, we only are
%%% interested in the index corresponding to the minimum pressure in
%%% the associated cycle. The find (...,10) finds the possible existing
%%% 10 indices corresponding to each minimum pressure and then the
%%% commands afterward makes sure that the chosen indice falls in the
%%% range of the corresponding cycle

temp_downstream=find(pressure_downstream==cycles_minpressure_downstream
(j),10); %saving the indice temporarily
temp_upstream=find(pressure_upstream==cycles_minpressure_upstream(j),10
); %saving the indice temporarily

%%%%%%%%%%%%%%%%%%%%%%%%%%%    Downstream     %%%%%%%%%%%%%%%%%%%%%%%%%%%
    if j==1
       for k=1:size(temp_downstream,1)
            if temp_downstream(k)>time_cycle_start_indice(j)
                 min_pressure_indice_downstream(j)=temp_downstream(k);
                 break
            end
       end
    else

        for k=1:size(temp_downstream,1)
            if temp_downstream(k)>=time_cycle_start_indice(j) &&
temp_downstream(k)>min_pressure_indice_downstream(j-1)
                 min_pressure_indice_downstream(j)=temp_downstream(k);
                 break
            end
        end
    end

%%%%%%%%%%%%%%%%%%%%%%%%%%%     Upstream     %%%%%%%%%%%%%%%%%%%%%%%%%%%
    if j==1
       for k=1:size(temp_upstream,1)
            if temp_upstream(k)>time_cycle_start_indice(j)
                 min_pressure_indice_upstream(j)=temp_upstream(k);
                 break
            end
       end
    else

        for k=1:size(temp_upstream,1)
            if temp_upstream(k)>=time_cycle_start_indice(j) &&
temp_upstream(k)>min_pressure_indice_upstream(j-1)
                 min_pressure_indice_upstream(j)=temp_upstream(k);
                 break
            end
        end
```

```
    end
end
%%%%%%%%%%%%%%%%%%%%%%%%%%%%%%%%%%%%%%%%%%%%%%%%%%%%%%%%%%%%%%%%%%%%%%%%%%%%
%%%%%%%%%%%%%%%%%%%%%%   PLOTTING Original DATA   %%%%%%%%%%%%%%%%%%%%%%%%%%
%%%%%%%%%%%%%%%%%%%%%%%%%%%%%%%%%%%%%%%%%%%%%%%%%%%%%%%%%%%%%%%%%%%%%%%%%%%%


set(0,'DefaultAxesFontSize', 18);

%%% Original data
xlabel('Time (s)')
ylabel('Pressure (cmH2o)')
figure(1)
plot(time,pressure_downstream, 'g')
xlabel('Time (s)')
ylabel('Pressure (cmH2o)')
legend('Downstream')

hold on
figure(2)
plot(time,pressure_upstream, 'g')
xlabel('Time (s)')
ylabel('Pressure (cmH2o)')
legend('Upstream')

%%%%%%%%%%%%%%%%%%%%%%%%%%%%%%%%%%%%%%%%%%%%%%%%%%%%%%%%%%%%%%%%%%%%%%%%%%%%
%%%%%%%   Making cuts and fitting a polynomial curve and plot   %%%%%%%
%%%%%%%%%%%%%%%%%%%%%%%%%%%%%%%%%%%%%%%%%%%%%%%%%%%%%%%%%%%%%%%%%%%%%%%%%%%%

%%% In this section a range of points before and after the prior found
%%% indices corresponding to the minimum pressure in each cycle is
%%% considered (a cut of the data around minimum pressure in each
%%% cycle). This would allow fitting a polynomial in that smaller range
%%% of data (in order to remove the noise and getting a smoother curve
%%% and finally a more accurate minimum value for the pressure in each
%%% of the cycle)

%%%%%%%%%%%%%%%%%%%%%%%%%     Downstream      %%%%%%%%%%%%%%%%%%%%%%%%%

for i=1:size(min_pressure_indice_downstream,2)

    %%% defining the cut range

cut_range_in_each_cyle_downstream=(min_pressure_indice_downstream(i)-
num_points_before_after_min_for_polyfit):(min_pressure_indice_downstrea
m(i)+num_points_before_after_min_for_polyfit);

    %%% time and pressure in the cut range

time_polyfit_downstream(i,:)=time(cut_range_in_each_cyle_downstream);

pressure_polyfit_downstream(i,:)=pressure_downstream(cut_range_in_each_
cyle_downstream);
```

```
    %%% plotting the time and pressure in the cut range
    figure(1)
    hold on

     plot(time_polyfit_downstream(i,:),pressure_polyfit_downstream(i,:),
     'b*')
    hold on

    %%% polynomially fitting the time and pressure in the cut range
     p_downstream(i,:)=polyfit(time_polyfit_downstream(i,:),
     pressure_polyfit_downstream(i,:), fit_order);

polynomial_fit_curve_downstream(i,:)=polyval(p_downstream(i,:),time_pol
yfit_downstream(i,:));

% Plotting the polynomial fit of the time and pressure in the cut range
    figure(1)
    hold on

plot(time_polyfit_downstream(i,:),polynomial_fit_curve_downstream(i,:),
'r')
    hold on
end


%%%%%%%%%%%%%%%%%%%%%%%%%      Upstream       %%%%%%%%%%%%%%%%%%%%%%%%%

for i=1:size(min_pressure_indice_upstream,2)


    cut_range_in_each_cyle_upstream=(min_pressure_indice_upstream(i)-
num_points_before_after_min_for_polyfit):(min_pressure_indice_upstream(
i)+num_points_before_after_min_for_polyfit);
    time_polyfit_upstream(i,:)=time(cut_range_in_each_cyle_upstream);

pressure_polyfit_upstream(i,:)=pressure_upstream(cut_range_in_each_cyle
_upstream);

    figure(2)
    hold on
    plot(time_polyfit_upstream(i,:),pressure_polyfit_upstream(i,:),
'b*')
    hold on

    p_upstream(i,:)=polyfit(time_polyfit_upstream(i,:),
pressure_polyfit_upstream(i,:), fit_order);

polynomial_fit_curve_upstream(i,:)=polyval(p_upstream(i,:),time_polyfit
_upstream(i,:));
```

```
    figure(2)
    hold on
    plot(time_polyfit_upstream(i,:),polynomial_fit_curve_upstream(i,:),
'r')
    hold on
end

%%%%%%%%%%%%%%%%%%%%%%%%%%%%%%%%%%%%%%%%%%%%%%%%%%%%%%%%%%%%%%%%%%%%%%%%%%%%
%%%%%%%%%%%%%%%%%%%%  Final average min pressure   %%%%%%%%%%%%%%%%%%%%
%%%%%%%%%%%%%%%%%%%%%%%%%%%%%%%%%%%%%%%%%%%%%%%%%%%%%%%%%%%%%%%%%%%%%%%%%%%%

%%%%%%%%%%%%%%%%%%%%%%%%%%%%%%%  Downstream  %%%%%%%%%%%%%%%%%%%%%%%%%%%%%%%

min_fit_pressure_downstream=min(polynomial_fit_curve_downstream,[],2);
average_min_pressure_downstream=mean(min_fit_pressure_downstream)
STD_min_pressure_downstream=std(min_fit_pressure_downstream)

%%%%%%%%%%%%%%%%%%%%%%%%%%%%%%%   upstream    %%%%%%%%%%%%%%%%%%%%%%%%%%%%%%%

min_fit_pressure_upstream=min(polynomial_fit_curve_upstream,[],2);
average_min_pressure_upstream=mean(min_fit_pressure_upstream)
STD_min_pressure_upstream = std(min_fit_pressure_upstream)

%%%% Printing the data %%%%

file_out = fopen('min_pressure_upstream_downstream.txt','a');
results_print=strcat(file1,...
    ', downstream_min_pressure(cmH2o),  ',
num2str(average_min_pressure_downstream),...
    ', downstream_min_pressure_STD,  ',
num2str(STD_min_pressure_downstream), ...
    ', upstream_min_pressure(cmH2o),  ',
num2str(average_min_pressure_upstream),...
    ', upstream_min_pressure_STD,  ',
num2str(STD_min_pressure_upstream),...
    ', Threshold_time, ', num2str(threshold_time),...
    ', Total_number_of_points_for_the_polynomial_fit, ',
num2str(2*num_points_before_after_min_for_polyfit+1),...
    ', number_of_cylcles_included_downstream, ',
num2str(size(min_pressure_indice_downstream,2)),...
    ', number_of_cylcles_included_upstream, ',
num2str(size(min_pressure_indice_upstream,2)), '\n');
fprintf(file_out,results_print);
fclose(file_out);
```

Catheter Pressure Code

Code #3 – Catheter Pressure Analysis

```
%%%%%%%%%%%%%%%%%%%%%%%%%%%%%%%%%%%%%%%%%%%%%%%%%%%%%%%%%%%%%%%%%%%%%%%%%%%%
%%%%%%%%%%%%%%%%%%%%%%%%%%%%%%%%%%%%%%%%%%%%%%%%%%%%%%%%%%%%%%%%%%%%%%%%%%%%
%AUTHOR: Masoud Moghaddam, Ph.D.
%LAST MODIFIED: 6/16/2017 by Kevin Garman
%DESCRIPTION: This code is a function that conducts quantification of
%downstream and upstream pressures measured by two separate OMEGA High
%Speed USB Output Pressure Transducers on either end of the collapsible
%conduit implemented in the experimental setup.  Outputs are an average
%of ten cycles' minimum pressure values and the the associated standard
%deviation. Outputs from this code are used to acquire data for all
%post-analysis calculations and discussion.
%%%%%%%%%%%%%%%%%%%%%%%%%%%%%%%%%%%%%%%%%%%%%%%%%%%%%%%%%%%%%%%%%%%%%%%%%%%%
%%%%%%%%%%%%%%%%%%%%%%%%%%%%%%%%%%%%%%%%%%%%%%%%%%%%%%%%%%%%%%%%%%%%%%%%%%%%

clear all;
clc;

%%%%%%%%%%%%%%%%%%%%%%%%%%%%%%%%%%%%%%%%%%%%%%%%%%%%%%%%%%%%%%%%%%%%%%%%%%%%
%%%%%%%%%%%%%%%%%%%%%%%%%%     Inputs      %%%%%%%%%%%%%%%%%%%%%%%%%%%%%
%%%%%%%%%%%%%%%%%%%%%%%%%%%%%%%%%%%%%%%%%%%%%%%%%%%%%%%%%%%%%%%%%%%%%%%%%%%%

file1='Cath&Flow_Diameter_12,70_Tube#d3_700_Stretch';

threshold_time=31;

%%%%%%%%%%%%%%%%%%%%%%%%%%%%%%%%%%%%%%%%%%%%%%%%%%%%%%%%%%%%%%%%%%%%%%%%%%%%
%%%%%%%%%%%%%%%%%%%%%%%   Reading from the files    %%%%%%%%%%%%%%%%%%%%%%%
%%%%%%%%%%%%%%%%%%%%%%%%%%%%%%%%%%%%%%%%%%%%%%%%%%%%%%%%%%%%%%%%%%%%%%%%%%%%

cycle_per_min=20;
file_size=size(xlsread(file1));
rows_in_text=num2str(file_size(1));
file_range=strcat('A2:H',rows_in_text);
imported_data=xlsread(file1, file_range);

%%%% reading the time, Catheter pressure
time=imported_data(:,2);
pressure_Catheter=imported_data(:,4);


%%%%%%%%%%%%%%%%%%%%%%%%%%%%%%%%%%%%%%%%%%%%%%%%%%%%%%%%%%%%%%%%%%%%%%%%%%%%
%%%%%%%%%%%%%%%%%    Finding the minumum pressure     %%%%%%%%%%%%%%%%%%%%%
%%%%%%%%%%%%%%%%%%%%%%%%%%%%%%%%%%%%%%%%%%%%%%%%%%%%%%%%%%%%%%%%%%%%%%%%%%%%

%%%% assigning a starting time_Threshold (neglecting the cycles before
%that threshold) and finding the indices corresponding to the start of
%the cycles.
```

```
threshold_time_indice=find(time>threshold_time,1);
period_cycle_sec=60/cycle_per_min;
time_cycles=threshold_time:period_cycle_sec:max(time);
num_cycles_after_threshold_time=size(time_cycles,2);
for i=1:num_cycles_after_threshold_time
    time_cycle_start_indice(i)=find(time>time_cycles(i),1);
end

%%%% Finding the minimum pressure in each of the cycles

for j=1: num_cycles_after_threshold_time-1
%     for j=1: 2

% This section looks for the minimum values in each cycle starting from
% 10 indices after the initial index of start of the cycle
% 10 is added here because in some cases the start of the cycle
% coincides with the minimum pressure value (resulting in some errors)

cycles_minpressure_Catheter(j)=min(pressure_Catheter((time_cycle_start_
indice(j)):time_cycle_start_indice(j+1)));

% finding the indices corresponding to the min pressure

% the min pressure value found in each of the cycles (in previous
% step) can be "not unique" and there is a chance that pressure with
% such value exit in other cycles as well. However, we only are
% interested in the index corresponding to the minimum pressure in the
% associated cycle. The find (...,5000) finds the possible existing
% 5000 indices corresponding to each minimum pressure and then the
% commands afterward make sure that the chosen index falls in the
% range of the corresponding cycle.

temp_Catheter=find(pressure_Catheter==cycles_minpressure_Catheter(j),50
00); %saving the index temporarily

%%%%%%%%%%%%%%%%%%%%%%%%%%%%   Downstream   %%%%%%%%%%%%%%%%%%%%%%%%%%%%

    if j==1
       for k=1:size(temp_Catheter,1)
            if temp_Catheter(k)>time_cycle_start_indice(j)
                 min_pressure_indice_Catheter(j)=temp_Catheter(k);
                 break
            end
       end
    else

        for k=1:size(temp_Catheter,1)
            if temp_Catheter(k)>=time_cycle_start_indice(j) &&
temp_Catheter(k)>min_pressure_indice_Catheter(j-1)
                 min_pressure_indice_Catheter(j)=temp_Catheter(k);
                 break
            end
        end
    end
```

```
end

%%%%%%%%%%%%%%%%%%%%%%%%%%%%%%%%%%%%%%%%%%%%%%%%%%%%%%%%%%%%%%%%%%%%%%%%%%%%
%%%%%%%%%%%%%%%%%%%%  PLOTTING Original DATA   %%%%%%%%%%%%%%%%%%%%
%%%%%%%%%%%%%%%%%%%%%%%%%%%%%%%%%%%%%%%%%%%%%%%%%%%%%%%%%%%%%%%%%%%%%%%%%%%%

set(0,'DefaultAxesFontSize', 18);

%%% Original data
figure(1)
plot(time,pressure_Catheter, 'g')
xlabel('Time (s)')
ylabel('Pressure (cmH2o)')
legend('Catheter')

%%% this part of the code shows beginning of each cycle (to check)

for i=1:size(time_cycle_start_indice,2)
 hold on
plot(time(time_cycle_start_indice(i)),
pressure_Catheter(time_cycle_start_indice(i)), 'r*')
hold on
end

for i=1:size(min_pressure_indice_Catheter,2)
 hold on
plot(time(min_pressure_indice_Catheter(i)),
pressure_Catheter(min_pressure_indice_Catheter(i)), 'bo')
hold on
end

%%%%%%%%%%%%%%%%%%%%%%%%%%%%%%%%%%%%%%%%%%%%%%%%%%%%%%%%%%%%%%%%%%%%%%%%%%%%
%%%%%%%%%%%%%%%%%%%%  Final average min pressure   %%%%%%%%%%%%%%%%%%%%
%%%%%%%%%%%%%%%%%%%%%%%%%%%%%%%%%%%%%%%%%%%%%%%%%%%%%%%%%%%%%%%%%%%%%%%%%%%%

average_min_pressure_Catheter=mean(cycles_minpressure_Catheter)
STD_min_pressure_Catheter=std(cycles_minpressure_Catheter)

%%%% Printing the data %%%%

file_out = fopen('min_pressure_Catheter.txt','a');
results_print=strcat(file1,...
    ', Catheter_min_pressure(cmH2o),  ',
num2str(average_min_pressure_Catheter),...
    ', Catheter_min_pressure_STD,  ',
num2str(STD_min_pressure_Catheter), ...
    ', Threshold_time, ', num2str(threshold_time) ,'\n');
fprintf(file_out,results_print);
fclose(file_out);
```

Collapsible Tube Buckling & Contact Point Code

Code #4 – Buckling Pressure/Flowrate & Contact Point Pressure/Flowrate Analysis

```
%%%%%%%%%%%%%%%%%%%%%%%%%%%%%%%%%%%%%%%%%%%%%%%%%%%%%%%%%%%%%%%%%%%%%%%%%%%%
                        ESTIMATE BUCKLING PRESSURE
%%%%%%%%%%%%%%%%%%%%%%%%%%%%%%%%%%%%%%%%%%%%%%%%%%%%%%%%%%%%%%%%%%%%%%%%%%%%
   THIS MATLAB CODE ESTIMATES THE BUCKING PRESSURE FROM KEVIN'S DATA
%%%%%%%%%%%%%%%%%%%%%%%%%%%%%%%%%%%%%%%%%%%%%%%%%%%%%%%%%%%%%%%%%%%%%%%%%%%%
%%%%%%%%%%%%%%%%%%%%%%%%%%%%%%%%%%%%%%%%%%%%%%%%%%%%%%%%%%%%%%%%%%%%%%%%%%%%
%AUTHOR: Guilherme Garcia, Ph.D.
%LAST MODIFIED: 6/18/2017 by Kevin Garman
%DESCRIPTION: This code is a function that conducts analysis of
%collapsible conduit pressures measured by the Millar Pressure Catheter
%measured at the center of the collapsible tube implemented in the
%experimental setup.  Outputs are graphical representations of the
%Buckling and Contact Point Pressures & Flowrates for the stretch and
%non-stretch %cases.  The Contact Point Curve is formed via Michaelis-
%Menten Function. The Buckling Point Curve is formed via Linear Piece
%Funtion. Specifically, this allows the user to accurately conduct
%analysis to estimate the Buckling Pressures/Flowrates and the Contact
%Point Pressures and Flowrates.  After processing, statistical analysis
%can be implemented.
%%%%%%%%%%%%%%%%%%%%%%%%%%%%%%%%%%%%%%%%%%%%%%%%%%%%%%%%%%%%%%%%%%%%%%%%%%%%
%%%%%%%%%%%%%%%%%%%%%%%%%%%%%%%%%%%%%%%%%%%%%%%%%%%%%%%%%%%%%%%%%%%%%%%%%%%%

clear all; %CLEARS ALL VARIABLES%
close all; %CLOSES ALL FIGURES%
clc; %CLEARS ALL INPUT AND OUTPUT FROM THE COMMAND WINDOW DISPLAY%

Buckling_threshold = 0.96;
Contact_point_threshold = 0.02;


%%%%%%%%%%%%%%%%%%%%%%%%%%%%%%%%%%%%%%%%%%%%%%%%%%%%%%%%%%%%%%%%%%%%%%%%%%%%
                            READ DATA FROM FILE
%%%%%%%%%%%%%%%%%%%%%%%%%%%%%%%%%%%%%%%%%%%%%%%%%%%%%%%%%%%%%%%%%%%%%%%%%%%%

%filename = 'L_7.5_Tube_3cut.csv';
%filename = 'H_2.2_TUBE_B.csv';
%filename = 'H_0.98_TUBE_E.csv';
filename = 'L_7.5_Tube#1cut.csv';

Npoints = 8; % Number of flowrates measured; Kevin used Volume of air
(ml) = 0, 100, 200, 300, 400, 500, 600, 700
P = zeros(2,Npoints);
rR_ratio = zeros(2,Npoints);

% Read flowrate
ROW=6; COL1=1; COL2=Npoints; % Row and column where data is located
Q = csvread(filename,ROW,COL1,[ROW COL1 ROW COL2]);
```

```
% Read Catheter Pressure - No stretch
ROW=8; % Row where data is located
P(1,:) = csvread(filename,ROW,COL1,[ROW COL1 ROW COL2]);

% Read Relative Displacement - No stretch
ROW=15; % Row where data is located
rR_ratio(1,:) = csvread(filename,ROW,COL1,[ROW COL1 ROW COL2]);

% Read Catheter Pressure - 0.5cm stretch
ROW=17; % Row where data is located
P(2,:) = csvread(filename,ROW,COL1,[ROW COL1 ROW COL2]);

% Read Relative Displacement - 0.5cm stretch
ROW=24; % Row where data is located
rR_ratio(2,:) = csvread(filename,ROW,COL1,[ROW COL1 ROW COL2]);

%%%%%%%%%%%%%%%%%%%%%%%%%%%%%%%%%%%%%%%%%%%%%%%%%%%%%%%%%%%%%%%%%%%%%%%%%%%%
                        ESTIMATE BUCKLING PRESSURE
%%%%%%%%%%%%%%%%%%%%%%%%%%%%%%%%%%%%%%%%%%%%%%%%%%%%%%%%%%%%%%%%%%%%%%%%%%%%

P_Fit = 0:0.01:20;
Npoints_P_Fit = size(P_Fit,2);
rR_ratio_Fit_P1 = zeros(2,Npoints_P_Fit) + 2;
rR_ratio_Fit_P2 = zeros(2,Npoints_P_Fit) + 2;

Q_Fit = 0:0.1:700;
Npoints_Q_Fit = size(Q_Fit,2);
rR_ratio_Fit_Q1 = zeros(2,Npoints_Q_Fit) + 2;
rR_ratio_Fit_Q2 = zeros(2,Npoints_Q_Fit) + 2;

P_buckling = zeros(2,1);
rR_ratio_buckling_P = zeros(2,1);
Q_buckling = zeros(2,1);
rR_ratio_buckling_Q = zeros(2,1);

P_contact_point = zeros(2,1);
rR_ratio_contact_point_P = zeros(2,1);
Q_contact_point = zeros(2,1);
rR_ratio_contact_point_Q = zeros(2,1);

Buckling_threshold = Buckling_threshold + 0.001;
Contact_point_threshold = Contact_point_threshold + 0.001;

for i=1:2 % No stretch: i=1; 0.5cm stretch: i=2

    % Truncate data to range of d/D > 0
    index_end = find(rR_ratio(i,:) < 0,1)-1;
    if isempty(index_end)==1 % If array is empty
        index_end = 8;
    end
    Truncated_rR_ratio = rR_ratio(i,1:index_end);
    Truncated_P = -P(i,1:index_end);
    Truncated_rR_ratio_Q1 = rR_ratio(i,2:index_end);
```

```
% For Michaelis-Menten fitting, I need to remove point Q=0
Truncated_Q1 = Q(2:index_end);
% For Michaelis-Menten fitting, I need to remove point Q=0
Truncated_rR_ratio_Q2 = rR_ratio(i,1:index_end);
Truncated_Q2 = Q(1:index_end);

x = Truncated_P';
y = Truncated_rR_ratio';
xQ1 = Truncated_Q1';
yQ1 = Truncated_rR_ratio_Q1';
xQ2 = Truncated_Q2';
yQ2 = Truncated_rR_ratio_Q2';

% Michaelis-Menten fit - Works best for rR_ratio near zero
% Michaelis-Menten fit - Pressure vs. rR_ratio
ft = fittype('Michaelis_Menten_Function(x,Km,m)');
f = fit(x,y,ft,'StartPoint',[1,4],'Upper',[20,10],'Lower',[0,0]);
best_m = f.m;
best_Km = f.Km;
 rR_ratio_Fit_P1(i,:) =
 Michaelis_Menten_Function(P_Fit,best_Km,best_m);

% Michaelis-Menten fit - Flowrate vs. rR_ratio
ft = fittype('Michaelis_Menten_Function(x,Km,m)');
f =
fit(xQ1,yQ1,ft,'StartPoint',[100,4],'Upper',[350,10],'Lower',[0,0]);
best_m = f.m;
best_Km = f.Km;
rR_ratio_Fit_Q1(i,:) =
Michaelis_Menten_Function(Q_Fit,best_Km,best_m);
%f = fit(xQ1,yQ1,'smoothingspline','SmoothingParam',0.8);
%rR_ratio_Fit_Q1(i,:) = f(Q_Fit);

% Polynomial fit
%poly_coefficients = polyfit(x,y,6);
%rR_ratio_Fit_2(i,:) = polyval(poly_coefficients,P_Fit);

% Smoothing spline fit
%f = fit(x,y,'smoothingspline','SmoothingParam',0.8);
%rR_ratio_Fit_2(i,:) = f(P_Fit);

% Piecewise linear interpolation - Works best for rR_ratio near 1.0
% Piecewise linear interpolation - Pressure vs. rR_ratio
f = fit(x,y,'linearinterp');
rR_ratio_Fit_P2(i,:) = f(P_Fit);

% Piecewise linear interpolation - Flowrate vs. rR_ratio
fQ = fit(xQ2,yQ2,'linearinterp');
rR_ratio_Fit_Q2(i,:) = fQ(Q_Fit);

% Find the Buckling pressure
index_P_buckling = find(rR_ratio_Fit_P2(i,:)<Buckling_threshold,1);
P_buckling(i) = -P_Fit(index_P_buckling);
rR_ratio_buckling_P(i) = rR_ratio_Fit_P2(i,index_P_buckling);
```

```
    % Find the Contact Point pressure
    index_P_contact_point =
     find(rR_ratio_Fit_P1(i,:)<Contact_point_threshold,1);
    if isempty(index_P_contact_point)==1 % If array is empty
        index_P_contact_point = Npoints_P_Fit;
    end
    P_contact_point(i) = -P_Fit(index_P_contact_point);
    rR_ratio_contact_point_P(i) =
    rR_ratio_Fit_P1(i,index_P_contact_point);

    % Find the Buckling flowrate
    index_Q_buckling = find(rR_ratio_Fit_Q2(i,:)<Buckling_threshold,1);
    Q_buckling(i) = Q_Fit(index_Q_buckling);
    rR_ratio_buckling_Q(i) = rR_ratio_Fit_Q2(i,index_Q_buckling);

    % Find the Contact Point flowrate
    index_Q_contact_point = find(rR_ratio_Fit_Q1(i,:)<0.02,1);
    if isempty(index_Q_contact_point)==1 % If array is empty
        index_Q_contact_point = Npoints_Q_Fit;
    end
    Q_contact_point(i) = Q_Fit(index_Q_contact_point);
    rR_ratio_contact_point_Q(i) =
     rR_ratio_Fit_Q1(i,index_Q_contact_point);
end


%%%%%%%%%%%%%%%%%%%%%%%%%%%%%%%%%%%%%%%%%%%%%%%%%%%%%%%%%%%%%%%%%%%%%%%%%%%%
                          PRINT RESULTS ON SCREEN
%%%%%%%%%%%%%%%%%%%%%%%%%%%%%%%%%%%%%%%%%%%%%%%%%%%%%%%%%%%%%%%%%%%%%%%%%%%%

'****************** BUCKLING PRESSURE ******************'

'BUCKLING PRESSURE (cmH2O) - NO STRETCH'
P_buckling(1)

'BUCKLING PRESSURE (cmH2O) - 0.5 cm STRETCH'
P_buckling(2)

'***************** CONTACT POINT PRESSURE ***************'

'CONTACT POINT PRESSURE (cmH2O) - NO STRETCH'
P_contact_point(1)

'CONTACT POINT PRESSURE (cmH2O) - 0.5 cm STRETCH'
P_contact_point(2)

'****************** BUCKLING FLOWRATE ******************'

'BUCKLING FLOWRATE (ml/s) - NO STRETCH'
Q_buckling(1)

'BUCKLING FLOWRATE (ml/s) - 0.5 cm STRETCH'
```

```
Q_buckling(2)

'**************** CONTACT POINT FLOWRATE ***************'

'CONTACT POINT FLOWRATE (ml/s) - NO STRETCH'
Q_contact_point(1)

'CONTACT POINT FLOWRATE (ml/s) - 0.5 cm STRETCH'
Q_contact_point(2)


P_Fit = - P_Fit;


%%%%%%%%%%%%%%%%%%%%%%%%%%%%%%%%%%%%%%%%%%%%%%%%%%%%%%%%%%%%%%%%%%%%%%%%%%%%
                FIGURE 1 - NO STRETCH - BUCKLING PRESSURE
%%%%%%%%%%%%%%%%%%%%%%%%%%%%%%%%%%%%%%%%%%%%%%%%%%%%%%%%%%%%%%%%%%%%%%%%%%%%

figure(1);
plot(P(1,:),rR_ratio(1,:),'sk','MarkerSize',8,'MarkerFaceColor','k');
hold on;
plot(P_Fit,rR_ratio_Fit_P2(1,:),'-b'); hold on;
plot(P_buckling(1),rR_ratio_buckling_P(1),'sr','MarkerSize',8,'MarkerFa
ceColor','r'); hold on;

xlabel('Catheter pressure (cmH_2O)','FontWeight','bold','FontSize',14);
ylabel('d/D','FontWeight','bold','FontSize',14);

title('No stretch'); hold on;

xlim([-8 0]);
ylim([0.75 1]);


%%%%%%%%%%%%%%%%%%%%%%%%%%%%%%%%%%%%%%%%%%%%%%%%%%%%%%%%%%%%%%%%%%%%%%%%%%%%
              FIGURE 2 - 0.5 cm STRETCH - BUCKLING PRESSURE
%%%%%%%%%%%%%%%%%%%%%%%%%%%%%%%%%%%%%%%%%%%%%%%%%%%%%%%%%%%%%%%%%%%%%%%%%%%%

figure(2);
plot(P(2,:),rR_ratio(2,:),'sk','MarkerSize',8,'MarkerFaceColor','k');
hold on;
plot(P_Fit,rR_ratio_Fit_P2(2,:),'-b'); hold on;
plot(P_buckling(2),rR_ratio_buckling_P(2),'sr','MarkerSize',8,'MarkerFa
ceColor','r'); hold on;

xlabel('Catheter pressure (cmH_2O)','FontWeight','bold','FontSize',14);
ylabel('d/D','FontWeight','bold','FontSize',14);

title('0.5 cm stretch'); hold on;

xlim([-8 0]);
ylim([0.75 1]);
```

```
%%%%%%%%%%%%%%%%%%%%%%%%%%%%%%%%%%%%%%%%%%%%%%%%%%%%%%%%%%%%%%%%%%%%%%%%
            FIGURE 3 - NO STRETCH - CONTACT POINT PRESSURE
%%%%%%%%%%%%%%%%%%%%%%%%%%%%%%%%%%%%%%%%%%%%%%%%%%%%%%%%%%%%%%%%%%%%%%%%

figure(3);
plot(P(1,:),rR_ratio(1,:),'sk','MarkerSize',8,'MarkerFaceColor','k');
hold on;
plot(P_Fit,rR_ratio_Fit_P1(1,:),'-b'); hold on;
plot(P_contact_point(1),rR_ratio_contact_point_P(1),'sr','MarkerSize',8
,'MarkerFaceColor','r'); hold on;

xlabel('Catheter pressure (cmH_2O)','FontWeight','bold','FontSize',14);
ylabel('d/D','FontWeight','bold','FontSize',14);

title('No stretch'); hold on;


%%%%%%%%%%%%%%%%%%%%%%%%%%%%%%%%%%%%%%%%%%%%%%%%%%%%%%%%%%%%%%%%%%%%%%%%
            FIGURE 4 - 0.5 cm STRETCH - CONTACT POINT PRESSURE
%%%%%%%%%%%%%%%%%%%%%%%%%%%%%%%%%%%%%%%%%%%%%%%%%%%%%%%%%%%%%%%%%%%%%%%%

figure(4);
plot(P(2,:),rR_ratio(2,:),'sk','MarkerSize',8,'MarkerFaceColor','k');
hold on;
plot(P_Fit,rR_ratio_Fit_P1(2,:),'-b'); hold on;
plot(P_contact_point(2),rR_ratio_contact_point_P(2),'sr','MarkerSize',8
,'MarkerFaceColor','r'); hold on;

xlabel('Catheter pressure (cmH_2O)','FontWeight','bold','FontSize',14);
ylabel('d/D','FontWeight','bold','FontSize',14);

title('0.5 cm stretch'); hold on;

%%%%%%%%%%%%%%%%%%%%%%%%%%%%%%%%%%%%%%%%%%%%%%%%%%%%%%%%%%%%%%%%%%%%%%%%
             FIGURE 5 - NO STRETCH - FLOWRATE AT BUCKLING
%%%%%%%%%%%%%%%%%%%%%%%%%%%%%%%%%%%%%%%%%%%%%%%%%%%%%%%%%%%%%%%%%%%%%%%%

figure(5);
plot(Q,rR_ratio(1,:),'sk','MarkerSize',8,'MarkerFaceColor','k'); hold
on;
plot(Q_Fit,rR_ratio_Fit_Q2(1,:),'-b'); hold on;
plot(Q_buckling(1),rR_ratio_buckling_Q(1),'sr','MarkerSize',8,'MarkerFa
ceColor','r'); hold on;

xlabel('Flowrate (ml/s)','FontWeight','bold','FontSize',14);
ylabel('d/D','FontWeight','bold','FontSize',14);

title('No stretch'); hold on;

xlim([0 250]);
ylim([0.75 1]);
```

```
%%%%%%%%%%%%%%%%%%%%%%%%%%%%%%%%%%%%%%%%%%%%%%%%%%%%%%%%%%%%%%%%%%%%%%%%
            FIGURE 6 - 0.5cm STRETCH - FLOWRATE AT BUCKLING
%%%%%%%%%%%%%%%%%%%%%%%%%%%%%%%%%%%%%%%%%%%%%%%%%%%%%%%%%%%%%%%%%%%%%%%%

figure(6);
plot(Q,rR_ratio(2,:),'sk','MarkerSize',8,'MarkerFaceColor','k'); hold
on;
plot(Q_Fit,rR_ratio_Fit_Q2(2,:),'-b'); hold on;
plot(Q_buckling(2),rR_ratio_buckling_Q(2),'sr','MarkerSize',8,'MarkerFa
ceColor','r'); hold on;

xlabel('Flowrate (ml/s)','FontWeight','bold','FontSize',14);
ylabel('d/D','FontWeight','bold','FontSize',14);

title('0.5 cm stretch'); hold on;

xlim([0 250]);
ylim([0.75 1]);


%%%%%%%%%%%%%%%%%%%%%%%%%%%%%%%%%%%%%%%%%%%%%%%%%%%%%%%%%%%%%%%%%%%%%%%%
            FIGURE 7 - NO STRETCH - CONTACT POINT FLOWRATE
%%%%%%%%%%%%%%%%%%%%%%%%%%%%%%%%%%%%%%%%%%%%%%%%%%%%%%%%%%%%%%%%%%%%%%%%

figure(7);
plot(Q(:),rR_ratio(1,:),'sk','MarkerSize',8,'MarkerFaceColor','k');
hold on;
plot(Q_Fit,rR_ratio_Fit_Q1(1,:),'-b'); hold on;
plot(Q_contact_point(1),rR_ratio_contact_point_Q(1),'sr','MarkerSize',8
,'MarkerFaceColor','r'); hold on;

xlabel('Flowrate (ml/s)','FontWeight','bold','FontSize',14);
ylabel('d/D','FontWeight','bold','FontSize',14);

title('No stretch'); hold on;

%xlim([0 350]);
%ylim([0 1]);
```

```
%%%%%%%%%%%%%%%%%%%%%%%%%%%%%%%%%%%%%%%%%%%%%%%%%%%%%%%%%%%%%%%%%%%%%%%%%%%%
           FIGURE 8 - 0.5 cm STRETCH - CONTACT POINT FLOWRATE
%%%%%%%%%%%%%%%%%%%%%%%%%%%%%%%%%%%%%%%%%%%%%%%%%%%%%%%%%%%%%%%%%%%%%%%%%%%%

figure(8);
plot(Q(:),rR_ratio(2,:),'sk','MarkerSize',8,'MarkerFaceColor','k');
hold on;
plot(Q_Fit,rR_ratio_Fit_Q1(2,:),'-b'); hold on;
plot(Q_contact_point(2),rR_ratio_contact_point_Q(2),'sr','MarkerSize',8
,'MarkerFaceColor','r'); hold on;

xlabel('Flowrate (ml/s)','FontWeight','bold','FontSize',14);
ylabel('d/D','FontWeight','bold','FontSize',14);

%xlim([0 350]);
%ylim([0 1]);

title('0.5 cm stretch'); hold on;
```

Code #5 – Michaelis Menten Function used in Buckling and Contact Point Flowrate Analysis

```
%%%%%%%%%%%%%%%%%%%%%%%%%%%%%%%%%%%%%%%%%%%%%%%%%%%%%%%%%%%%%%%%%%%%%%%%%%%%
             ESTIMATE BUCKLING AND CONTACT POINT FLOWRATE
 %%%%%%%%%%%%%%%%%%%%%%%%%%%%%%%%%%%%%%%%%%%%%%%%%%%%%%%%%%%%%%%%%%%%%%%%%%%
        THIS MATLAB CODE ESTIMATES THE FLOWRATE FROM KEVIN'S DATA
%%%%%%%%%%%%%%%%%%%%%%%%%%%%%%%%%%%%%%%%%%%%%%%%%%%%%%%%%%%%%%%%%%%%%%%%%%%%
%%%%%%%%%%%%%%%%%%%%%%%%%%%%%%%%%%%%%%%%%%%%%%%%%%%%%%%%%%%%%%%%%%%%%%%%%%%%
%AUTHOR: Guilherme Garcia, Ph.D.
%LAST MODIFIED: 6/19/2017 by Kevin Garman
%DESCRIPTION: This code is used in analysis of buckling and contact
%point flowrate values.
%%%%%%%%%%%%%%%%%%%%%%%%%%%%%%%%%%%%%%%%%%%%%%%%%%%%%%%%%%%%%%%%%%%%%%%%%%%%
%%%%%%%%%%%%%%%%%%%%%%%%%%%%%%%%%%%%%%%%%%%%%%%%%%%%%%%%%%%%%%%%%%%%%%%%%%%%

function y = Michaelis_Menten_Function(x,Km,m)

    y = zeros(size(x));

    for i=1:length(x)
        y(i) = 1 - x(i)^m /((Km)^m + x(i)^m);
    end
end
```